Aircraft Noise Shielding Assessment

The creation of a software tool to predict aircraft noise shielding

F.H.V. Dewitte

Technische Universiteit Delft

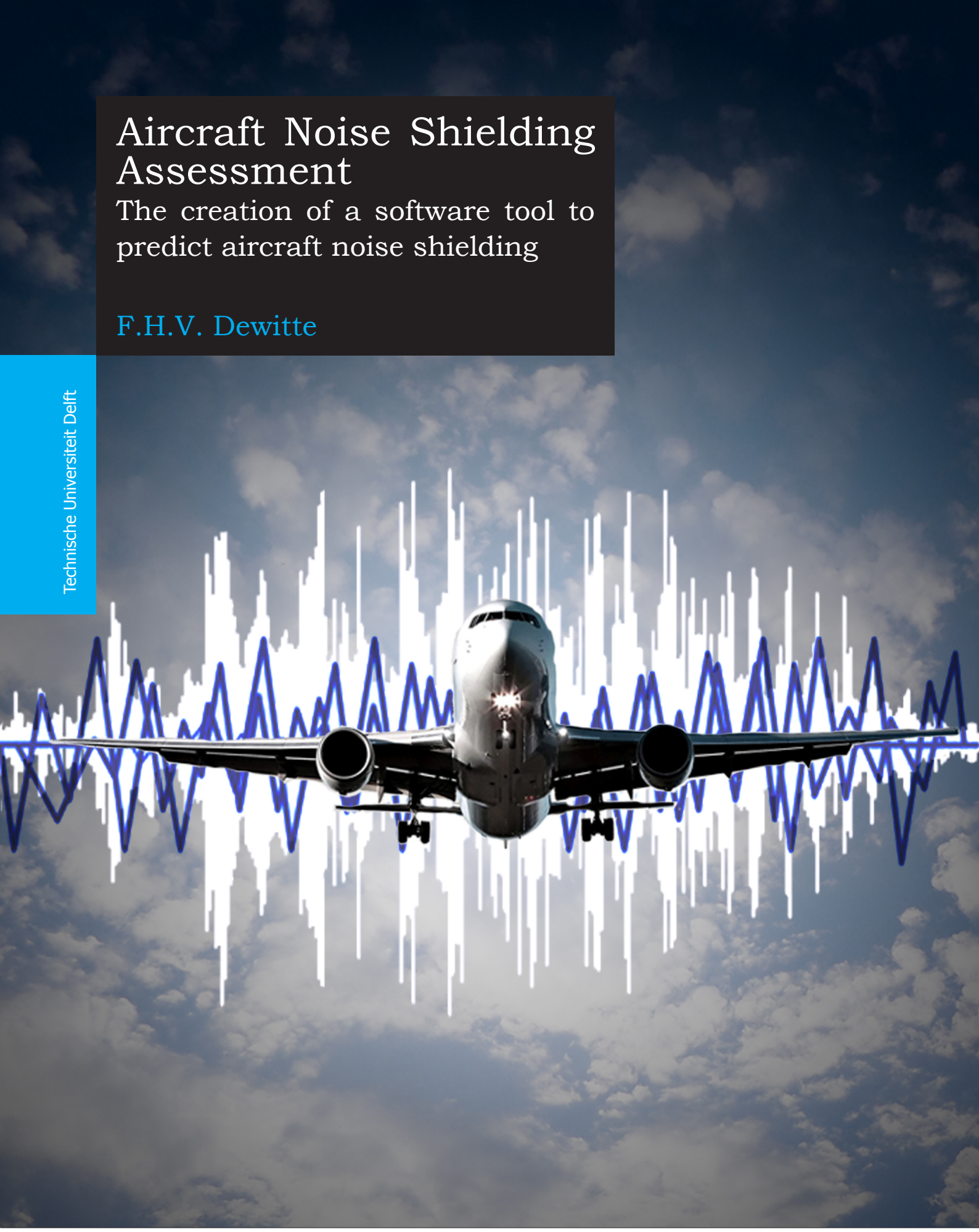

TU Delft Delft University of Technology

Challenge the future

Aircraft Noise Shielding Assessment

The creation of a software tool to predict aircraft noise shielding

by

F.H.V. Dewitte

in partial fulfillment of the requirements for the degree of

Master of Science
in Aerospace Engineering

at the Delft University of Technology,
to be defended publicly on Monday January 28, 2016 at 10:00 AM.

Student number:	4111729		
Thesis number:	070#16#MT#FPP		
Supervisor:	Dr. ir. M. Snellen		
	Prof. dr. D.G. Simons		
Thesis committee:	Prof. dr. D.G. Simons,	TU Delft	ANCE
	Dr. ir. M. Snellen,	TU Delft	ANCE
	Dr. ir. R. Vos,	TU Delft	FPP

This thesis is confidential and cannot be made public until January 28, 2016.

TU Delft Delft University of Technology

Preface

Preface...

To conclude my Aerospace Engineering studies at the Delft University of Technology I have performed this thesis project. I started my studies in this field because I have a very keen interest in the science behind aeronautics. I have chosen the topic of aircraft noise shielding for this project so that more people can enjoy the beauty of aircraft and flying in general without the inconvenience of noise disturbance.

In recognition of the people who helped me in some way or another during my thesis project, I would like to take the opportunity to thank them. I would like to thank Dr. ir. M. Arntzen who set me on track with this thesis project. Also Dr. ir. M. Snellen for taking over the project and for her guidance and support. I would also like to thank Prof. dr. D.G. Simons for giving me new insights and a critical view on the noise shielding calculation methods.

My highest gratitude goes to my parents E. Dewitte and A. Schockaert for always believing in my capabilities, even when I questioned myself. Also for giving me the opportunity to study at the Delft University of Technology. I would like to thank my brother R. Dewitte for creating such a nice image for the cover page of this report and G. Mc Phillips for proofreading.

Further, I would like to thank all my friends and family members who supported me during my studies. Especially my grandfathers O. Dewitte and J. Schockaert who passed away during my graduation studies and where proud of everything I did and will do. I would also like to thank my fellow students for the helpful discussions.

Finally, my very special thanks to my love C. Reuse for her patience and support in every way possible. Your encouragement is highly appreciated.

F.H.V. Dewitte
Delft, December 2015

Summary

The amount of air traffic is increasing and cities become more and more populated. Since airports tend to be located close to or inside cities, an increasing amount of people suffer from aircraft noise pollution. More silent aircraft are needed to be able to reduce this noise pollution. One way to reduce the aircraft noise is through engine noise shielding. To be able to shield the aircraft engine noise efficiently, a noise shielding assessment tool is required. In this thesis project, such a tool is developed for conventional tube with wing aircraft. This tool needs to have low computational cost while the accuracy should be sufficient for the preliminary design.

Firstly it is necessary to look at the available noise shielding calculation methods. The most accurate methods are the the boundary element method and the ray tracing method. The computational cost of these methods are however too high to use them in the design loop. The computational time of the equivalent source method is slightly lower than that of the boundary element method. This comes with the penalty of reduced accuracy. The optimal positions and number of equivalent sources is difficult to find which makes this method difficult to use for various aircraft configurations. The computational cost of the barrier shielding method is the least expensive but it can only solve for plane screen problems. The Kirchhoff diffraction method can solve more complex shape outlines than the barrier shielding method but, as well as the barrier shielding method, it only captures sharp edge diffracted rays.

To create a fast and accurate noise prediction tool, the aircraft's fuselage is modeled as a cylinder and the wings as two planar surfaces. The engine is represented by a monopole sound source. The most suitable noise shielding calculation methods are found to be the barrier shielding method for the wings and the analytic solution of a cylinder for the fuselage. The analytic solution is used to increase the accuracy of the barrier shielding method. This is done by including the creeping rays at the fuselage. Because the barrier shielding method is developed for a half-finite barrier, it has to be modified for finite barriers. This is done in the same way as used in the NASA Aircraft Noise Prediction Program. For the analytic solution of the cylinder, the scattered and incident acoustic pressure need to be defined. Here, a derivation for a line source is used. This is a valid assumption since to determine the noise shielding, the relative pressure is needed. It is however important that the sound waves are cylindrical in the two dimensional plane.

The two methods are then added together and compared with the results of an aircraft with a plane fuselage. When adding the two methods together, the rays that are diffracted by the fuselage and then by the wing also need to be taken into account. This is done by including the part of the fuselage located in the center of the wings in the wing shielding calculation. Because the attenuation of the fuselage is not provided by the wings, next, the attenuation of that part of the fuselage is subtracted from the total result. Finally, the attenuation of the cylinder, obtained with the analytic solution, is added. This results in a smooth noise shielding transition between the wings and the fuselage which indicates that the double shielded rays are indeed taken into account.

The wing shielding assessment tool is validated against results obtained with the Kirchhoff theory of diffraction. First, the Kirchhoff diffraction theory is compared with the aircraft noise shielding calculated with the barrier shielding method. It is concluded that the modification to the barrier shielding for finite shapes overestimates the region of highest shielding of the wing. In addition, the horizontal plane is not a good representation of the fuselage if the source is not centered right above the fuselage plane. It tends to underestimate the noise attenuation.

When the fuselage is substituted by the cylinder. The fuselage has higher shielding compared to the Kirchhoff theory of diffraction. This is caused by the creeping rays. The analytic solution includes creeping rays. The creeping rays continuously sheds rays as it travels around the surface reducing the strength of the ray. The reduction in sound ray strength results in higher shielding. This effect is amplified by increasing the frequency.

The noise shielding prediction tool developed in this thesis project has shown to be able to determine the noise attenuation by a point source of different aircraft configurations with low computational cost. The addition of the analytic results of the cylinder to the barrier shielding method has increased the accuracy by including the creeping rays.

Contents

1

Introduction

The amount of air traffic is increasing. As, cities become even more populated. Since airports tend to be located close to or inside cities, an increasing amount of people suffer from aircraft noise pollution. This has already resulted in air traffic restrictions. To be able to accommodate the need for air traffic and the noise pollution restrictions, more silent aircraft are needed.

There are different methods to reduce aircraft noise. For example designing engines that produce less noise. Also a redesign of the high lift devices to reduce the noise which they create, especially at take-off and approach conditions. Another method to reduce the noise created by an aircraft is blocking the noise propagation with elements of the aircraft itself. For example, block the engine noise with the aid of a wing. This method is called noise shielding. Aircraft noise shielding is the reduction of noise by blocking it by the aircraft geometry. A noise shielding example is given in Figure 1.1.

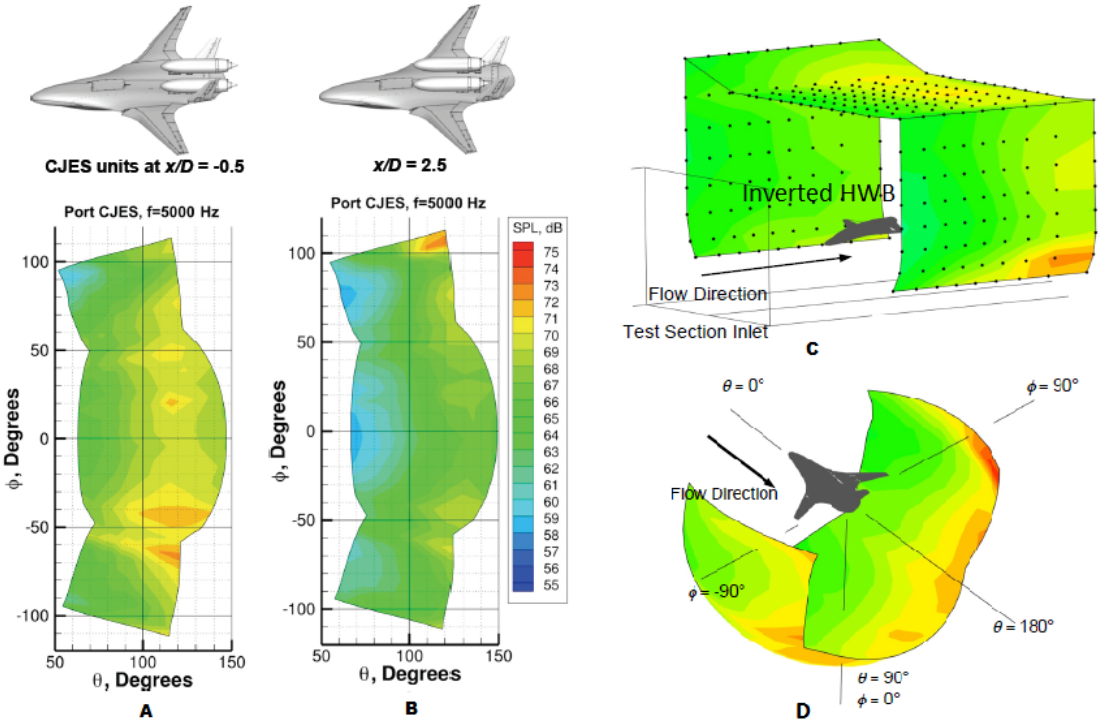

Figure 1.1: θ (polar) - ϕ (azimuth) noise hemispheres of shielding effect off different engine positions with f = 5000 Hz. D is the fan nozzle exit diameter and x the axial distance from the fan nozzle exit plane to the trailing edge of the hybrid wing body. Positive x means that the fan nozzle exit plane is located upstream of the HWB trailing edge. CJES stands for Compact Jet Engine Simulators. Figure A is the un-shieldied noise contour (x/D = -0.5), B the shielded noise contour (x/D = 2.5) C shows the microphone locations and D an example of the 3D noise contour [1].

In Figure 1.1, the shielding effect of placing the engines more to the center of the fuselage is examined. The shielding is obtained experimentally over an azimuth angle of 180 [deg]. In the experiment, the jet noise is simulated by so called Compact Jet Engine Simulators (CJES). Each dot in Figure 1.1 C represents a microphone. With interpolation, the result between the microphones is obtained. The results are than converted to a noise hemisphere as shown in Figure D. Figure C and D are example noise contours which are given to make clear what the observer locations are. For clarity, the shielding contour plots are projected on a two-dimensional plane in plot A and B. In case A, where the engines are un-shielded, the sound pressure levels are higher. When the engines are shielded by the fuselage, as is the case for Figure 1.1 B, the sound pressure level is lower. This is the case because the fuselage blocks the noise coming from the engine.

To be able to (re)design an aircraft configuration for optimum noise shielding, a noise shielding assessment tool is needed. This tool must have the capabilities to predict the noise created by existing and new concept aircraft configurations. With assessing the amount of sound attenuation due to shielding, one can assess which aircraft configuration will result in the least amount of noise pollution. The main goal of this thesis project is to develop a fast prediction tool to asses where noise shielding is effective such that it can be used in the design loop.

1.1. Prior Work

One of the most basic methods to assess noise shielding is the barrier shielding method. The barrier shielding method predicts the noise shielding of screens as is explained in section 2.1. This method basically provides the shielding amount of a screen for each location after the screen. This method is based on empirical results and is designed to obtain the noise shielding of rigid barrier screens [2–4]. The wing shielding of the NASA Aircraft Noise Prediction program is based on the barrier shielding method [5].

NASA has also started the Environmentally Responsible Aviation Project. The aim of this project is to develop technology to reduce the produced aircraft noise with 42 [dB], the NOx emission with 75 [%] and the fuel burn with 50 [%] compared to conventional aircraft, before 2020. These requirements are called the N+2 requirements [6]. A key element to reach the N+2 requirements is the hybrid wing body aircraft noise shielding. Therefore, aircraft noise shielding needs to be assessed. In [6], this is done with the Kirchhoff theory of diffraction. The Kirchhoff diffraction theory is a high frequency diffraction approximation of a spherical sound source diffracting through an aperture as is explained in section 2.2.

Noise shielding calculation methods tend to be computationally expensive. To reduce the computational cost, NASA has developed the fast scattering code [7–9]. The fast scattering code basically speeds up the calculations done for the equivalent source method. The equivalent source method makes use of fictive sources to represent the shielding object. This is explained in section 2.6.

The Cambridge-MIT institute funded a project called ”The Silent Aircraft Airframe” [10]. In this project, the boundary element method is used for low frequency noise shielding in [10] and the ray tracing method is used in [11]. The boundary element method and the ray tracing method are explained in section 2.3 and section 2.4 respectively. These two methods are complex and have a high computational cost. The ray tracing method is also used by DLR to create a tool for the noise assessment of different aircraft configurations [12]. In [10], ray tracing is used to asses the acoustic shielding of a hybrid wing body aircraft. It was shown that the ray tracing shielding results compared well with experimental results.

Currently, there are different noise shielding prediction tools available. The available prediction tools lack in aspects of computational time and or accuracy. Therefore, a noise shielding prediction program that can give a good indication of the noise attenuation at low computational costs has been developed in this thesis project. It is important for the assessment tool that the computational time is low while keeping a sufficient amount of accuracy such that it can be used in the design loop. Since noise shielding becomes more significant for high frequencies, the method should perform well in the high frequency region.

1.2. Project Build up

Firstly it is important to look at the different available noise shielding calculation methods. In chapter 2, the barrier shielding method, the Kirchhoff theory of diffraction, the boundary element method, the fast multipole method and the ray tracing method are briefly discussed which leads to a trade-off. In conclusion of this trade-off it has been decided to use a combination of two separate methods. The barrier shielding method for the wings and the analytic solution of a cylinder for the fuselage.

The barrier shielding method is computationally fast, but less accurate for round shapes. This inaccuracy is overcome by using the analytic solution of a cylinder for the fuselage. The latter is done in order to take the so-called creeping rays into account. These are sound rays that partially follow the contour of the shielding object. The separate noise shielding calculation methods are discussed in detail in chapter 3 and chapter 4.

Next, these methods are combined in chapter 5. To the best of the authors knowledge, this has not been done before. Since the method to determine the noise shielding is determined, a noise shielding prediction tool needs to be created. In chapter 6, the implementation of the method into the noise shielding assessment tool is discussed. The noise shielding prediction tool is then validated against the Kirchhoff theory of diffraction in chapter 7.

Finally, it is concluded that the noise shielding prediction program gives a good indication of the noise shielding at low computational cost in chapter 9. Recommendations towards future work are also stated in chapter 9.

2

Noise Shielding Calculation Methods

In this chapter, the different methods to model aircraft noise shielding will be discussed. After the analysis of the different methods, a trade-off is made. The noise shielding modeling method that is chosen in the trade-off will be used in the noise shielding model. The noise shielding modeling methods to be discussed are:

- The barrier shielding method
- The Kirchhoff theory of diffraction
- The boundary element method
- The fast multipole method
- The ray tracing method
- The equivalent source method
- The combination of the barrier shielding method with analytic solution of a cylinder

To be able to make this trade-off in section 2.7, each method will be discussed in its own respective section. The advantages and disadvantages are listed and a short explanation on how they work is given.

2.1. Barrier Shielding Method

The diffraction of the sound by a half finite barrier can be assessed with the barrier shielding method. Maekawa [2, 3] has measured the sound pressure levels at many points in the shadow zone for different geometries, frequencies and locations. The shadow zone is the region where the direct sound ray cannot penetrate.
An important parameter for determining the shielding is the Fresnel Number. This parameter is denoted by N in Equation 2.1 [3, 4].

$$N = \frac{2}{\lambda}\delta$$
$$\begin{cases} N < 0 & \text{Observer in bright zone} \\ N > 0 & \text{Observer in geometrical shadow zone} \end{cases} \tag{2.1}$$

With λ the wavelength of sound. δ is the path difference from the source to the observer with and without the screen as shown in Figure 2.1.

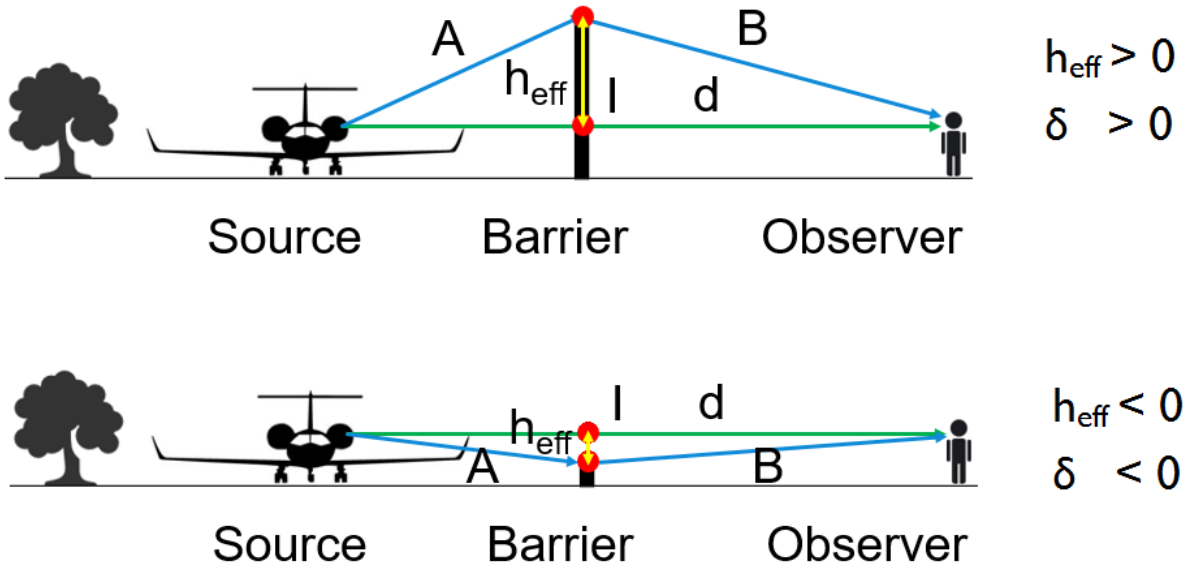

Figure 2.1: Schematic view of the path difference $\delta = \pm(|A| + |B| - |d|)$. Where d is the direct sound ray, A and B the diffracted sound ray, I the intersection point of the direct sound ray with the barrier. h_{eff} is the effective height of the barrier.

The Fresnel number shown in Equation 2.1 changes sign because of the way the path length difference is defined. The path length difference is defined positive if the effective height of the barrier is positive and negative if the effective height is negative. This is shown in Figure 2.1. The effective height is defined negative if the barrier is lower than the line of sight.

The path difference is applicable to different geometries other than screens as can be seen in Figure 2.2.

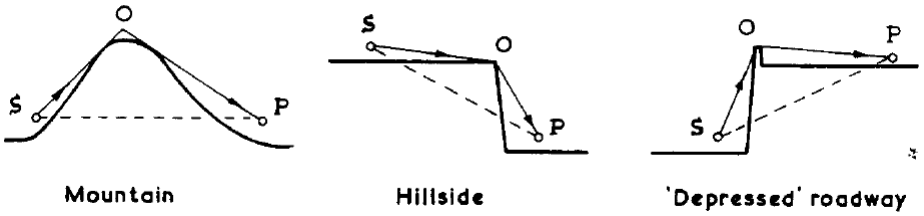

Figure 2.2: Examples of different barriers for which δ holds. S is the source, P the observer [3]

In the barrier shielding method, it is assumed that the diffracting edge is a knife edge, i.e. very thin barrier. When the thickness of the screen is smaller than the wavelength, this assumption is valid [2]. For the analysis of the wing, this is assumed to be the case.

Maekawa has plotted the experimentally obtained sound attenuation against the Fresnel number denoted in Equation 2.1. The results are fitted by the straight line in Figure 2.3.

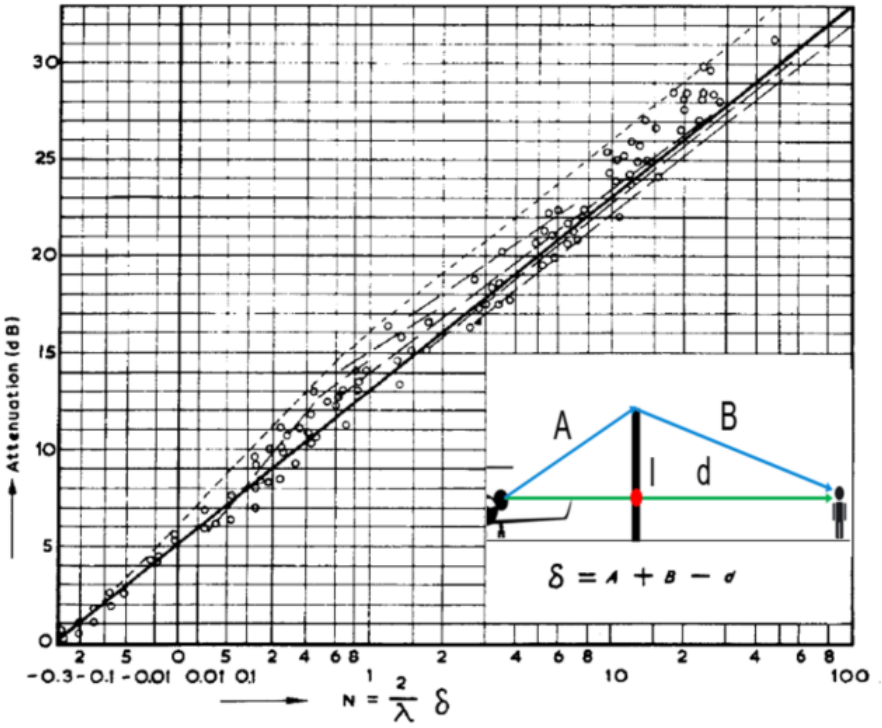

Figure 2.3: Attenuation of sound by a semi-infinite screen versus Fresnel zone number N [3].

Equation 2.2 provides the expression corresponding to the fit [4, 5].

$$A_{tt}(f_i) = \begin{cases} 20\log\frac{\sqrt{2\pi N}}{\tanh\sqrt{2\pi N}} + 5.0 & \text{for } N \geq 0 \\ 20\log\frac{\sqrt{2\pi|N|}}{\tan\sqrt{2\pi|N|}} + 5.0 & \text{for } -0.2 \leq N < 0 \\ 0 & \text{for } N < -0.2 \end{cases} \tag{2.2}$$

This means that once the Fresnel number is known, the sound attenuation of a barrier can be calculated. The advantage of the barrier shielding method is that it is computationally inexpensive [13]. However, it can only be used for sharp edge diffraction from planar shielding objects. It has to be noted that ground reflection is not taken into account. This is done to focus on the shielding effects and it is assumed that the distance to the ground is sufficient enough to neglect ground reflection.

2.2. Kirchhoff Theory off Diffraction

The Kirchhoff diffraction method is used to solve a contour integral. The contour is taken around the line separating the illuminated side from the shadow side of the shielding object. Once this separating line is known, the shielding object can be treated as a screen with an aperture. Babinet's principle states that the sum of the diffracted pressures of the screen with an aperture and a screen with the form of the aperture result in the incident field, i.e. the scattering of two complementary shapes create the incident field as shown in Figure 2.4.

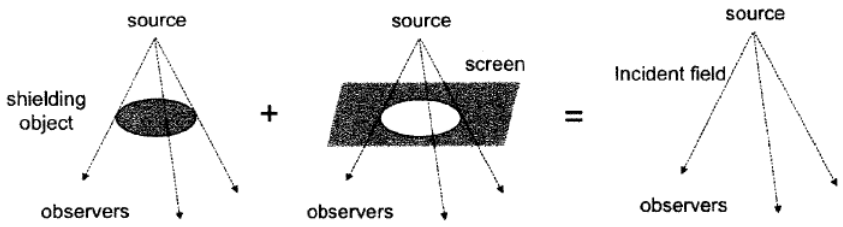

Figure 2.4: Sketch of Babinet's Principle [13]

This means that if one subtracts the acoustic pressure from the noise screen with the aperture from the incident sound pressure, the resulting pressure will be that of the shielding object. [6, 14]. This is shown in Equation 2.3.

$$p_{sc,O} = p_{inc} - p_{sc,S_{ap}} \tag{2.3}$$

Here, $p_{sc,O}$ is the acoustic pressure scattered by the obstacle. $p_{sc,S_{ap}}$ is the acoustic pressure scattered by aperture. p_{inc} is the un-scattered acoustic pressure of the free-field obtained by $\frac{e^{ikd}}{d}$, where k is the wave number and d the distance between the source and receiver. It is clear that the edge of the aperture has to be chosen to lie on the border of the shielding object.
The noise attenuation can then be determined by:

$$A_{tt} = -20 \log \left| \frac{p_{inc} + p_{sc,O}}{p_{inc}} \right| \tag{2.4}$$

Where $(p_{inc} + p_{sc,O})$ is the total acoustic pressure with the scattering object present and p_{inc} is the incident acoustic pressure without scattering. The Kirchhoff diffraction theory is in fact a high frequency diffraction approximation of a spherical sound wave diffracting through an aperture as sketched in Figure 2.5.

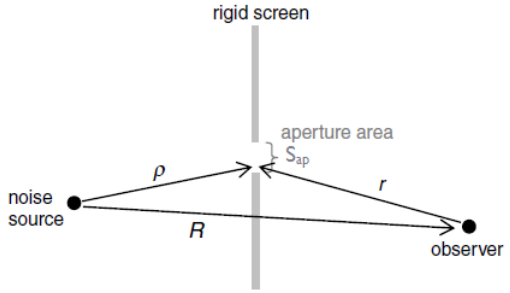

Figure 2.5: Sketch of the geometry used to derive the Kirchhoff diffraction integral [6]

The Kirchhoff diffraction integral is given in Equation 2.5 [14].

$$p_{sc,S_{ap}}\left(\vec{d}\right) = \frac{1}{4\pi} \int \int_{S_{ap}} \left[\frac{e^{ikB}}{B} \frac{\partial}{\partial n} \left(\frac{e^{ikA}}{A} \right) - \frac{e^{ikA}}{A} \frac{\partial}{\partial n} \left(\frac{e^{ikB}}{B} \right) \right] dS \tag{2.5}$$

Where the scattered field through the aperture at d is represented by $p_{sc,S_{ap}}\left(\vec{d}\right)$. $\vec{d}$ is the vector from the source to the observer location. S_{ap} is the control surface as shown in Figure 2.5, n is the direction normal to the control surface. A is the distance from the noise source to the aperture and B is the distance from the observer as shown in Figure 2.5. k is the wave number and dS indicates a surface integral.

Equation 2.5 is obtained by applying the following assumptions to the Green's theorem solution of the Helmholtz equation. The surface acoustic pressure on the back side of the shielding screen is assumed to be zero. The acoustic pressure in the aperture region can assumed to be the free field [6, 14].

The surface integral of Equation 2.5 is transformed into a contour integral to reduce computational costs. This reduces computational costs since the contour integral can be solved by one-dimensional numerical integration. The transformation obtained with the Maggi-Rubinowicz transformation is shown in Equation 2.6. [6, 14, 15]

$$p_{sc,S_{ap}}\left(\vec{d}\right) = \frac{1}{4\pi}\oint_{\partial S_{ap}} \frac{e^{ikA}}{A}\frac{e^{ikB}}{B}\frac{\left(\vec{A}\times\vec{B}\right)\cdot d\vec{s}}{AB+\vec{A}\cdot\vec{B}} + \chi\frac{e^{ikd}}{d} \tag{2.6}$$

The integration contour ∂S_{ap} is defined by the edge of the aperture. The variable χ is 1 if the integration contour ∂S_{ap} is enclosed by $\vec{d}$ and 0 otherwise. A is the distance from the noise source to the aperture and B is the distance from the observer as shown in Figure 2.5. $\vec{A}$ is the vector from the noise source to the aperture and $\vec{B}$ the vector from the observer to the aperture.

The assumptions made to derive the Kirchhoff diffraction integral imply that this method does capture the edge diffracted rays, but not the creeping rays (see Figure 2.9) [6]. This implies that this method is not accurate for smooth objects. In addition, this method is only developed for monopole sources [6].

This method can be used as long as the border of the shielding geometry is defined. It is faster than the boundary element method and still accurate at high frequencies. It can also solve more complex geometries than the barrier shielding method, which is only useful for rectangular shields [6].

2.3. Boundary Element Method

The boundary element method is used in the shielding prediction tool BEMPAR, developed by DLR [16]. It is more accurate than the barrier shielding method, Kirchhoff theory of diffraction and ray tracing method at any source frequency [13], however it gets more computationally demanding as the frequency increases [10].

In the boundary element method, a finite element method discretization is applied to a boundary integral equation of a certain problem [17]. This boundary integral equation consists of two integrals. The first integral equation is defined on the boundary of the domain of interest. The second integral relates this boundary solution to the solution at points in the domain [18]. This build up is called a boundary integral equation. The boundary of the problem is discretized instead of the whole field of interest as is the case for the finite element method [19]. For scattering models, this means that the equation governing the infinite domain is reduced to an equation over the finite boundary [18]. This makes it possible to calculate complex shielding geometries.

The aim of the boundary element method is to substitute the partial differential equation of the domain by an equation that only embodies the boundary [18]. For example, an integral of the form shown in Equation 2.7 can be used instead of the Laplace equation $\nabla^2\varphi(p) = 0$ for the domain D bounded by surface S as shown in Figure 2.6 [18].

$$\int_S \frac{\partial G\,(P,Q)}{\partial n_Q}\varphi\,(Q)\,dS_Q + \frac{1}{2}\varphi\,(Q) = \int_S G(P,Q)\frac{\partial\varphi}{\partial n_Q}dS_Q \tag{2.7}$$

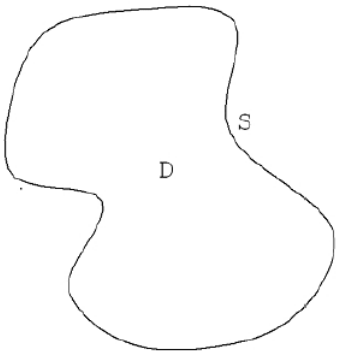

Figure 2.6: Schematic view of the domain D and boundary S [18].

The acoustic potential is represented by φ. The $e^{i\omega t}$ time dependence convention has been used, with ω the angular frequency. dS_Q indicates that the surface integral is executed with respect to the variable Q. The integrand is dependent on both variables P and Q. However the integration completed is fixed in relation to P.

It has to be noted that Equation 2.7 relates the potential and its derivatives only with respect to the boundary. Equation 2.7 is used to determine the unknown boundary functions from the given boundary data [17, 18].

The Green's function $G(P,Q)$ represents the effect of point location P of a unit source at the point Q and $\frac{\partial}{\partial n_Q}$ is the partial derivative with respect to the unit outward normal at the point Q on the boundary. The Green's function, denoted as G, for two and three dimensions are given in Equation 2.8 and Equation 2.9 respectively [17, 20].

$$G(P,Q) = -\frac{1}{4i}\left(H_0^1(kd)\right) \quad P,Q \in \mathbb{R}^2 \tag{2.8}$$

$$G(P,Q) = -\frac{e^{ikd}}{4\pi d} \quad P,Q \in \mathbb{R}^3 \tag{2.9}$$

Here, $d = \| P - Q \|$, k is the wave number and $i = \sqrt{-1}$. H_0^1 is the Hankel function of the first kind and order zero.

To be able to solve the integral Equation 2.7 numerically, the boundary of the problem is divided in a set of panels or straight lines for the two dimensional case as shown in Figure 2.7. Now, the boundary functions can be represented by a characteristic form in each panel. This makes it possible to make a linear system of equations from the boundary integral equations [18].

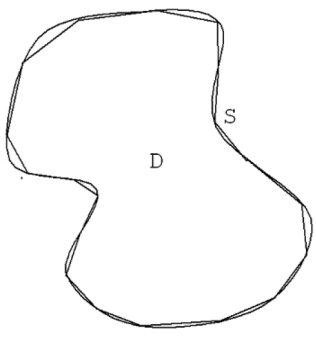

Figure 2.7: Schematic view of the descritization of the boundary S of the domain D [18].

Numerical solvers are available based on the boundary element method for the Helmholtz and the Laplace equation. The acoustic potential can be calculated with the Helmholtz equation and the acoustic pressure field with the Laplace equation independently [10].

The boundary element method is capable of dealing with complex sources [21]. This technique permits the precise evaluation of the diffracted pressure field by barriers [20]. Since the matrix size depends on the size of the shielding object, the computation can become expensive [13].
The representation of the Helmholtz equation by an integral over the outer boundary can also be solved with equivalent sources [13]. The boundary edges are then represented by a set of equivalent sources. This reduces the boundary integral to a numerical solvable set of linear equations. This will be discussed in section 2.6.

From the boundary element method, the fast multipole method is created. It is developed to lower the computational time of the standard boundary element method [22]. This is done by accelerating the matrix vector products arising from the Helmholtz and Laplace BEM equations [23]. However, this is out of the scope of this project.

2.4. Ray Tracing Method

In the ray tracing method each sound ray of interest is traced. Only the ray that reaches the receiver has to be further processed. The field of acoustic rays only needs to be calculated once for multiple frequencies, so there is no penalty for higher frequencies. The ray tracing method is not memory intensive and is amenable to a parallel implementation. It also provides visualization for sound rays at any location [11, 24] and it is accurate for scattering problems [13].

Complex sound sources are difficult to handle [21]. Therefore, ray tracing is generally used for monopole noise sources. On top of that, since the path of each ray has to be evaluated, ray tracing is computationally expensive [13]. However, only the rays of interest have to be evaluated.
This method is used by DLR to create a tool for the noise assessment of aircraft configurations [12]. In [10], ray tracing is used to asses the acoustic shielding of a hybrid wing body aircraft. It was found that the ray tracing results compared well with experiments. The sound rays are divided into a direct field, a sharp edge diffracted field and a creeping field as discussed in the following paragraphs.

2.4.1. Direct Field

When the velocity is zero and the medium is homogeneous, the individual sound rays are straight lines. Consider an arbitrary ray field as depicted in Figure 2.8, where the sound rays propagate in two perpendicular planes with different caustic locations. The caustic is the location to which all the sound rays are tangent.

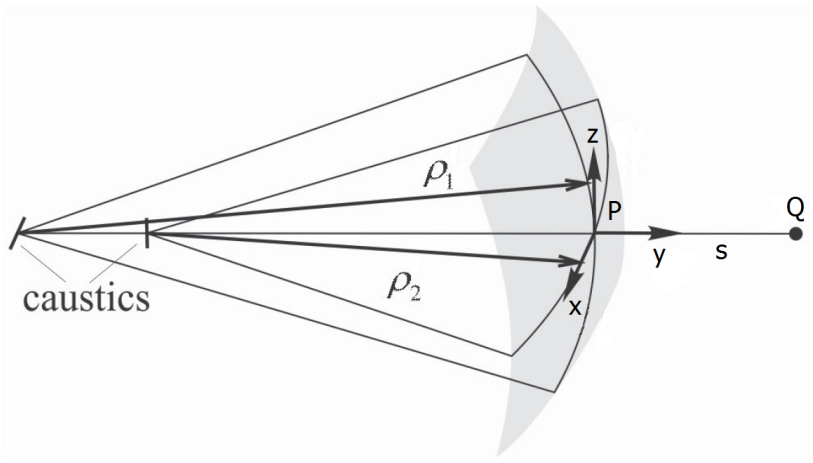

Figure 2.8: Sketch of the incident ray field and the principle radii ρ_1 and ρ_2. P is the reference point and Q the point of interest. s is the distance between P and Q [25].

The area ratio of the wavefront sections is then denoted by Equation 2.10 [26].

$$\frac{\rho_1 \rho_2}{(\rho_1 + s)(\rho_2 + s)} \tag{2.10}$$

Where ρ_1 and ρ_2 are the principle radii of curvature of the wave front of a tube of rays through the point P. If the sound pressure field at P is known, the sound pressure field at the observer location Q can be determined. This field is denoted by $p(Q)$ in Equation 2.11 [11].

$$p\,(Q) = p\,(P)\left[\frac{\rho_1 \rho_2}{(\rho_1 + s)\,(\rho_2 + s)}\right]^{1/2} e^{-iks} \tag{2.11}$$

The time dependence is $e^{i\omega t}$ and the wave number $k = \frac{\omega}{c}$. The distance the ray travels between P and Q is denoted by s. $p(P)$ is the total sound pressure field at point P. P is a point along the sound ray where the pressure field needs to be known. In most cases, this will be the location of the sound source.

If s is large and the principle radii of curvature are finite, the sound pressure field decreases with $\frac{1}{s}$. This represents a spherical wave. If one of the radii of curvature is infinite one gets a cylindrical wave. If both radii are infinite the plane wave is obtained.

2.4.2. Sharp Edge-Diffracted Field

On the edges of the barrier, multiple diffractions can occur. Such as creeping rays for round edges and edge diffracted rays for sharp edges. This can be seen in Figure 2.9. According to [10], if the wavelength is large compared to the radius of curvature of the edge then the edge will behave as a sharp edge.

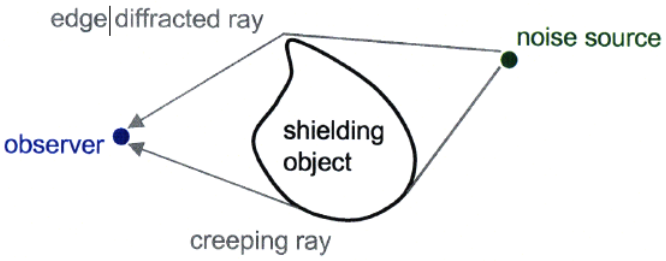

Figure 2.9: Sketch of edge diffraction versus creeping ray [27]

Fermat's principle of edge diffraction states that the edge diffracted ray path from a source at P towards the point of interest Q has a stationary length of the path from P to Q. i.e. the ray will follow the path that takes the least amount of time. As a consequence for a homogeneous medium, the incident and diffracted rays make equal angles with the edge at the diffraction point Q_e, denoted by θ_0 in Figure 2.10, and lie on opposite sides of the plane normal to the edge [11]. This results in a cone of possible diffracted rays shown in Figure 2.10 [11].

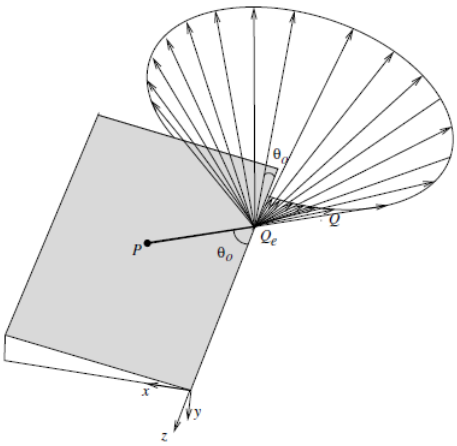

Figure 2.10: Sketch of sharp edge diffraction into a cone of rays with Q_e the diffraction point, θ_0 angle between sound ray and edge, P is the source location and Q the point of interest [11].

One defines the radius of cuvrature ρ as the distance between the point on the edge Q_e and the caustic as shown in Figure 2.11.

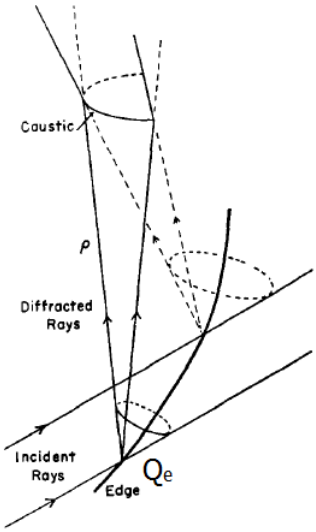

Figure 2.11: Sketch of two incident rays hitting a thin curved edge and the diffracted rays. The two diffracted ray cones intersect at the caustic. ρ is the distance between this caustic and the edge at the diffraction point Q_e. [26].

According to [11], the analytic solution of an edge diffracted field of a point source can then be given by Equation 2.12.

$$p\left(P\right) = p_{inc}\left(Q_e\right) D \sqrt{\frac{\rho}{s\left(s+\rho\right)}} e^{-iks} \tag{2.12}$$

Where Q_e is the diffraction point as shown in Figure 2.10, $p_{inc}\left(Q_e\right)$ is the incident field at Q_e, ρ is the principal radius as shown in Figure 2.11 and Q is the location where the ray attaches or leaves the object. The length s is the distance between the diffraction point Q_e and the observation point. D is the diffraction coefficient obtained from Equation 2.13 [11, 26, 28].

$$D = -\frac{e^{i\pi/4}}{2\sin\beta\sqrt{2\pi k}} \cdot \left[\sec\frac{\theta-\alpha}{2} \pm \csc\frac{\theta+\alpha}{2}\right] \tag{2.13}$$

The diffraction coefficient is dependent on the geometry of the edge and the wave number. The angle α is the angle between the incident sound ray and the normal to the shielding object. θ is defined as the angle between the diffracted sound ray and the normal to the shielding object. These angles are shown in Figure 3.5. β is the angle between the diffracting edge and the incident ray [26].

2.4.3. Creeping Field

The determination of creeping rays is more difficult than that of the sharp edge diffrated rays. The creeping ray strikes and leaves the surface at tangent points. Illustrated by points Q_1 and Q_2 respectively in Figure 2.12. Therefore, first of all, the shadow line of a set of sampling points has to be found i.e. $|PQ_1|$. The shadow line is a locus of tangent points from the source to the curved surface. For each sample point on the shadow line, the geodesic curve is traced and crossed over the ray between different surfaces when needed. This is represented by t in Figure 2.12. Finally, the surface is exited at the receiver shadow line $|Q_2Q|$ [11].

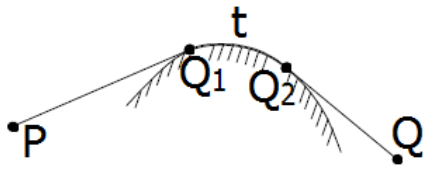

Figure 2.12: Sketch of a creeping ray with source point P receiver Q, geodesic curve t. Sound ray strikes the object at $Q1$ and leaves the object at $Q2$ [11]

The creeping ray field is given by Equation 2.14 obtained from [11].

$$p\,(Q) = p_{inc}\,(Q_1)\,T\,(Q_1, Q_2)\sqrt{\frac{\rho}{s\,(s+\rho)}}e^{-iks} \tag{2.14}$$

The radius of curvature ρ of the diffracted wave front is defined is shown in Figure 2.13.

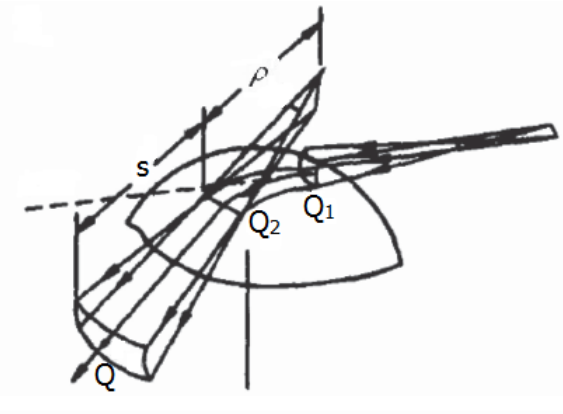

Figure 2.13: Sketch of the creeping ray paths with receiver Q Sound ray strikes the object at $Q1$ and leaves the object at $Q2$, ρ is the radius of curvature of the diffracted wave front, s is the distance between Q_2 and Q [25].

In Equation 2.14, $T(Q_1, Q_2)$ is a transfer function that relates the diffracted field at Q_2 to the incident field at Q_1. The transfer function is shown in Equation 2.15 [11].

$$T\,(Q_1, Q_2) = \sum_m D_m\,(Q_1)\left[e^{\left(ikt - \int_0^t \alpha_m(\tau)d\tau\right)}\sqrt{\frac{d\sigma\,(Q_1)}{d\sigma\,(Q_2)}}\right]D_m\,(Q_2) \tag{2.15}$$

Here, $D_m\,(Q_1)$ and $D_m\,(Q_2)$ are the diffraction coefficients at Q_1 and Q_2 respectively . The diffraction coefficient depends on the wave number k and the local geometry. The geodesic length is given by t

as can be seen in Figure 2.12. The decay coefficient is given by α_m. This coefficient depends on the frequency and on the local surface properties. It can be seen from Equation 2.15 that the creeping ray reduces exponentially with creeping length. This is the case because a creeping ray continuously sheds rays as it travels along the surface. The attenuation of the creeping ray field caused by the divergence of two proximate creeping rays from the attachment point Q_1 to the exit point Q_2 is represented by $\sqrt{\frac{d\sigma(Q_1)}{d\sigma(Q_2)}}$ where $d\sigma$ indicates the cross sectional area of the wave front. In the special case of a cylindrical field, the nearby rays would not diverge and the ratio would be unity [11].

2.5. Barrier Shielding Method and Analytic Solution Combined

In this section, the barrier shielding method and analytic solutions are combined. This is to make the shielding computations less complex and faster. However, when the barrier shielding method as described in section 2.1 is used solely, it is considered not to be accurate enough for doing the analysis of the fuselage. This is the case because it only uses edge diffracted rays and performs less accurately for complex shapes. The ray tracing method, as discussed in section 2.4, becomes complex and computationally demanding once round shapes such as the fuselage are involved. Therefore, in this thesis, the barrier shielding method is combined with the analytic solution of the sound pressure field around a cylinder. This is explained in this section. To the best of the authors knowledge, this has not been done before.

2.5.1. Barrier Shielding Method for the Aircraft Wing

First, the noise shielding by the aircraft wing is discussed. The wing of an aircraft can be modeled by a barrier. The diffraction of the sound by this type of barrier can be assessed with the barrier shielding method, as discussed in section 2.1. Some modifications need to be applied to the barrier shielding method so it can be used on a wing. Reflection of the sound on the ground is neglected. As the wing is finite, three edge refraction barriers need to be considered. This method is based on the shielding method developed for the NASA ANOPP program [5, 29, 30] and is also used by [31].

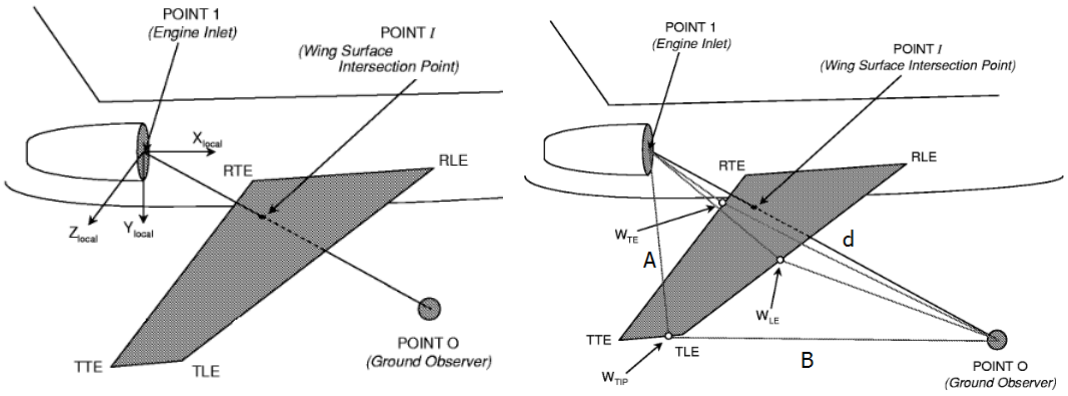

Figure 2.14: Sketch of the wing conventions used for the wing. On the left the intersection point of the direct sound ray, on the right the diffraction distances are shown [29].

First the intersection point with the wing needs to be determined. Then the points on the wing edges that are the closest to this intersection point need to be defined, as shown on the left in Figure 2.14. To be able to determine the Fresnel number, the difference in path length between the direct and diffracted sound rays must be known. This means that for each wing edge, the distance from the source to the closest point on the wing edge $W_{TE,LE,TIP}$ to the intersection point needs to be known. The distances from $W_{TE,LE,TIP}$ to the observer also needs to be determined. The diffracted sound rays

to the close points $W_{TE,LE,TIP}$ are shown on the right in Figure 2.14. When the diffracted sound rays are known, the path differences can be calculated. This is done for the wing tip edge as following:

$$\delta = \pm(|A| + |B| - |d|) \tag{2.16}$$

Where,

$$\begin{cases} \delta > 0 : \text{Intersection point on wing surface} \\ \delta = 0 : \text{Intersection point on boundary edge} \\ \delta < 0 : \text{Intersection point not on wing surface i.e, no attenuation of the noise source.} \end{cases}$$

The sign of the path length difference is defined as the sign of the effective height of the barrier as shown in Figure 2.1. The lengths A, B and d are defined in Figure 2.14.
The equation of the Fresnel Number is repeated here for clarity [32]:

$$N = \frac{2\delta}{\lambda} = \frac{2\delta f_i}{c_\infty} \tag{2.17}$$

where f_i is the frequency of interest, c_∞ is the speed of sound and λ the wave length. From the Fresnel number, the sound attenuation can be calculated for all edges with the frequency of interest as shown in Equation 2.18 [4, 29, 31].

$$A_{tt_j}(f_i) = \begin{cases} 20\log\frac{\sqrt{2\pi N}}{\tanh\sqrt{2\pi N}} + 5.0 & \text{for } N \geq 0 \\ 20\log\frac{\sqrt{2\pi|N|}}{\tan\sqrt{2\pi|N|}} + 5.0 & \text{for } -0.2 \leq N < 0 \\ 0 & \text{for } N < -0.2 \end{cases} \tag{2.18}$$

The attenuation of all the edges at a certain frequency can be combined with the aid of Equation 2.19.

$$A_{tt_{tot}} = -10\log\sum 10^{(-A_{tt_j}/10)} \tag{2.19}$$

Where $A_{tt_{tot}}$ is the total attenuation of sound. j is the leading edge, trailing edge and tip of the wing. Summing the edge attenuation in this manner, makes the barrier shielding method valid for finite barriers.

2.5.2. Analytic Solution Fuselage

Next, the shielding by the aircraft fuselage is discussed. To be able to solve the noise shielding of the fuselage analytically, the fuselage will be approximated by a long acoustic hard walled cylinder [33, 34]. Modeling exact shapes with simple geometrical objects is common practice in noise calculations [35, 36].

The total sound around the cylinder is the sum of the incident and scattered sound. The incident sound is the sound that would be generated if the cylinder was not present. The scattered sound is the noise radiated from the body caused by the incident field, i.e. due to reflecting and diffracting waves from the surface of interest [13, 37–39].

The incident sound pressure field caused by the plane waves traveling normal to the surface of the cylinder with the assumption that the source is at a infinite distance is given by Equation 2.20 [37, 39–41].

$$p_{inc}(r_P, k, \phi) = p(d)\sum_{m=0}^{\infty}\epsilon_m i^m cos(m\phi)J_m(k \cdot r_P) \tag{2.20}$$

where $p(d)$ is the incident sound pressure amplitude. k is the wavenumber and J_m is the Bessel function of the first kind and order m. The conventions used for the fuselage are shown in Figure 2.15 where d is the distance between the sound source and the observer, r is the distance between the

source and cylinder center and r_P the distance between the cylinder center and observer. Note that Equation 2.20 is the expression of plane waves undisturbed by the cylinder written in terms of cylindrical waves [41, 42]. This will be explained in chapter 4.

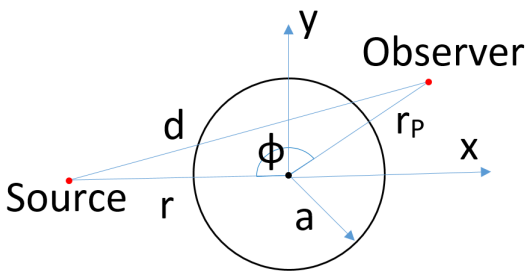

Figure 2.15: Sketch of the conventions used for the fuselage

Now, the distortion of the sound waves due to the cylinder need to be taken into account. Since the boundary is assumed to be hard, the scattered field can be simulated as a source where all the waves travel away from the cylinder's surface [37]. Here, each element of the cylinder is assumed to scatter like a circular cylinder. For the sound scattering, the circular cylinder cross section is assumed to be perpendicular to the radiation direction and behaves as it is in two dimensions [13].
According to [37, 40, 41], the pressure of the scatter field caused by a cylinder can be described by Equation 2.21.

$$p_{sc}(r_P, k, \phi) = -p(d) \sum_{m=0}^{\infty} \epsilon_m i^{m+1} e^{-i\gamma_m} \sin\gamma_m \cos(m\phi) H_m(k \cdot r_P) \tag{2.21}$$

The geometric conventions used are shown in Figure 2.15. Where H_m is the Hankel function of the first kind and order m. The Hankel function is a combination of the Bessel function of the first kind denoted by J_m and second kind denoted by Y_m, see Equation 2.22.

$$H_m = J_m + iY_m \tag{2.22}$$

Using Hankel's transform, an exact solution can be found for the scattered field of the cylinder. The boundary conditions applied to the cylinder are that there is continuous pressure and continuous radial velocity on the cylinder boundary [36, 43].

The incident pressure field obtained with Equation 2.20 is only valid for a source located at infinity producing plane waves. Because the engines are located close to the fuselage and are represented by point sources, the equations need to be modified such that they hold for a point source located close to the cylinder.

As stated before, a point source is used in the aircraft model. The free space Green's function shown in Equation 2.23 describes the radiation of a point source in an unbounded medium [37, 44].

$$G(d) = -\frac{e^{ikd}}{4\pi d} \tag{2.23}$$

An expression based on Equation 2.23 that describes the sound pressure produced by a point source in the far field $(kd >> 1)$ dependent on the distance between the point source and the observation point location is given in Equation 2.24 [45].

$$p(d) = -i\omega\rho_0 Q_s \frac{e^{ikd}}{d} \tag{2.24}$$

Where k is the wave number, ω the radial frequency, ρ_0 the air density Q_s is the complex source strength amplitude [45]. One can substitute Equation 2.24 into Equation 2.20 and Equation 2.21 to

obtain the incident and scattered sound pressure field of a finite distance point source.

Now, the acoustic pressure outside the cylinder can be represented by the summation of the incident and scattered field [38], as shown in Equation 2.25.

$$p_{tot} = p_{inc} + p_{sc} \tag{2.25}$$

The sum of the scattered and incident field can be rearranged into a scattering coefficient. This is the coefficient of how much the cylinder scatters. This coefficient is given by C_s in Equation 2.26 obtained from [36].

$$C_s = \left| \frac{p_{inc} + p_{sc}}{p_{inc}} \right| \tag{2.26}$$

The scattering coefficient is the division of the pressure field with the cylinder present $(p_{inc} + p_{sc})$ over the sound pressure without the shielding cylinder present (p_{inc}). This causes the scattering coefficient to be smaller than one if acoustic noise shielding does occur.

The scattering coefficient can be determined for different cylinders and observer locations, from which a look up table can be made. From here, the scattering coefficient can be easily looked up from the table, without the need to calculate the scattering and induced field every time. This reduces the computational cost of the simulation [36]. The total pressure field can then be obtained from Equation 2.27.

$$p_{tot} = C_s \cdot p_{inc} \tag{2.27}$$

From the scattering coefficient, the sound attenuation due to the cylinder can be obtained. This is done with Equation 2.28.

$$A_{tt} = -20 \log_{10}(C_s) \quad [dB] \tag{2.28}$$

Finally, to be able to calculate the noise shielding capabilities of the entire aircraft, the fuselage and the wings need to be combined. This means that both theories, discussed above, for the wings and fuselage need to be combined. For the wing, the amount of shielding is calculated with the barrier shielding method and for the fuselage the analytic solution of a cylinder is used. Further research needs to be done in this thesis project to be able to combine these two methods. Combining these two methods has not been done before.

2.6. Equivalent Source Method

For the equivalent source method, the boundary value problem from the boundary element method is replaced with different sources that are put inside the scattering object of interest. This allows the source to be monopole or multipole [13]. The strength of the sources is adjusted to satisfy the boundary conditions.

The main advantage of the equivalent source method compared to the boundary element method is that the linear system of equations is smaller, which results in a lower computation time [46]. However, at high frequencies, the equivalent source method's system of equations can become impractical [13]. Also, when the number of sources is higher than the number of prescribed boundary data, the equivalent source method is slower than the boundary element method [47].

The optimal position and number of the equivalent sources is difficult to find and requires experience [47]. The determination of the sources is computationally challenging and there is little theory available to evaluate the type, location and number of equivalent sources [7]. Taking this into account, the boundary element method tends to be more accurate than the equivalent source method [47].

To decrease the computational time of the equivalent source method, NASA developed the Fast Scattering Code (FSC). This code is developed to be able to predict the three-dimensional scattered acoustic field produced by the interaction of known incident sound with aerostructures [7].
The fast scattering code is created as a tool for analyzing the effects of changes in configurations and operating conditions on noise radiation and scattering [8]. However, when bodies are located close to each other, the code gets less accurate [9].

To be able to find a solution for a three-dimensional boundary problem, the fast scattering code makes use of the equivalent source method. This is done by expanding the scattered acoustic pressure into a series of point source monopoles or dipoles. Those point sources are located inside the scattering object on an imaginary source surface [48]. These source surfaces are discretized, as well as the scattering surfaces.

On each equivalent source point and collocation point on the scattering surface, the acoustic boundary is evaluated, creating complex matrix equations. The matrix equations are solved using the lower upper decomposition. Finally, the acoustic field is obtained by evaluating the equivalent source distribution at the desired locations[7].

2.7. Trade-off

In this section a trade-off is made. The different noise shielding methods as formerly discussed and their findings are summarized in Table 2.1. The capability of the methods is illustrated with three '+' symbols if the result is very good and three '-' symbols if it performs bad on that particular category.

The first category of interest is the computational cost. Then, the accuracy of the results, as well as the dimensions and type of sources the method can cope with are discussed. It has to be kept in mind that the directionallity of the sources can be approximated by applying a weighting factor to a monopole source. The category "Shielding Object" is the capability of the method to cope with complex noise shielding object shapes. The last category is complexity. With this, it is implied the build up of the method. The easier it is to apply the method, the more points it gets. From this trade-off table shown in Table 2.1, a final choice is made on which method will be used during the thesis project.

	Comp. Cost	Accuracy	Dimensions	Source	Shielding Object	Complexity
Barrier Shielding method	+++	- - -	2D	Monopole	- - -	+++
Kirchhoff	++	- - -	3D	Monopole	- -	++
BEM	- -	+	3D	Monopole/Dipole	+++	- - -
Ray Tracing	+	+++	3D	Monopole	+++	-
ESM	-	+	3D	Multipoles	++	- - -
Barrier shielding and analytic	+++	- -	3D	Monopole	-	+

Table 2.1: Trade-off between the assessed noise shielding calculation methods

The barrier shielding method is the simplest method that is discussed here. However, it can solve for plane screen problems only. Therefore, it will not be used for the noise shielding model. The Kirchhoff diffraction method can solve more complex shapes. However, because of the assumptions made for the derivation of the Kirchhoff diffraction integral, only sharp edge diffracted rays can be computed. As an aircraft consist mostly of round shapes, it is expected that there will be a lot of creeping rays. As a consequence, the Kirchhoff diffraction method is considered not accurate enough and received three "-" symbols for accuracy in Table 2.1.

The boundary element method is considered more accurate than the ray tracing method and around the same accuracy as the equivalent source method as can be seen in Table 2.1. The BEM is able to solve for complex shielding geometries. Only the boundary of the object of interest has to be discretized. Because the BEM is computationally expensive (compared to the ray tracing method [13]), the fast multipole method is developed. This method accelerates the matrix vector products arising

from the Helmholtz and Laplace BEM equations.

Since the ray tracing method is accurate for shielding problems at low Mach numbers, it is a good method for the noise shielding of more advanced designs. It is less computationally expensive than the BEM and ESM [13]. However, complex sound sources are more difficult to handle. The visualization of the sound rays at every location is also beneficial in assessing the shielding capabilities of an aircraft. Here, only the rays of interest need to be evaluated which is an advantage for the computational cost.

The computational time of the equivalent source method is slightly lower than that of the BEM but higher than the ray tracing method. However, the optimal positions and number of equivalent sources is difficult to find and requires experience. It also falls short on accuracy compared to the BEM as shown in Table 2.1. A fast scattering code is developed by NASA based on the ESM to speed up the calculations. The code tends to be less accurate when bodies are located close to each other. The fast scattering code is considered not accurate enough for close bodies and too complex to implement.

What can be observed from Table 2.1 is that there is a conflict between the accuracy and the solvable degree of complexity of the shielding object on the one side, and the complexity of the method used and its computational time on the other side. This is exactly what is tried to be solved with the combination of the barrier shielding method with the analytic method. The accuracy of this method is thought to be sufficient while its computational cost and complexity to implement is low. If a correct way can be found to combine the barrier shielding method with analytic solutions, a good starting method can be created to asses the influence of different shielding geometries rapidly. Due to its simplicity and reasonable accuracy, the combination of the barrier shielding method with analytic solutions has been chosen as the shielding assessment method for this thesis project.

2.8. Note on Flight Effects

In this thesis project, the flight effects influencing the aircraft noise shielding are not taken into account. This is the reason why the incorporation of flight effects is not a variable in the trade-off. In this section, the expected influence of the flight effects on the noise shielding prediction are discussed.

To determine the influence of the flight effects on the aircraft noise shielding, the shielding of a monopole sound source with a sphere as shown in Figure 2.16 is investigated.

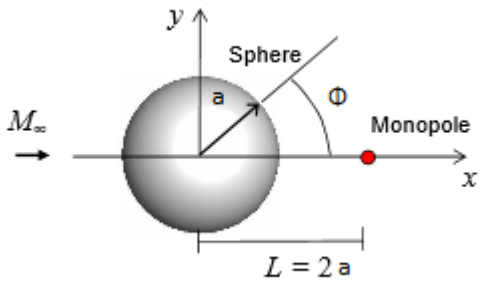

Figure 2.16: Sketch of the geometry used of the monopole source shielded by the cylinder [49].

In [49], polar plots of the total acoustic pressure field around the sphere defined in Figure 2.16 are created. This is done with the use of the boundary element method. Because the source and shielding object are moving, the Mach number is varied from 0 to 0.6. The ka value is varied from 5, 20 and 50. Where k is the wavenumber and a the radius of the sphere. The observer locations are placed on a circle a distance $3a$ around the center of the sphere. The results are shown in Figure 2.17.

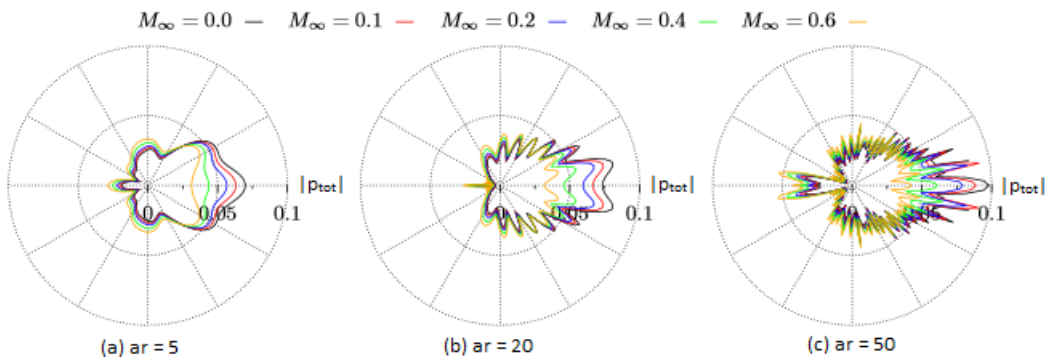

Figure 2.17: Polar plots of the influence of the Mach number on the total pressure field of a monopole shielded by a sphere for ka = 5, 20 and 50 [49].

In Figure 2.17, one can see that the sound emitted aft of the cylinder becomes more compact. There is a small region of upstream amplification which becomes more prominent as the frequency increases. The main effect of the Mach number according to [49, 50] is the compaction of the downstream extent of the noise source. This phenomena will benefit the amount of noise shielding at each frequency. In this thesis project, all calculations are done for static conditions. This results in an underestimation of the shielding effects.

In [51], no significant difference in the shielding results between uniform and non-uniform flow fields are found. However, a small increase in noise shielding in the non-uniform flow can occur due to refraction at the wake of the aircraft. It is concluded in [51] that the wake has a weak effect on the shielding. As a result, the non-uniform flow effects can be neglected in the noise shielding prediction tool created here.

From the results shown in [49–51] it can be concluded that for low-Mach number flows, the differences in acoustic shielding due to the flight effects is negligible. Low-mach numbers occur at approach and take-off conditions. Therefore, only static shielding conditions are looked at in the noise shielding prediction tool created in this thesis project.

3

Application of the Barrier Shielding Method for the Aircraft Wing

To be able to make the trade-off, in subsection 2.5.1, the barrier shielding method applied to the aircraft's wing is described shortly. Since this method is chosen, it is discussed in more detail here. In the barrier shielding method, sound rays are traced to determine the noise shielding. This is also the case for the ray tracing method. Therefore, the barrier shielding method can be considered a simplified ray tracing approach.

The aim of this thesis project is to determine the amount of noise shielding. Therefore, the diffracted sound rays are the ones of interest. A diffracted ray is caused when an incident wave hits edges and corners of an obstacle or grazes a shielding obstacle [28]. Since the medium in which the sound travels is homogeneous and only sharp edge diffraction is considered, the sound rays are assumed to travel along straight lines. Sharp edge diffraction occurs when the wavelength is large compared to the radius of curvature of the edge [10].

The sound source is represented by a point source in a uniform medium. This causes the sound waves to be spherical waves. Note that the transmission of noise through the wing is neglected. This causes the shadow zone of the wing to depend solely on the diffracted sound rays. The barrier shielding method is a semi-empirical method which is based on the Fresnel number as will be explained in the following sections.

3.1. Fresnel Number

Instead of using the Fresnel integral equations to determine the diffracted sound field in the shadow zone of a semi-infinite thin rigid plate, a more practical approach is introduced [52]. The variable used instead is the Fresnel Number as shown in Equation 2.1. This approach is also used by the NASA ANOPP program [29, 53]. The Fresnel number depends on the path length difference which is shown in Equation 3.1.

$$\delta = \pm(|A| + |B| - |d|) \tag{3.1}$$

For the Path Difference denoted by δ, d is the direct sound ray and $(A + B)$ is the shortest path over the edge as shown in Figure 3.1. δ is positive in the shadow zone and negative in the bright zone [4]. The sign of the path length difference is defined as shown in Figure 2.1.

The Fermat's principle states that the sound ray path, is the one that takes the shortest amount of time. This is also the case here. This means that the closest point on the wing edge to the wing intersection point needs to be taken as the diffraction point. This is shown for the trailing edge in Figure 3.1.

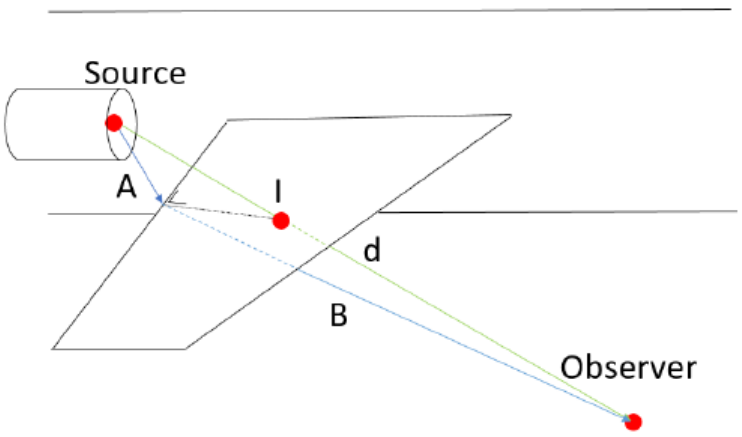

Figure 3.1: Sketch of diffracted sound rays A and B, and the direct sound ray d for the wing's trailing edge

Here, the equivalent diffraction method is used. This means that the points on the wing boundary which are closest to the intersection point are used to calculate the diffraction of that boundary. This means that the diffraction at the intersection point determines the diffraction of the complete boundary.

To be able to define the path difference, first of all the intersection point (x_I, y_I, z_I) with the wing needs to be determined. This is done by solving two so-called two-point form equations of the source (x_1, y_1, z_1) observer (x_0, y_0, z_0) line shown in Equation 3.2 and Equation 3.3 [29].

$$\frac{x_I - x_0}{x_1 - x_0} - \frac{y_I - y_0}{y_1 - y_0} = 0 \tag{3.2}$$

$$\frac{x_I - x_0}{x_1 - x_0} - \frac{z_I - z_0}{z_1 - z_0} = 0 \tag{3.3}$$

Because there are three unknown variables a third equation is needed. This is the so-called three-point form equation for the wing plane denoted by Equation 3.4 [29].

$$\begin{vmatrix} x_I - x_{RLE} & y_I - y_{RLE} & z_I - z_{RLE} \\ x_{RTE} - x_{RLE} & y_{RTE} - y_{RLE} & z_{RTE} - z_{RLE} \\ x_{TLE} - x_{RLE} & y_{TLE} - y_{RLE} & z_{TLE} - z_{RLE} \end{vmatrix} = 0 \tag{3.4}$$

To determine the intersection point in Equation 3.4, only three points are used to describe the wing surface. While the wing itself is defined by four points. This means that for the calculations there is assumed that the wing is in one plane. With location conditions in the prediction tool, it is ensured that the intersection point lies withing the wing edges.

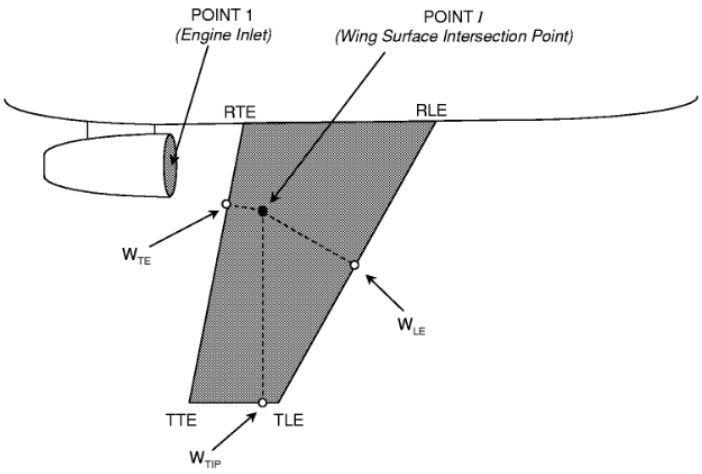

Figure 3.2: Sketch of the points closest to the wing surface intersection point at the trailing edge W_{TE}, leading edge W_{LE} and tip W_{tip} [29].

The points on the wing edges closest to the intersection point are shown in Figure 3.2. These points are obtained by imposing the line from the intersection point (I) to the point on the boundary $(W_{TE}, W_{LE}, W_{TIP})$ to be perpendicular to the wing boundary. This is obtained by setting the dot product of the vector of the line $|IW_{TE,LE,TIP}|$ and the wing boundary equal to zero. This is shown for all the border points in Equation 3.5, 3.6 and 3.7 [29].

$$(x_I - x_{WLE})(x_{RLE} - x_{TLE}) + (y_I - y_{WLE})(y_{RLE} - y_{TLE}) + (z_I - z_{WLE})(z_{RLE} - z_{TLE}) = 0 \tag{3.5}$$

$$(x_I - x_{WTIP})(x_{TTE} - x_{TLE}) + (y_I - y_{WTIP})(y_{TTE} - y_{TLE}) + (z_I - z_{WTIP})(z_{TTE} - z_{TLE}) = 0 \tag{3.6}$$

$$(x_I - x_{WTE})(x_{RTE} - x_{TTE}) + (y_I - y_{WTE})(y_{RTE} - y_{TTE}) + (z_I - z_{WTE})(z_{RTE} - z_{TTE}) = 0 \tag{3.7}$$

There is also imposed that the points $(W_{TE}, W_{LE}, W_{TIP})$ have to lie on the boundary of the wing. This means that the points $(W_{TE}, W_{LE}, W_{TIP})$ have to satisfy the two-point form equation of the wing edge line they are located on. For the leading edge, this gives Equation 3.8 and Equation 3.9 for example.

$$\frac{x_{WLE} - x_{RLE}}{x_{TLE} - x_{RLE}} - \frac{y_{WLE} - y_{RLE}}{y_{TLE} - y_{RLE}} = 0 \tag{3.8}$$

$$\frac{x_{WLE} - x_{RLE}}{x_{TLE} - x_{RLE}} - \frac{z_{WLE} - z_{RLE}}{z_{TLE} - z_{RLE}} = 0 \tag{3.9}$$

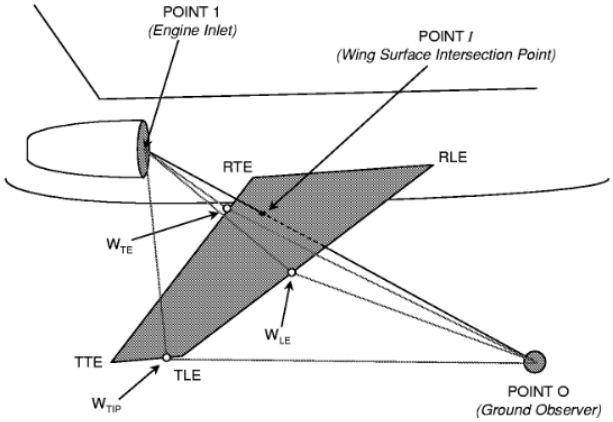

Figure 3.3: Sketch of the direct and diffracted sound rays of the aircraft wing [29]

Now that all the necessary points and corresponding sound rays are known, the Fresnel number can be obtained. The Fresnel number needs to be determined for every diffracting wing edge. The diffraction of a semi-infinite plane can be used for a wing if the wavelength is much smaller than the wing edge length. This is the case because for this condition, the diffraction is governed by local conditions of the edge only [54]. This means that the solution of the wing will become more accurate as the frequency increases. The limiting edge will be the wing tip because this is the shortest edge. However, in the NASA ANOPP approach, the barrier shielding method is modified to hold for finite planes. The finite length limitations will be elaborated more in subsection 3.1.2.

3.1.1. Noise Attenuation in Relation to the Fresnel Number

Now that the method to determine the Fresnel number is known, the relation between the Fresnel number and the amount of noise shielding needs to be derived. To be able to determine the sound attenuation due to a barrier, the sound field with and without the screen needs to be known. To do this, Maekawa has measured the sound pressure level of a thin rigid barrier at multiple points in the shadow zone. This is done for a wide range of frequencies and geometries. A trend line of the attenuation results versus the Fresnel number is shown in Figure 3.4. This line can be used to determine the sound attenuation of a barrier given that the Fresnel number is known. The Fresnel number only depends on the geometry of the barrier [3].

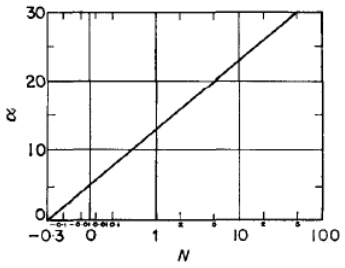

Figure 3.4: Trend line of the experimental results of the sound attenuation (α) by a semi-infinite screen in free space versus the Fresnel number (N) as obtained by Maekawa [52].

Rathe [52] has developed a more practical approach than Maekawa for the case $N \geqslant 0$. A characteristic frequency is derived from the case $N = 0.5$ to describe the geometric situation as shown in Equation 3.10.

$$N = 0.5 = \frac{2\delta}{\lambda} = \frac{2\delta f_c}{c} \Rightarrow f_c = \frac{c}{4\delta} \tag{3.10}$$

The attenuation of each octave step of the center frequency is given in Table 3.1 based on Figure 3.4. Here, only one characteristic center frequency needs to be calculated to obtain the complete frequency range.

Attenuation by an acoustic barrier							
Frequency [Hz]	$< \frac{f_c}{64}$	$\frac{f_c}{64}$	$\frac{f_c}{32}$	$\frac{f_c}{16}$	$\frac{f_c}{8}$	$\frac{f_c}{4}$	$\frac{f_c}{2}$
Attenuation [dB]	5	5	6	6	7	8	9
Frequency [Hz]	f_c	$2f_c$	$4f_c$	$8f_c$	$16f_c$	$32f_c$	$> 32f_c$
Attenuation [dB]	11	13	16	19	22	24	24

Table 3.1: Attenuation by an acoustic barrier for different characteristic frequencies as determined by Rathe [52].

Since a point source is used, the sound waves will be spherical waves. The spherical waves cause the incident waves to be oblique. However, the method used by Rathe is developed for the two-dimensional plane. It is thus assumed that the incident waves are perpendicular to the shielding screen. As a consequence, also the diffracted ray will be perpendicular to the shielding screen. To show that the results of Rathe are applicable to the oblique incident waves, the geometrical theory of diffraction developed by Keller is used [28].

With the geometrical theory of diffraction, an approximate solution of the sound attenuation due to a barrier between source and observer can be derived [4, 28]. This approximation is given in Equation 3.11.

$$\Delta L_k = -20 \log \frac{d}{2 \sin\beta \left(2\pi/\sqrt{\lambda}\right) \sqrt{AB(A+B)}} \left[\sec\frac{\theta-\alpha}{2} \pm \csc\frac{\theta+\alpha}{2}\right] \tag{3.11}$$

ΔL_k indicates the sound attenuation due to a barrier as derived by Keller [26]. The angles in Equation 3.11 are defined as shown in Figure 3.5. The angle α is the angle between the incident sound ray and the normal to the shielding object. θ is defined as the angle between the diffracted sound ray and the normal to the shielding object. β is the angle between the incident sound ray and the edge of the diffracting object. The angle β can be obtained with $(\sin(\beta) = A'/A)$. Here A is the incident sound ray in three-dimensions and A' is the projection of the incident sound ray onto the two-dimensional plane [26].

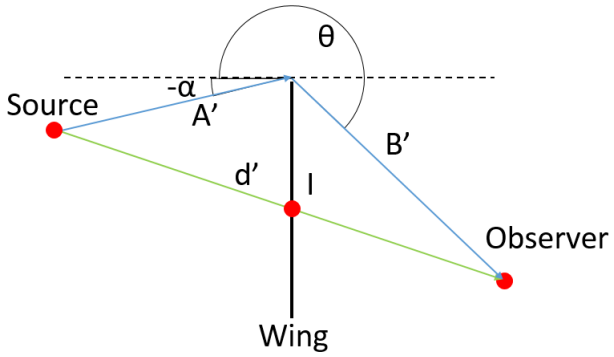

Figure 3.5: Conventions used for the barrier shielding method. The prime symbols means that it is projected from 3D to 2D with A the incident sound ray, B the diffracted sound ray. d the direct sound ray and I the intersection point of the direct sound ray with the barrier.

The negative sign between the brackets in Equation 3.11 applies to the acoustic hard condition ($\frac{\delta p_{tot}}{\delta n} = 0$ at the boundary) and the positive sign to the acoustic soft condition ($p_{tot} = 0$ at the boundary) [28, 54]. For the acoustic hard condition, there is no displacement of the sound wave at the boundary. The polarity of the reflected wave is inverted. When the boundary is assumed soft, there is displacement at the boundary but the net vertical force must be zero. Here, the polarity of the sound wave remains the same. In this thesis project, the acoustic hard condition is used.

The attenuation is dependent on the geometrical spreading of the sound rays and on the diffraction coefficient. The diffraction coefficient shown in Equation 2.13 and used in Equation 3.11 is determined such that Equation 2.12 agrees with the asymptotic expansion of Sommerfeld's exact solution of the diffracted pressure field for large values of kd [26, 28, 55]. The derivation of the diffraction coefficient can be obtained in appendix II of [26].

Seen from Figure 3.5, Equation 3.12 follows.

$$\cos\frac{\theta-\alpha}{2} = \pm\frac{1}{2}\sqrt{\frac{(A'+B')^2 - d'^2}{A'B'}} = \pm\frac{1}{2}\sqrt{\frac{(A+B)^2 - d^2}{AB}} \cdot \frac{1}{\sin\beta} \tag{3.12}$$

Where the minus sign is for the shadow zone and the positive sign for the bright zone [4].
Using Equation 3.12 and introducing the path length difference defined in Equation 3.1, Equation 3.11 can be rewritten to obtain Equation 3.13 [4].

$$\Delta L_k = -20\log\frac{1}{2\pi\sqrt{\delta/\lambda}} - 20\log\frac{d}{A+B} - 20\log\frac{\sqrt{2}}{\sqrt{1+d/(A+B)}} - 20\log\frac{1}{\sqrt{2}}\left(1-\frac{\cos\frac{1}{2}(\theta-\alpha)}{\sin\frac{1}{2}(\theta+\alpha)}\right) \quad (3.13)$$

The first term of Equation 3.13 can be rewritten as shown in Equation 3.14. This equation, is identical to Rathe's data for $N \geqslant 1$ and $N < 8$ [4]. In Rathe's results, the path of the diffracted ray is perpendicular to the barrier's edge [52]. Rathe's results are thus only valid in the two-dimensional projected plane shown in Figure 3.5.

$$\Delta L_r = -20\log\frac{1}{2\pi\sqrt{\delta/\lambda}} = -10\log\frac{\lambda}{4\pi^2\delta} = 10\log\frac{4\pi^2\delta}{\lambda} \quad (3.14)$$

For each frequency in Table 3.1, the attenuation with Equation 3.14 can be obtained. Here, $\lambda = c/f$ and $\delta = 0.5\ [m]$. Both results are compared in Figure 3.6. For $N \geqslant 1$ and $N < 8$ the results are identical as stated in [4]. As $N > 8$, small differences start to occur again. This is the case because the shielding is limited with 24 [dB] in Rathe's data. The results of Rathe are also not valid for path-length differences smaller than half the wavelength [4].

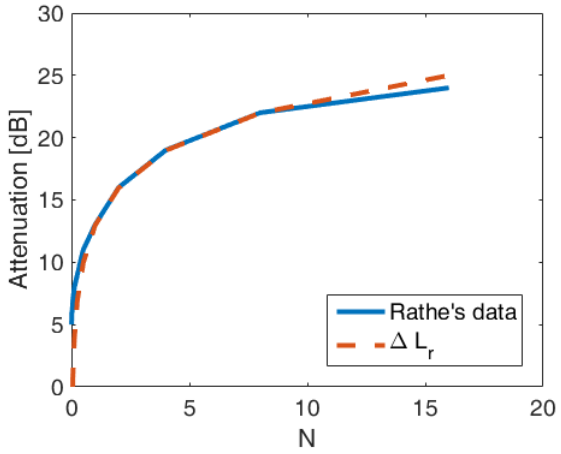

Figure 3.6: Comparison of the attenuation result for different Fresnel numbers N from Rathe's data [52] with the first term of Keller's Formula ΔL_r [4]

Term two, three and four of Equation 3.13 are correction factors. Since Equation 3.13 is obtained by rearranging Equation 3.11, the correction factors are also included implicitly in Equation 3.11.
The second term of Equation 3.13 is a correction factor which accounts for increased spherical divergence of the diffracted rays relative to the direct sound ray [4]. The corrected term is large when both the source and observer are close to the barrier and small if they are far away. This is the case since the larger the distance d, the smaller the effect of the oblique incidence on the length of the sound ray will be.

The third term is the path-length correction term and the fourth term is the angular correction term. Both their magnitudes are shown in Figure 3.8. Their variation is within $\pm 3[dB]$. Despite the correction factors, there is stated in [4] that there is no substantial difference between the results of Rathe and the formula by Keller. This can also be concluded by the scattering in the experimental results of Meakawa. This scattering shown in Figure 3.7 occurs in a range of $\pm 3[dB]$ and can be linked to the third and fourth correction term of Equation 3.13 [4].

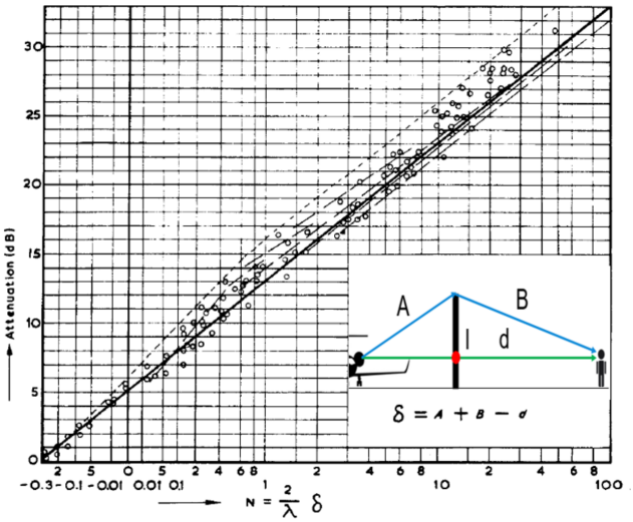

Figure 3.7: Sound attenuation of semi-infinite screen in free space against Fresnel Number N [3].

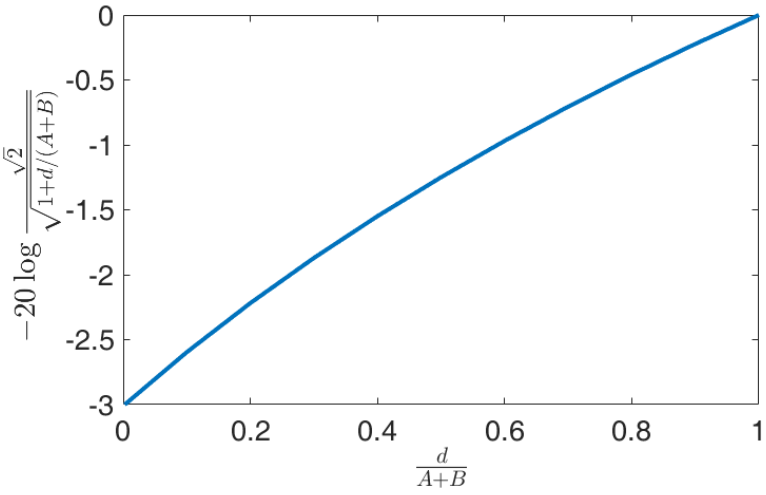

(a) Path-length correction term

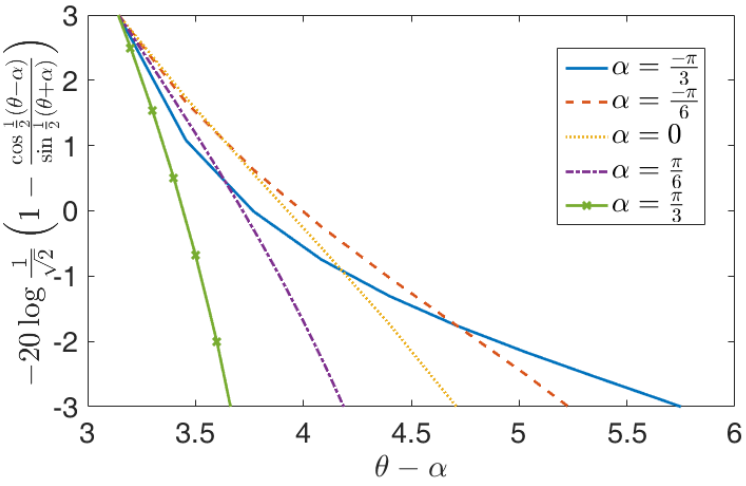

(b) Angular correction term

Figure 3.8: Correction terms of Equation 3.13

However, since the second correction term is large when both the source and receiver are close to the noise barrier, a correction needs to be done to Rathe's results. This means that close to the barrier, Equation 3.14 is no longer valid. From Rathe's data, it can be seen that for $N = 0$, the attenuation must be 5 [dB] [52]. When $N = 0$, the source, wing edge limit and observer are on a straight line. This means, that a correction needs to be applied to Equation 3.14 because it is not valid for Fresnel numbers smaller than unity.

When the Observer is located close to the barrier θ goes to $\frac{3\pi}{2}$ $[rad]$ as shown in Figure 3.9. The correction should then be Equation 3.15 [4].

$$\Delta L_r = 5 + 10 \log \frac{2\pi\delta}{\lambda} \tag{3.15}$$

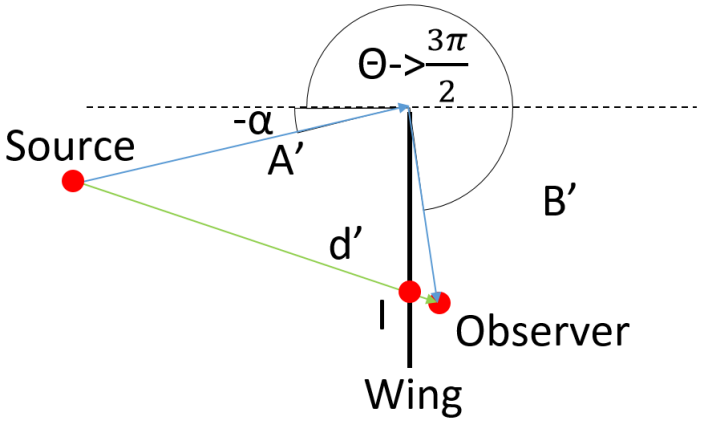

Figure 3.9: Conventions used for the barrier shielding method with $\theta \to \frac{3\pi}{2}$. With the direct sound ray d and diffracted sound rays A and B.

If the barrier height is small as shown in Figure 3.10, the Fresnel number also becomes small. Here, $\theta - \alpha \to \pi$ $[rad]$ holds. The equation then becomes [4]:

$$\Delta L_r = 5 + 10 \log \frac{8\pi\delta}{\lambda} \tag{3.16}$$

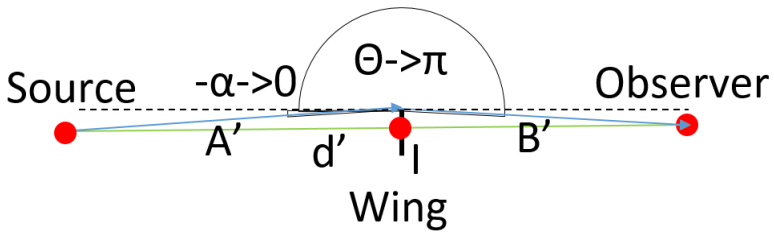

Figure 3.10: Conventions used for the barrier shielding method with $\theta - \alpha \to \pi$ $[rad]$. With the direct sound ray d and diffracted sound rays A and B.

As a result, the correction that needs to be implemented needs to be 0 if $N \geq 1$ and cancels the second term of Equation 3.15 and Equation 3.16 if $N \to 0$. To implement the corrections such that the attenuation holds for both cases, Equation 3.17 is used [4]. As can be seen in Figure 3.11, this equation is consistent with the results of Rathe for $N < 12.5$.

$$\Delta L_a = 5 + 20 \log \frac{\sqrt{2\pi N}}{\tanh \sqrt{2\pi N}} \tag{3.17}$$

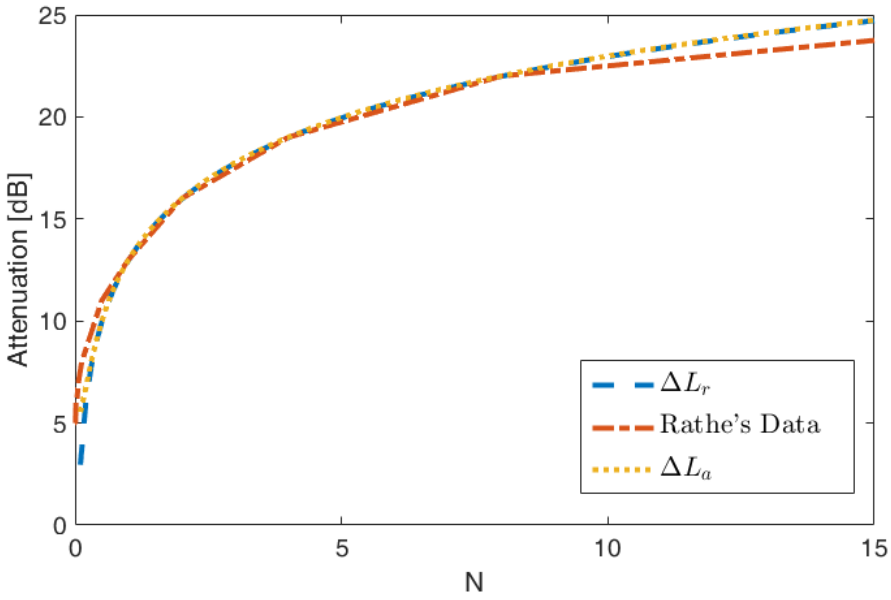

Figure 3.11: Comparison of the attenuation of an acoustic barrier for different Fresnel numbers (N) of Equation 3.14 (ΔL_r), Rathe's data and Equation 3.17 (ΔL_a) [4].

One can conclude that the attenuation is 0 for $N < -0.2$ to incorporate the excess attenuation of sound rays passing slightly above the wing. Finally, the equation used for determining the noise attenuation of the wing is [4, 5, 29]:

$$\Delta L_a = \begin{cases} 20\log\frac{\sqrt{2\pi N}}{\tanh\sqrt{2\pi N}} + 5.0 & \text{for } N \geq 0 \\ 20\log\frac{\sqrt{2\pi|N|}}{\tan\sqrt{2\pi|N|}} + 5.0 & \text{for } -0.2 \leq N < 0 \\ 0 & \text{for } N < -0.2 \end{cases} \tag{3.18}$$

The attenuation of all the wing edges at the frequency of interest needs to be combined with the aid of Equation 3.19. Where j = leading edge, trailing edge and tip of the wing. With this summation, the diffraction around multiple edges is included. This means that the solution holds for finite planes instead of semi-infinite planes. This method is also used for wing shielding by the NASA ANOPP program [29].

$$A_{tt_{tot}} = -10\log\sum 10^{(-A_j/10)} \tag{3.19}$$

3.1.2. Comparison Theories

In this section, the method explained in subsection 3.1.1 will be compared with a theory that makes use of a correction factor for the side edges to determine the Fresnel number based sound attenuation of a finite barrier. The method explained in subsection 3.1.1 will be called the NASA ANOPP method [29]. This is because it has been developed for the NASA Aircraft Noise prediction program.

The method which makes use of correction factor is obtained from [56]. The semi-infinite noise barrier is made finite by implementing a correction based on the Fresnel number from both side edges. The formula for the noise attenuation with the correction factor becomes Equation 3.20 [56].

$$A_{tt} = 20\log\frac{\sqrt{2\pi N}}{\tanh\sqrt{2\pi N}} + 5.0 - 10\log\left(1 + \frac{N}{N_{side1}} + \frac{N}{N_{side2}}\right) \tag{3.20}$$

Where, N is the Fresnel number of the longest edge. N_{side1} and N_{side2} are the Fresnel number of the side edges. This equation is only valid for N, N_{side1} and $N_{side2} > 1$. The correction term of the equation needs to be applied to the attenuation of a semi-infinite barrier if the side edges are

closer than five times the effective height. The effective height of the barrier is the distance from the intersection point of the direct sound ray with the barrier to the top of the shielding barrier [56].

Since this method is developed for a screen with one edge on the ground, it needs to be adjusted for a barrier which is not attached to the ground. This is a better resemblance of the wing. For the comparison of the two theories, a rectangular barrier in free-space is used. Such a shape has two long edges. As a result, Equation 3.20 needs to be calculated for both these edges. When both the long edge attenuation with correction for the side edges are obtained, they need to be summed up. This addition is done with the aid of Equation 3.21 [29].

$$A_{tt,tot} = -10 \log_{10} \left(10^{-A_{tt,1}/10} + 10^{-A_{tt,2}/10} \right) \tag{3.21}$$

To see if the two methods are consistent with each other, the result of the NASA ANOPP method is compared with the correction factor method explained above. The sound attenuation of the different methods is shown in Figure 3.12. As can be seen, the results are in the same order of magnitude. The center region with the highest shielding is longer for the NASA ANOPP approach but the magnitude of shielding is the same. Because this approach is already used for wing shielding by NASA in previous work [29] and the method described in Figure 3.12 is only valid for Fresnel numbers higher than one, the NASA ANOPP approach will be used during this thesis project. Because the two methods give similar results, the adjustment of the barrier shielding method to hold for finite barriers is assumed correct for both methods.

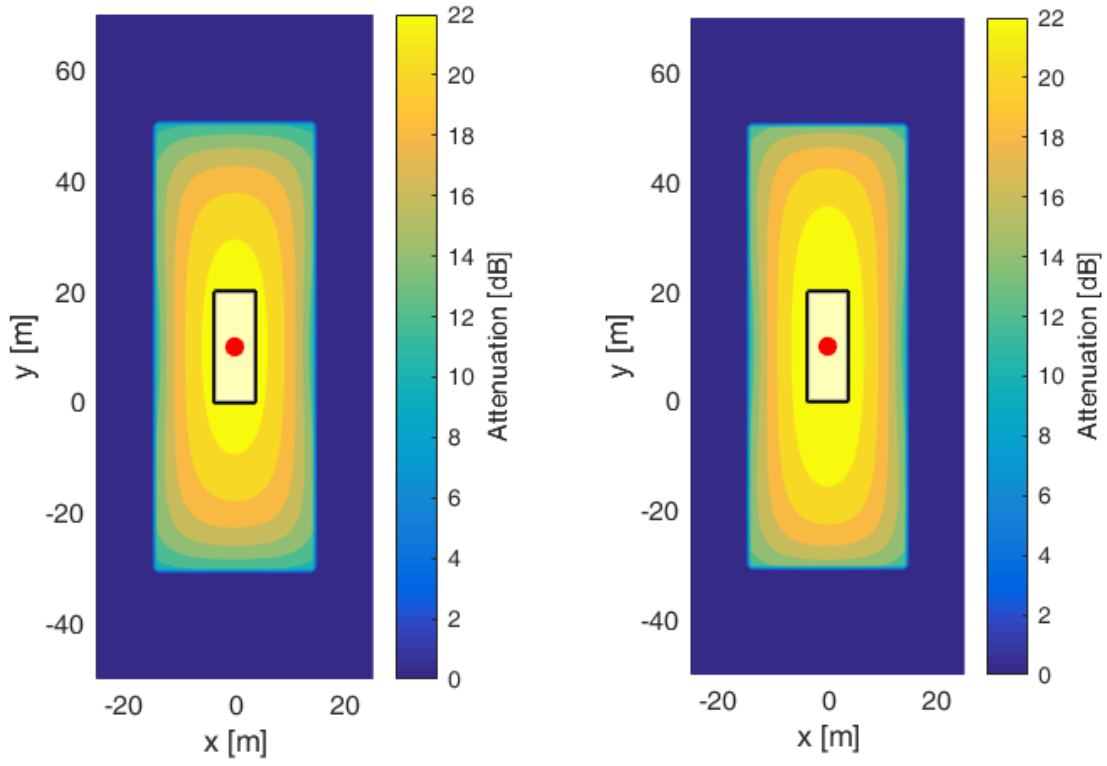

(a) Correction factor

(b) NASA ANOPP method

Figure 3.12: Comparison of the shielding results of a plane screen. On the left, the shielding is calculated with the use of the correction factor for the side edges. On the right, the NASA ANOPP method is used. The parameters used are f=5 kHz, Source located 10 [m] above plane. Height between plane and ground is 30 [m], barrier length 20 [m], barrier width 8 [m].

3.2. Validation

The results of the wing shielding are compared with the results of the NASA Aircraft Noise Prediction Program [5, 29, 30]. This is because the same method for determining the noise shielding by the aircraft wing is used in ANOPPP. Comparing the results is difficult since the exact geometry used in the ANOPP test case is not known. It is known however that a business jet is used for the test case. Therefore, the location of the source and the wing geometry is based on a FALCON 2000 Business jet. It is also known that the observer angle is 48 [deg], this angle is also used in the wing shielding program developed in the thesis research here. For comparison, the attenuation due to the wing is plotted against the frequency. In Figure 3.13, the results of the prediction tool developed in this thesis project and NASA ANOPP program are plotted respectively. The calculation is done for all 1/3 Octave band center frequency levels from 50 to 10 000 [Hz].

It can be seen that there are differences in the results. The higher the frequency, the greater the difference. This difference is probably due to the different geometries. The noise attenuation increases with frequency. This results in a greater difference in attenuation results due to different geometries at high frequencies. The order of magnitude is the same. The largest difference is 3 [dB]. From this and the comparison with the correction factor method, it is concluded that the wing shielding program based on the barrier shielding method gives a good estimation of the wing shielding.

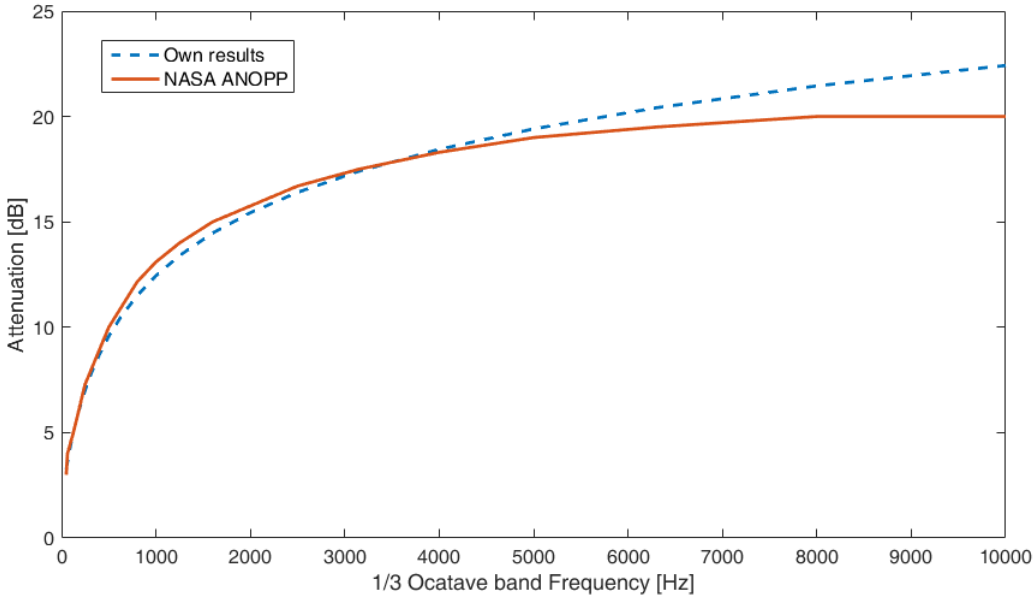

Figure 3.13: Camparision of the frequency versus attenuation of the own results and the NASA ANOPP results

4

Application of the Analytic Solution of a Cylinder

In subsection 2.5.2, the analytic solution of the noise attenuation due to a cylindrical shielding object is briefly discussed. In this chapter, it will be discussed again but further elaborated and applied to the aircraft's fuselage. The analytic solution of the cylinder is used for the fuselage to increase the accuracy of the barrier shielding method. At the same time, the computational cost is kept as low as possible.

Several assumptions have been made to be able to use the analytic solution. The cylinder is assumed to be of infinite length. i.e. diffraction of sound waves at the end of the cylinder are not taken into account. Also, the fuselage is assumed acoustic hard such that all the scattered sound waves travel outward from the cylinder. The fact that the fuselage can be modeled as a cylinder is also an assumption.

Two analytic methods are described here. It is concluded that the first method is insufficient to calculate the noise shielding of a fuselage with an engine modeled as a point source. This is due to the assumption that the source is in the far field. Therefore a second method is looked at in section 4.6. This solution is valid when the source is in the near field. Since the engines are located close to the fuselage, the second method is used in the noise shielding prediction tool developed in this thesis project.

4.1. Incident Field

The total sound pressure field is created by two fields. The incident field and the scattered field. The incident field is the sound pressure caused by the source as if the scattering object is not present. The scattered sound pressure is, in the case of an acoustic hard boundary, the pressure field radiating outward of the shielding object.

Since for the incident field, the cylinder is looked at cross section per cross section, the pressure field is defined in a two-dimensional plane. The acoustic waves of a point source in a two-dimensional plane are represented by plane waves if the source is assumed in the far field. The incident sound pressure equation can thus be expressed by the plane wave equation defined in Equation 4.1 [41].

$$p_{inc} = p(d)e^{-i(\omega t - kx)} \tag{4.1}$$

Where k is the wave number, ω the angular frequency. The geometric dependent variables used are defined in Figure 4.2. In Equation 4.1, the plane waves are defined to travel normal to the fuselage's z-axis and in the direction of the positive x-axis. The time dependent part in Equation 4.1 can be omitted for simplicity. Rewritten in polar coordinates one gets Equation 4.2 [41].

$$p_{inc} = p(d)e^{ik(r_P \cos\phi)} \tag{4.2}$$

Where r_p is the distance to the point of interest in the fuselage two-dimensional section of interest. The azimuth angle is represented by ϕ. The incident waves are sketched in Figure 4.1.

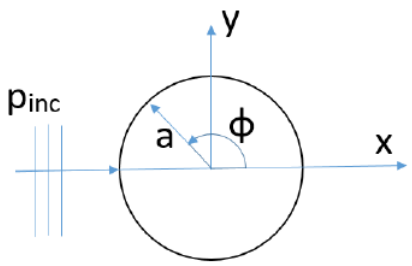

Figure 4.1: Sketch of two-dimensional plane waves normal to the cylinder. Where a is the radius and ϕ the azimuth angle. p_{inc} is the incident pressure field.

Note that the sound pressure due to the plane wave is only dependent on the x-coordinate. However, the results are obtained on a circle located outside the cylinder. The observer location in this circle is described by ϕ and r_P. By geometry $r_p \cos\phi$ is equal to x which is the only variable the plane wave is dependent on. In other words, the plane wave is only dependent on x but the observer location can be varied in the y direction.

Assuming that the incident sound waves are not disturbed due to the presence of the cylinder, the incident plane waves can be expressed in terms of cylindrical waves with Equation 4.3 [41, 42].

$$p_{inc}(r_P, k, \phi) = p(d) \sum_{m=0}^{\infty} \epsilon_m i^m cos(m\phi) J_m(k \cdot r_P) \tag{4.3}$$

Where the factor $\epsilon_m = 1$ if $m = 0$ and 2 otherwise. J_m is the Bessel function of the first kind and of order m. $p(d)$ is the sound pressure amplitude.

Equation 4.3 can be approximated by Equation 4.4.

$$p_{inc}(r_P, k, \phi) = p(d) \sum_{m=0}^{M-1} \epsilon_m i^m cos(m\phi) J_m(k \cdot r_P) \tag{4.4}$$

Where M is the total number of terms needed for the series expansion. It was found that the summation part goes to zero if m increases. M needs to be set in the noise shielding prediction tool such that the division of $\sum^{M-1}$ over $p_{inc,M}$ approaches zero.

Although Equation 4.4 does not account for disturbances by the cylinder, the sound pressure varies with the distance from the cylinder origin to the point of interest (r_P) [41]. The distortion due to the cylinder is taken into account in the scattered field which will be discussed in the next section.

4.2. Scattered Field

The scattered sound pressure field is caused by the reflection of sound waves from the surface of the cylinder. For the scattered sound pressure field, the influence of the cylinder on the sound waves is taken into account. This is done by simulating the fuselage as a cylindrical sound source. Since the surface of the fuselage is assumed acoustic hard, all the sound waves will travel outwards of the cylinder. The scattered sound pressure on the cylinder's boundary surface can be calculated with Equation 4.5 [41].

$$p_{sc}(a, k, \phi) = -p(d) \sum_{m=0}^{M-1} A_m cos(m\phi) H_m(ka) \tag{4.5}$$

Where $p(d)$ is the sound pressure amplitude, a is the radius of the cylinder as shown in Figure 4.1. The wavenumber is depicted by k. H_m is the Hankel function of order m. The Hankel function is a combination of the Bessel function of the first and second kind as shown in Equation 4.6

$$H_m(ka) = J_m(ka) + iN_m(ka) \tag{4.6}$$

The coefficient A_m has to satisfy the hard wall boundary condition which states that the sum of the scattered and incident velocities needs to be zero $(u_{inc} + u_{sc} = 0)$ at the boundary. The expression for A_m is given in Equation 4.7 [41].

$$\begin{cases} A_0 = \epsilon_0 i e^{-i\gamma_0} \sin(\gamma_0) & \text{for } m = 0 \\ A_m = \epsilon_m i^{(m+1)} e^{-i\gamma_m} \sin\gamma_m & \text{for } m > 0 \end{cases} \tag{4.7}$$

The sine term and $e^{-i\gamma_m}$ make sure that the combination of incident and scattered waves is correct. The phase angles γ_m are defined as shown in Equation 4.8 and represent the angle between the incident and scattered wave [41].

$$\begin{cases} \tan(\gamma_0) = -\frac{J_1(ka)}{N_1(ka)} & \text{for } m = 0 \\ \tan(\gamma_m) = -\frac{J_m'(ka)}{N_m'(ka)} & \text{for } m > 0 \end{cases} \tag{4.8}$$

Now, Equation 4.5 needs to be modified such that it holds for the scattered sound pressure field for any distance of interest (r_P). For the noise shielding prediction tool, the sound pressure needs to be known at different observer locations further away than the cylinder's surface. The velocity potential at an arbitrary distance from the cylinder is defined in Equation 4.9 [41].

$$\Psi_{sc,m}(k, \phi) = \epsilon_m i^{m+1} e^{-i\gamma_m} \sin\gamma_m \cos(m\phi) \tag{4.9}$$

To obtain this velocity potential, one has to take the phase angles and direction of the scattered waves from the cylinder into account. Here, the same phase angles as defined in Equation 4.8 are used dependent on the cylinder radius a. $\Psi_{sc,m}$ is also dependent on the wave number k and azimuth angle ϕ [41]. The scattered sound field is then represented by Equation 4.10 derived from Equation 4.7 and Equation 4.9 [41].

$$\begin{aligned} p_{sc}(r_P, k, \phi) &= -p(d) \sum_{m=0}^{M-1} \Psi_{sc,m} H_m(k \cdot r_P) \\ &= -p(d) \sum_{m=0}^{M-1} \epsilon_m i^{m+1} e^{-i\gamma_m} \sin\gamma_m \cos(m\phi) H_m(k \cdot r_P) \end{aligned} \tag{4.10}$$

4.3. Sound Source

In section 4.1 and section 4.2, the sound source was assumed to lie at infinity. In the aircraft model, the sound sources will be located close to the fuselage. Therefore, the previous described incident and scattered field need to be modified to hold for source at finite distances.

To do this, first of all, the sound pressure radiated due to a point source itself needs to be determined. A harmonic point source, with time dependence $e^{i\omega t}$, radiates an acoustic pressure $p(x)$ that satisfies the Helmholtz equation shown in Equation 4.11 [44].

$$\left(\Delta + k^2\right) p(x) = f(x) \quad , k = \frac{\omega}{c} \tag{4.11}$$

where $f(x)$ is a function which describes the physical system the sound waves come from. The variable x is a spatial location of the domain considered.

The Helmholtz equation is based on the principle of energy conservation. The solution of the Helmholtz equation may not be unique. This is caused because it also includes incoming waves which come from infinity and move towards the shielding object. These waves do not exist physically. To exclude these rays, the Sommerfeld's radiation condition is used. The Sommerfeld's radiation conditions is shown in Equation 4.12 [44, 57].

$$\lim_{r_P \to \infty} \left(r_P \left(\frac{\partial p}{\partial_{r_P}} - ikp \right) \right) = 0 \tag{4.12}$$

Sommerfeld's condition makes sure that the energy is radiated away from the scattering object. Here, r_P is the distance between the observation point and the origin of the scattering object. This distance is defined in Figure 4.2.

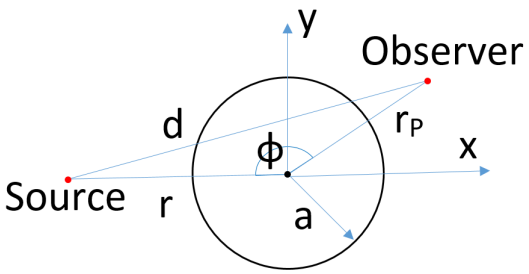

Figure 4.2: Sketch of the conventions used for the fuselage. Where a is the radius, ϕ the azimuth angle.

The free space Green's function is an elementary kernel of the Helmholtz equation and satisfies the Sommerfeld's condition. This means that Equation 4.11 can be rewritten to Equation 4.13 [44, 57].

$$(\Delta + k^2)G = f \tag{4.13}$$

Where G is the Green's function.
The free space Green's function shown in Equation 4.14 describes the radiation of a point source in free-space [37, 44].

$$G(d) = -\frac{e^{ikd}}{4\pi d} \tag{4.14}$$

Where the distance d is defined in Figure 4.2.

The far field $(kd >> 1)$ of an acoustic point source dependent on the distance between the point source and the observation point can be represented by Equation 2.24 based on the Green's function [41, 45]. The formula is repeated in Equation 4.15 for clarity.

$$p(d) = -i\omega\rho_0 Q_s \frac{e^{ikd}}{4\pi d} \tag{4.15}$$

Where k is the wave number, ρ_0 the density of air and the distance d is defined in Figure 4.2. Q_s is the complex source strength amplitude which represents the volume of fluid displaced at the source by the rate [45]:

$$Qe^{i\omega t} = \int\int \vec{u} \cdot \hat{n} dS \tag{4.16}$$

Where $\vec{u}$ represents the velocity on some point on the source's surface. For the analysis of the fuselage noise shielding, the complex source strength amplitude is taken as 1+i $\left[\frac{m^3}{s}\right]$. The magnitude of the source strength is not important because it will be divided out in the end when the attenuation is determined.

4.4. Validation

The theory described above is implemented in a Matlab program. To test if the program works correctly, the results are compared with that of Morshed [37] in Figure 4.3. Morshed [37] has presented the results of an experiment, using a numerical and analytic approach. The analytic approach is described above. As can be seen in Figure 4.3, the results for the analytic solutions are exactly the same. This means that the method is implemented correctly. The results are normalized to the maximum sound pressure level at an azimuth angle of +/-180 [deg]. The variables used are a cylinder radius of 0.057 [m]. The source is placed at an azimuth angle of 180 [deg]. The distance from the source to the face of the cylinder is 4.1 [m]. The difference with the analytic approach and the experiment at f = 700 and 1500 [Hz] originate from the reflection of sound at low frequencies of the test chamber walls [37].

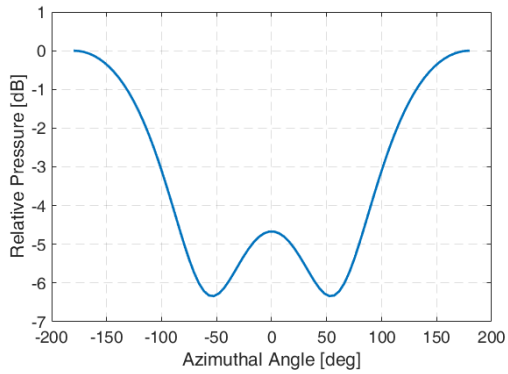

(a) Own Results, f = 700 [Hz], ka = 0.73.

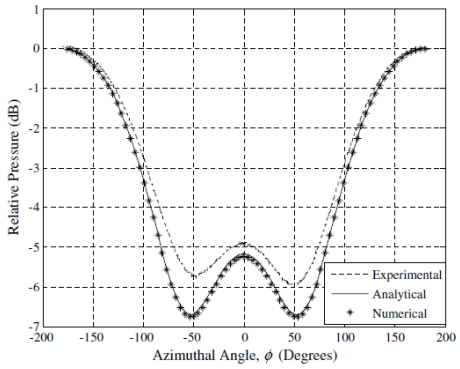

(b) Results of Morshed [37], f = 700 [Hz], ka = 0.73.

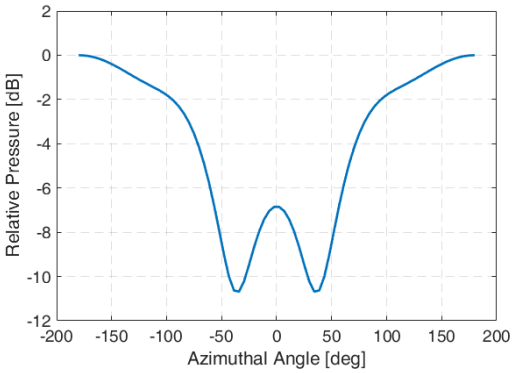

(c) Own Results, f = 1500 [Hz], ka = 1.57.

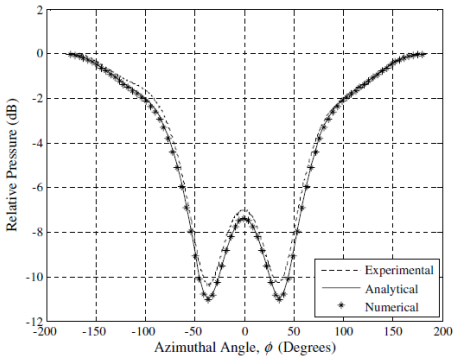

(d) Results of Morshed [37], f = 1500 [Hz], ka = 1.57.

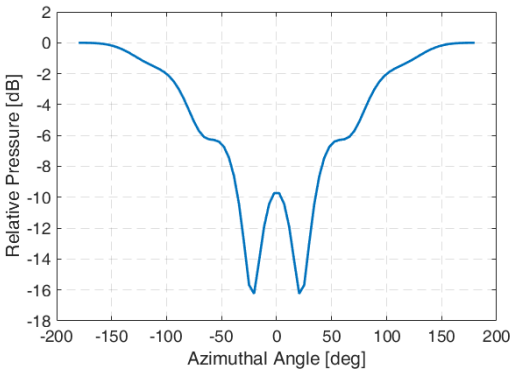

(e) Own Results, f = 3000 [Hz], ka = 3.13.

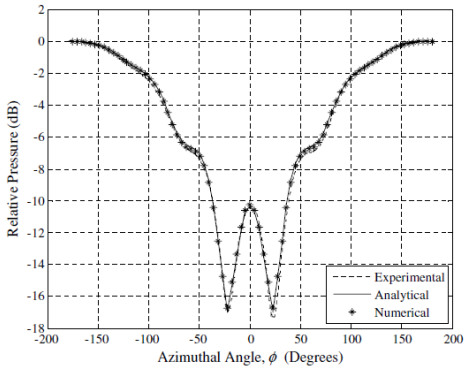

(f) Results of Morshed [37], f = 3000 [Hz], ka = 3.13.

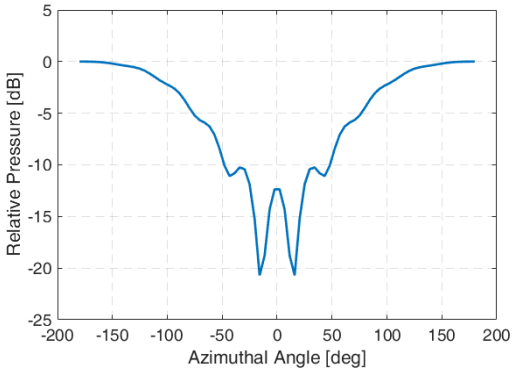

(g) Own Results, f = 5000 [Hz], ka = 5.22.

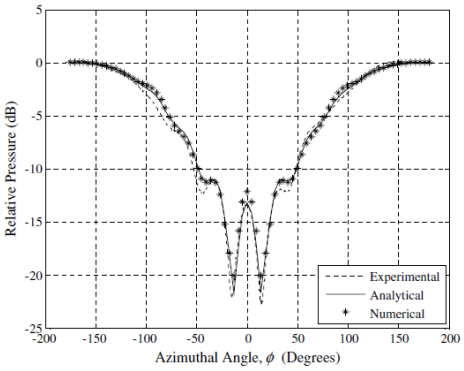

(h) Results of Morshed [37], f = 5000 [Hz], ka = 5.22.

Figure 4.3: Comparison of the own results with the results of Morshed [37]

4.5. Fuselage Noise Shielding

To predict the noise shielding of the fuselage represented by a cylinder with a circular cross section, first of all, the total pressure field needs to be determined. The total pressure field consists of the incident and scattered field. Adding the incident and scattered field together is done with a simple addition. This is shown in Equation 4.17 [13, 38, 39].

$$p_{tot} = p_{inc} + p_{sc} \tag{4.17}$$

Now that the total sound pressure can be determined, the amount of attenuation in [dB] can be obtained with Equation 4.18.

$$SPL_{att} = -20\log_{10}\left|\frac{p_{tot}}{p_{inc}}\right| = -20\log_{10}\left|\frac{p_{inc}+p_{sc}}{p_{inc}}\right| \tag{4.18}$$

To obtain the reduction in sound due to the cylinder, the total acoustic pressure needs to be divided by the pressure without the cylinder present. This is equal to the incident sound pressure.

Since this calculation method is for a finite cylinder, a correction has been implemented for the front and aft of the fuselage. This decreases the shielding region if the source is further away from the fuselage. This correction is based on the line of sight. When the line of sight is not blocked by the fuselage, the attenuation is set to zero. This results in an equivalent cylinder length on the observer plane as is shown in Figure 4.4.

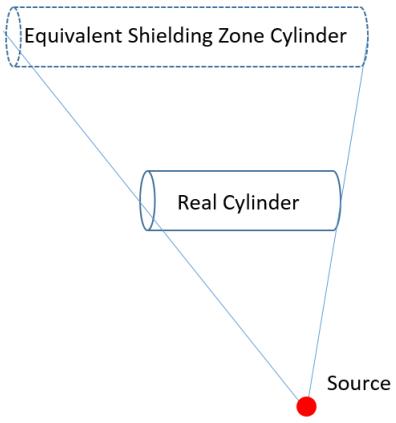

Figure 4.4: Sketch of the line of sight correction to the length of the infinite cylinder

With this method, the diffraction at the front and aft of the fuselage is not taken into account. But, since the engine noise shielding is in scope, it is assumed that the end points of the fuselage will not contribute significantly to the shielding capabilities of the aircraft. As a result, the regions before and behind the fuselage are not of great interest.

As a final note on the cylinder shielding method, the inclined source, i.e. the source is not located at an azimuth angle of 180 [deg] but at any other angle, is looked at. When the source is inclined, the attenuation magnitudes and directivity patterns are exactly the same but rotated the inclined angle around the center of the fuselage [41].

If one substitutes the scattered field and incident field into Equation 4.18 the term $p(d)$ is divided out as can be seen in Equation 4.19.

$$A_{tt} = -20\log_{10}\left|\frac{-\sum_{m=0}^{M-1}\epsilon_m i^{m+1}e^{-i\gamma_m}\sin\gamma_m\cos(m\phi)H_m(k\cdot r_P)+\sum_{m=0}^{M-1}\epsilon_m i^m cos(m\phi)J_m(k\cdot r_P)}{\sum_{m=0}^{M-1}\epsilon_m i^m cos(m\phi)J_m(k\cdot r_P)}\right| \tag{4.19}$$

This means that the attenuation does not depend on the correction of the source at finite distance incorporated in $p(d)$. As a result, the shielding contour does not increase or decrease as the radial distance of the source is varied. This can be seen in Figure 4.5. Clearly, this result can not be valid.

In Figure 4.5, the distance of the source to the fuselage is varied. Here the fuselage diameter is 3.76 [m], the height of the cylinder with respect to the ground plane is 30 [m]. The distance of the cylinder center to the sound source is varied from 5 to 20 [m]. As can be seen on the plots, the distance of the source has no influence on the shielding range and magnitude. It is concluded that the assumption of plane waves is not valid here. Therefore, another method will be used which is discussed in section 4.6.

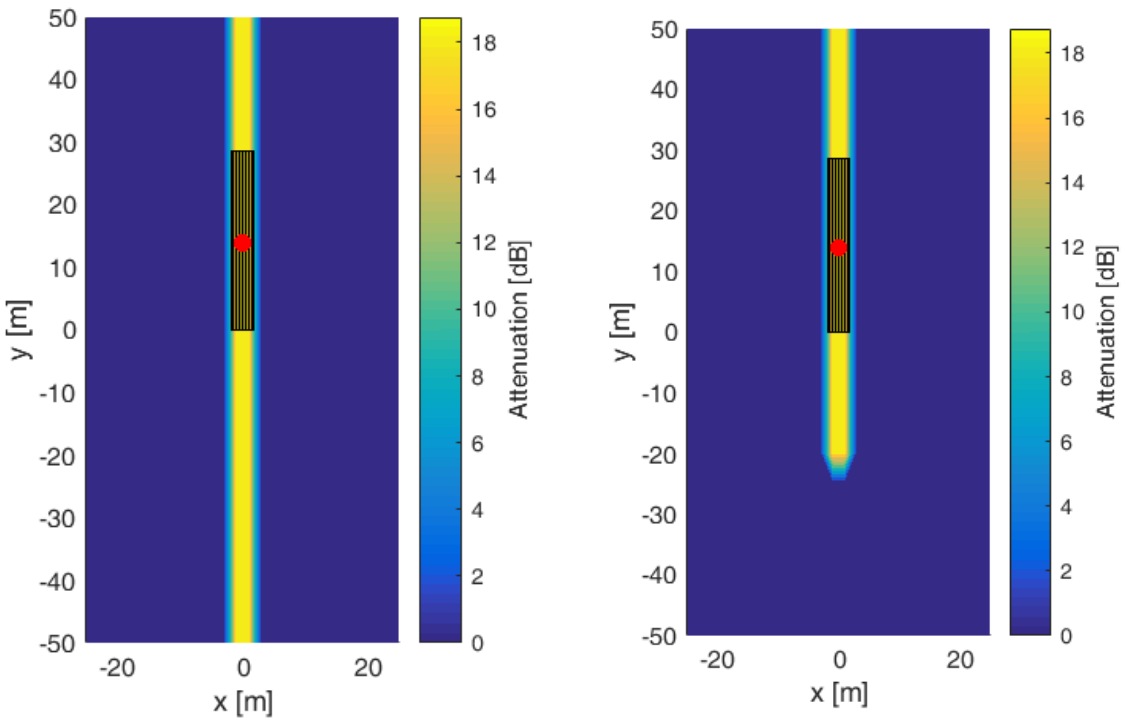

(a) r = 5 [m]

(b) r = 20 [m]

Figure 4.5: Comparison of the change in source distance relative to the cylinder, f = 20 [kHz], a = 1.88 [m], length = 28.65 [m]

4.6. Cylindrical Waves

In this section, the attenuation due to the cylinder with the use of spherical incident waves is discussed. To derive the incident and scattered field, a line source is used. This causes the incident sound waves to be cylindrical in the two-dimensional field. Note that the individual source of a three dimensional line source acts as a point source in two dimensions [36]. Since the length of the cylinder is assumed infinite and the fact that the relative sound pressure difference is sought, the cylinder incident and pressure field are only depended on two dimensional variables and are independent of the source strength. In the previous section, the cylinder's sound attenuation was also only valid on the two dimensional variables.

The cylindrical wave incident field is given by Equation 4.20 [39] and a sketch of the incident field is shown in Figure 4.6. This is the expression for the Greens function for the two-dimensional wave equation and represents the sound pressure of a point source in the two-dimensional plane.

$$p_{inc} = \frac{1}{4i} H_0(k_0 d) \tag{4.20}$$

Where H_0 is the Hankel function of the first kind and order zero. k_0 is the wave number outside the cylinder.

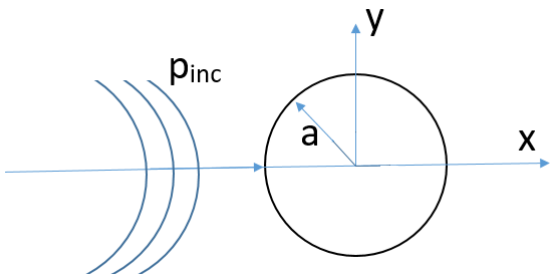

Figure 4.6: Sketch of two-dimensional cylindrical incident waves normal to the cylinder

The scattered field is represented by Equation 4.21 obtained from [36].

$$p_{sc} = A_0 H_0(k_0 r_P) + \sum_{m=1}^{\infty} A_m H_m(k_0 r_P) \cos(m\theta) \tag{4.21}$$

This equation is similar to Equation 4.5. The difference is due to the coefficients A_m and A_0. Here, the coefficients have to satisfy the cylindrical wave conditions. Also note that the term $p(d)$ is no longer needed since no correction has to be made to make it valid for cylindrical waves. The conventions used are defined in Figure 4.2. The used coefficients are given by:

$$A_0 = \frac{iH_0(k_0 r)}{4\Delta_0} \cdot -J_0(k_1 a) J_1(k_0 a) \tag{4.22}$$

$$\Delta_0 = -J_0(k_1 a) H_1(k_0 a) \tag{4.23}$$

$$A_m = \frac{iH_m(k_0 r)}{2\Delta_m} \left(-J_m(k_1 a) \left(J_{m-1}(k_0 a) - J_{m+1}(k_0 a)\right)\right) \tag{4.24}$$

$$\Delta_m = -J_m(k_1 a) \left(H_{n-1}(k_0 a) - H_{n+1}(k_0 a)\right) \tag{4.25}$$

Where the subscript 0 means inside and 1 means outside the cylinder. It has to be noted that the coefficients are the same as in [39], but here the ratio of impedance $\frac{\rho_0 c_0}{\rho_1 c_1}$ is set equal to zero since the fuselage is assumed acoustic hard. By doing this, the scattered field coefficients are simplified to the ones shown above.

4.7. Validation

To be able to see if the theory discussed in section 4.6 is implemented correctly, it is compared with the results of [36]. In Figure 4.7 the shielding coefficient is shown. This coefficient is calculated with the use of Equation 4.26 [36].

$$Cs = \left| \frac{p_{inc} + p_{sc}}{p_{inc}} \right| \tag{4.26}$$

If the shielding coefficient Cs is one, there is no shielding. If it is lower than one, there is acoustic shielding. If it is higher than one, the sound field is amplified due to positive interference of the incident and scattering wave.

In Figure 4.7 the source is located on the right and the cylinder in the center of the figure. The shadow region after the cylinder is created by the fact that the incident and scattered field are out of phase and reduce each other. From the comparison of the results in Figure 4.7, it is concluded that the method is implemented correctly. Any distinct difference are due to the use of different calculation meshes. By using different calculation meshes a difference in accuracy exists. Also, the color scheme of the plot is not exactly identical.

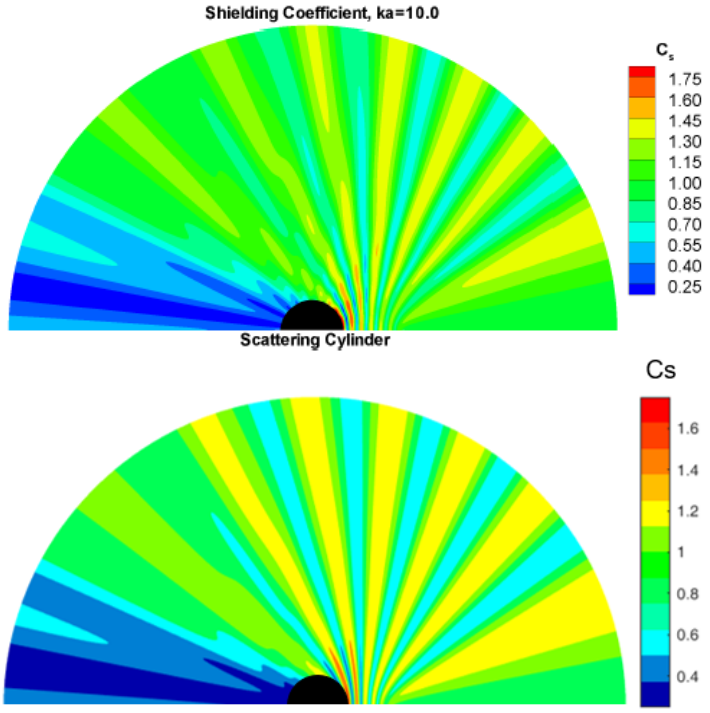

Figure 4.7: Comparison of the Shielding coefficient of the own results on the bottom with the solution of [36] on the top. ka = 10, distance between source and cylinder is 3 times the radius of the cylinder to the right of the cylinder.

In contrast to what one might expect, the highest shielding region is not at the center of the fuselage but occurs just beside the fuselage's center in the shadow region. The higher sound pressure at the center of the shielding region occurs because the sound pressure is reinforced there. A diffracted wave travels around both sides of the cylinder. At the center of the cylinder the two waves can collide and increase the pressure field. This results in a reduction in the shielding coefficient [40].

In Figure 4.8, the influence of moving the source further away from the cylinder is examined. The shielding contour becomes smaller as the source moves further away and the amount of shielding reduces. Because the shielding method behaves as expected, this method is considered valid for the fuselage shielding and will be used in the noise shielding prediction program.

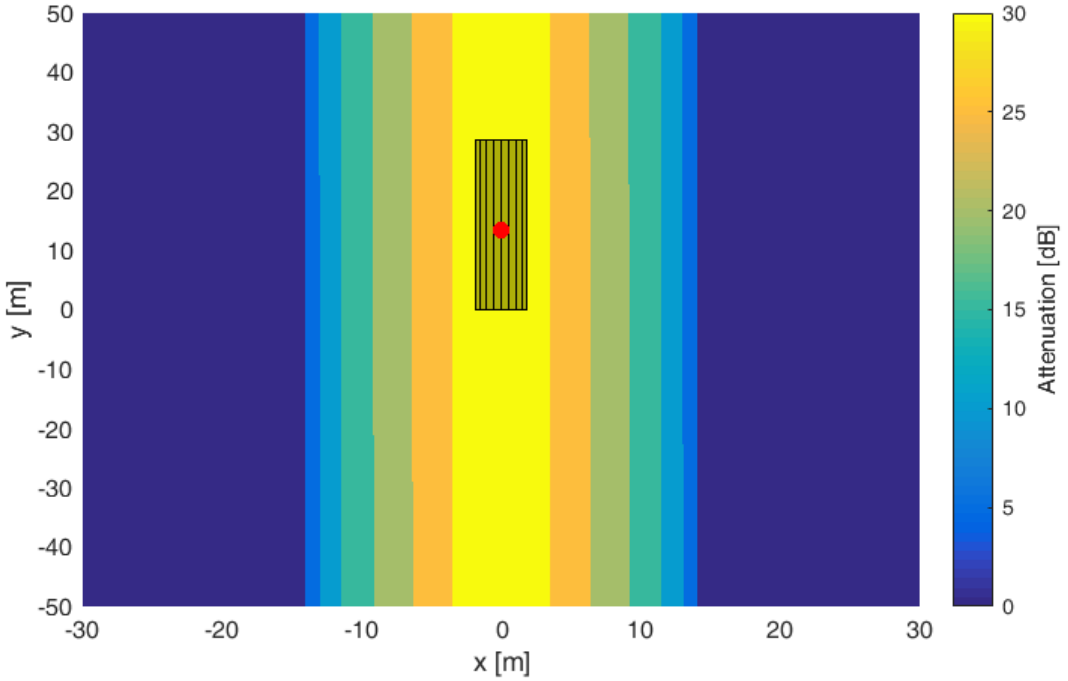

(a) r = 5 [m]

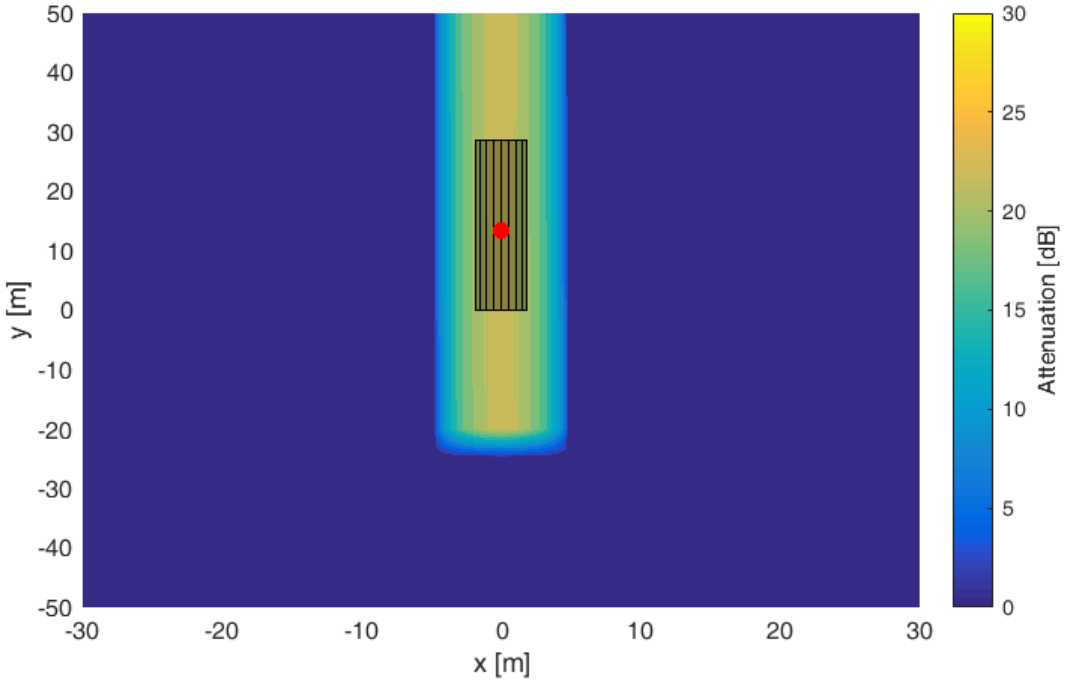

(b) r = 20 [m]

Figure 4.8: Comparison of the change in source distance relative to cylinder denoted by r for, f = 20 [kHz], a = 1.88 [m], length = 28.65 [m]

5

Combination of the Fuselage and Wings

In the previous chapters it is shown that separate methods are available for both the fuselage and the wings. Now, a way to combine these two methods has to be developed. To the best of the authors knowledge, this has not been done before. The combination of the methods is approached step by step. Firstly by looking at the wing and plane fuselage noise shielding separately. Then, the wings and the plane fuselage are combined. The result of the cylindrical fuselage is compared with the plane fuselage calculated with the barrier shielding method. Finally, the wings are added to the cylindrical fuselage and the result is compared with the plane fuselage and wing combination.

5.1. Wings

For both wings, the barrier shielding method described in chapter 3 is used. First, the shielding of the two wings without a fuselage is calculated. The inputs used in this chapter are given in Appendix A. The wing is located 30 [m] above the observer plane. The location of the source is in the center and 10 [m] above the aircraft. The coordinates used for the source are (0,-10,13.5).
Since the fuselage will block the diffraction at the root edge, this edge is assumed to be non diffracting. Therefore, a sudden stop in noise shielding will take place at the root. The wing noise attenuation results are shown in Figure 5.1. The noise shielding contour itself is as expected. The highest wing shielding takes place at the wing root because the path difference is largest there. At the root, the wing is widest and the distance to the tip edge is maximum.

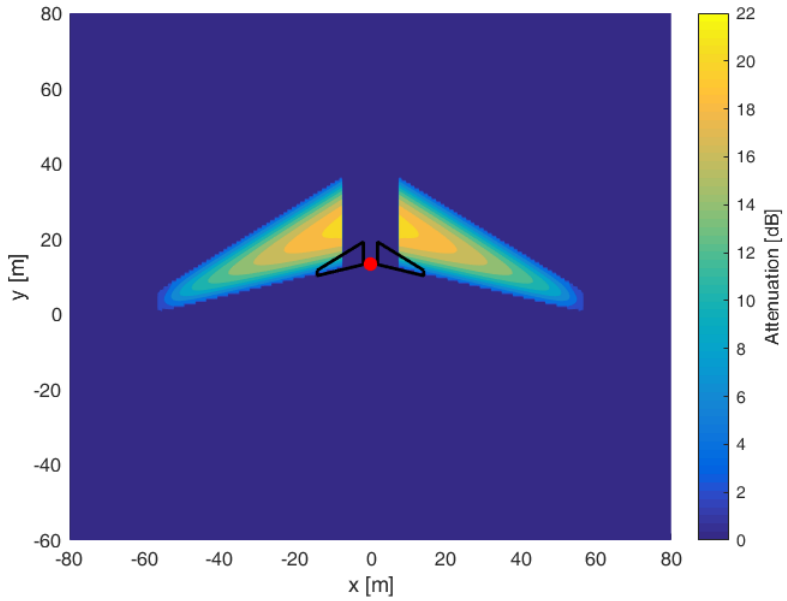

Figure 5.1: Noise Shielding of two wings. The source is represented by the red dot and placed 10 [m] above the wings. f = 5000 [Hz]. The observer plane is placed 30 [m] below the wings.

5.2. Plane Fuselage

The method described for the wings is also performed for the plane fuselage. When the fuselage is considered separately, all its edges are considered diffraction edges. For the plane fuselage, the shielding reduces towards the edges. The shielding is dominated by the closest edge. The highest shielding occurs at the center of the fuselage. This is due to the fact that the path difference is largest there. The noise shielding result is shown in Figure 5.2.

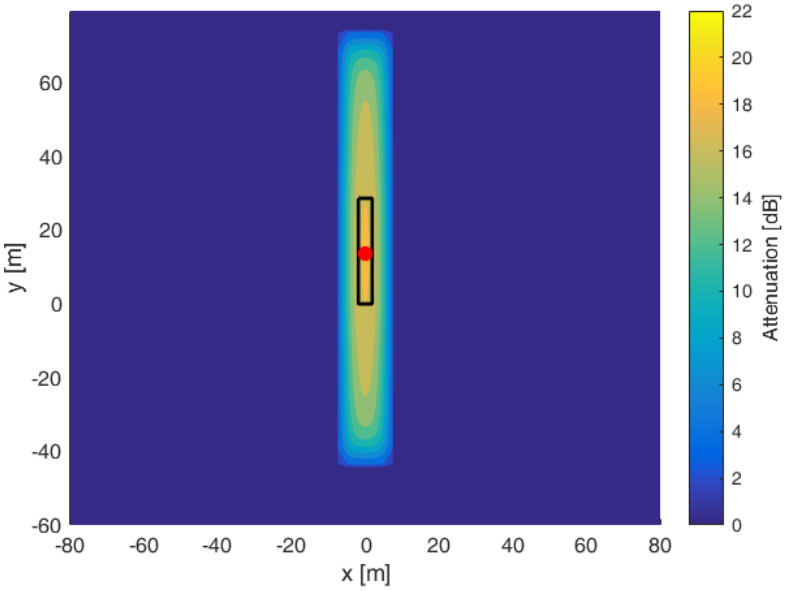

Figure 5.2: Noise Shielding contour of a plane fuselage. The source is represented by the red dot and placed 10 [m] above the fuselage. f = 5000 [Hz]. The observer plane is placed 30 [m] below the barrier.

5.3. Plane Fuselage and Wings

Now that the wings and the plane fuselage can be calculated with the barrier shielding method, both of them are combined. When the direct sound ray intersects the fuselage, it has a diffracted sound ray at each of the fuselage edges. These sound rays go through the fuselage close points denoted by $Cf_{1,2,3,4}$ shown in Figure 5.3.

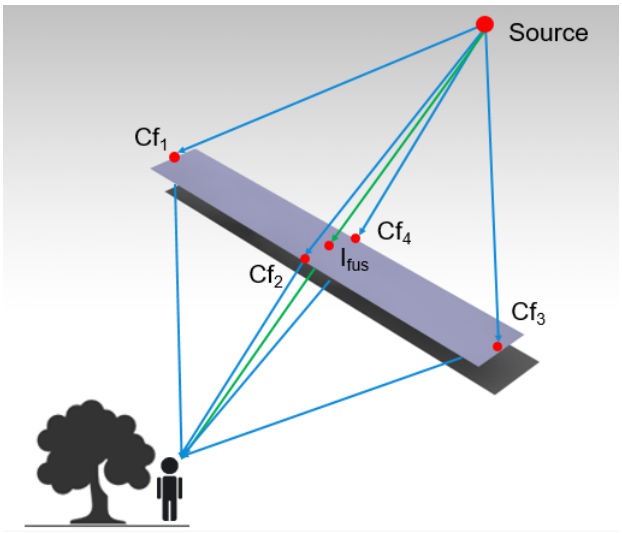

Figure 5.3: Sketch of the diffracted sound rays at each edge of the fuselage. I_{fus} is the intersection point of the direct sound ray with the fuselage, $Cf_{1,2,3,4}$ are the closest points to this intersection point on the fuselage boundary.

These sound rays can intersect one of the wings. This is the case for both points Cf_2 and Cf_4 shown in Figure 5.4. Here, a closer look is taken and the sound ray coming from the source to the point Cf_2, indicated with the bold red line in Figure 5.4.

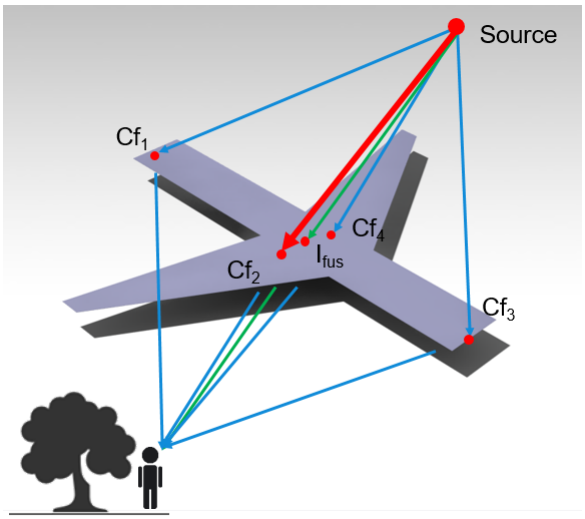

Figure 5.4: Sketch of the diffracted sound rays at each edge of the fuselage with the wings present. I_{fus} is the intersection point of the direct sound ray with the fuselage, $Cf_{1,2,3,4}$ are the closest points to this intersection point on the fuselage boundary.

As this sound ray intersects the wing, it is shielded by the wing as well. The procedure for the wing is the same as if the sound ray would come directly from the source. The closest points on each wing edge $Cw_{1,2,3}$ from the wing intersecting point I_{wing} are sought. Then, the sound rays will go from the source, through Cw_1, Cw_2 and Cw_3 to the observer. This is shown in Figure 5.5.

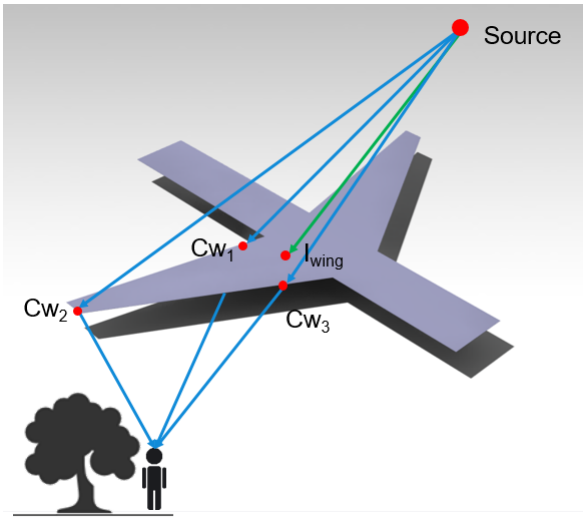

Figure 5.5: Sketch of the diffracted sound rays at each wing edge. I_{wing} is the intersection point of the direct sound ray with the fuselage. $Cw_{1,2,3}$ are the closest points to the wing intersection point on the wing edges.

The sound rays which are only blocked by the fuselage and the ones coming from the other wing need to be added with the others as shown in Figure 5.5. All the sound rays used to determine the attenuation with the use of the barrier shielding method are shown in Figure 5.6.

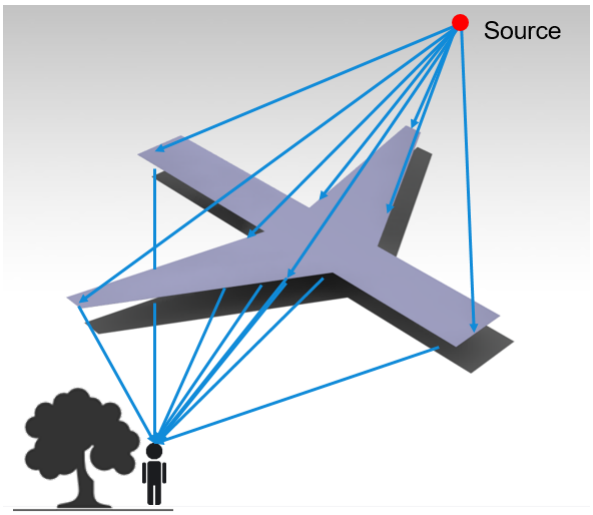

Figure 5.6: Sketch of the used diffracted sound rays when both wing and fuselage noise shielding is considered.

The attenuation of all the diffracted sound rays are added together with Equation 3.19 to obtain the noise shielding result with the barrier shielding method for a finite barrier in the shape of a plane fuselage with two planar wings. The result of this addition technique is shown in Figure 5.7. The outline of the aircraft is clearly visible in the shielding contour. The amount of shielding also runs smoothly from the wing to the fuselage. Except for the regions of maximum shielding at the wing root. This is due to the assumption that no diffraction occurs at the wing root. This is why the regions with the highest amount of shielding at the wing root and at the fuselage located between the wings do not coincide.

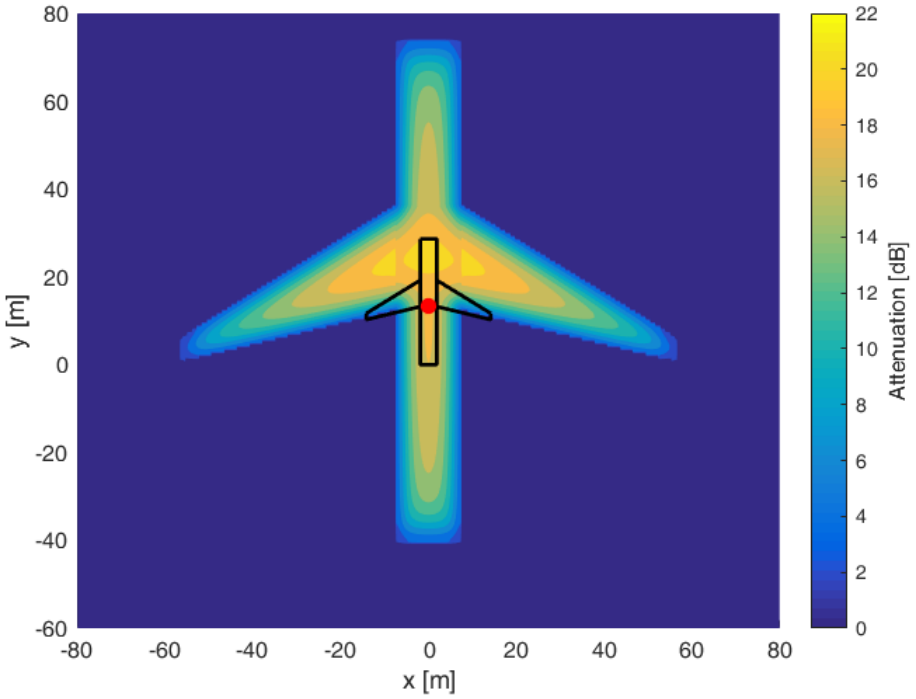

Figure 5.7: Noise Shielding of a plane fuselage with wings. The source is represented by the red dot and is placed 10 [m] above the aircraft. f = 5000 [Hz]. The observer plane is located 30 [m] below the aircraft.

5.4. Cylindrical Fuselage

Since the barrier shielding method only incorporates sharp edge diffracted rays, the analytic solution of a cylinder is used for the fuselage. This is because the fuselage is a cylindrical shape which is expected to have a lot of creeping rays. The analytic solutions takes these creeping rays into account. As a consequence, the analytic solution will be more accurate for the fuselage shielding than the barrier shielding method.

The barrier shielding method does not distinguish between different shapes which have the same outline. This also holds for the diffraction integral method. This method is based on the Kirchhoff theory of diffraction. In [58], the shielding results of the diffraction integral method, the analytic solution and the Fast Scattering Code are compared. This comparison is done for a sphere with a geometry as denoted in Figure 5.8.

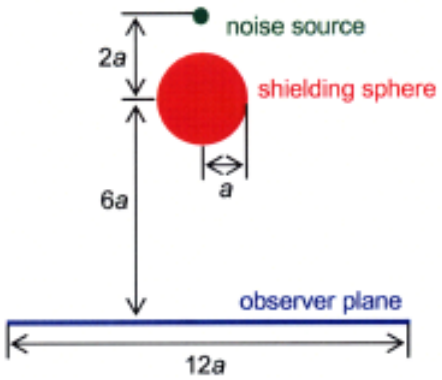

Figure 5.8: Sketch of the geometry used for the sphere shielding with the point source placed above the sphere [58].

This comparison is presented because it is expected that, for the fuselage shielding, the same trend in comparing the barrier shielding method with the analytic solution will exist as with the Kirchhoff theory of diffraction and the analytic solution for the sphere. This is the case because the barrier shielding method has similar limitations as the diffraction integral method.

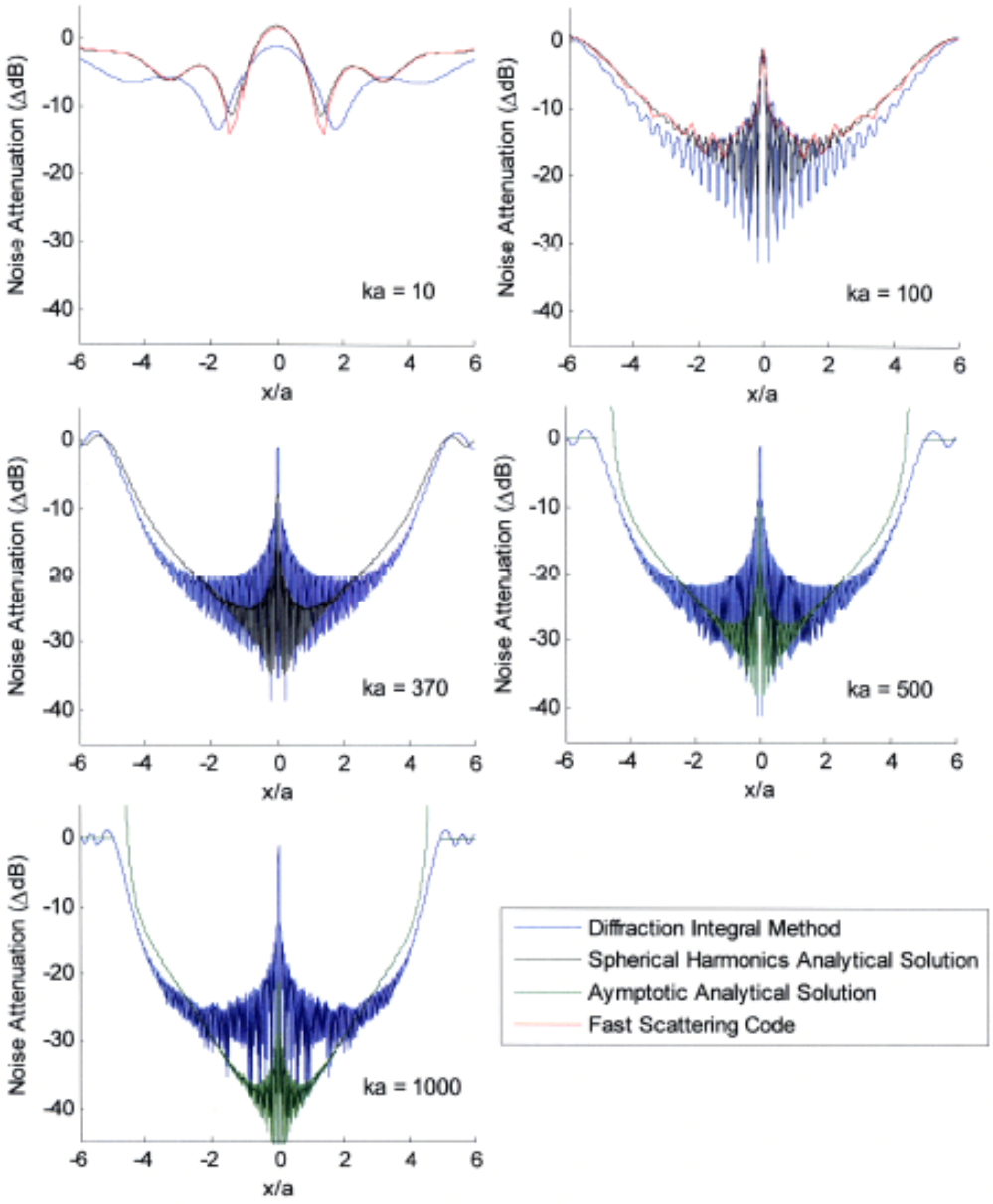

Figure 5.9: Comparison of the shielding results of a sphere with a point source placed above it as defined in Figure 5.8, obtained with the diffraction integral method, analytic solution and NASA's Fast Scattering Code [58]

In Figure 5.9 the so-called spherical harmonics analytic solution is used for ka values lower than 370. This solution is obtained by expanding the Helmholtz equation in spherical harmonics [58]. For higher ka values, the asymptotic analytic solution described in [58] is used. The results of the Fast scattering code are only present until $ka = 100$ [58].

As can be seen in Figure 5.9, The Fast Scattering Code and the analytic solution have similar results. At $ka = 100$, the fast scattering code oscillates less. This is caused by insufficient observer density [58].

It can be seen that the diffraction integral method deviates more from the analytic solution as the frequency increases. As stated earlier, the creeping rays continuously sheds rays as it travels around the surface reducing the strength of the ray. As the frequency increases, the creeping ray will reduce in strength. The reduction in ray strength results in higher shielding. The diffraction integral method is incapable of capturing those creeping rays and represents the diffracted rays with sharp edge diffracted rays resulting in lower shielding at high frequencies [58].

In conclusion, it is expected that the analytic solution of the cylinder will have higher shielding results than predicted with the barrier shielding method. It can also be seen that results of the analytic solution oscillates heavily at high frequencies. This means that the step size of the observer location will need to be sufficiently small.

The results of the cylinder obtained with the noise shielding assessment tool is shown in Figure 5.10. The outer contour of the shielding is the same as in Figure 5.2 but, as expected from the reasoning above, the amount of shielding is higher, especially at the center of the cylinder. This is caused by the creeping rays. The more to the center, the longer the creeping distance. Because the creeping ray is longer, more rays will be shed tangentially to the creeping ray reducing the strength of the sound ray. It has to be noted that the results presented here is that of an infinite cylinder but the length of the cylinder is limited with the line of sight condition. Diffraction at the front and aft of the cylinder are not taken into account. This causes the shielding to stop abruptly at the front and aft of the fuselage.

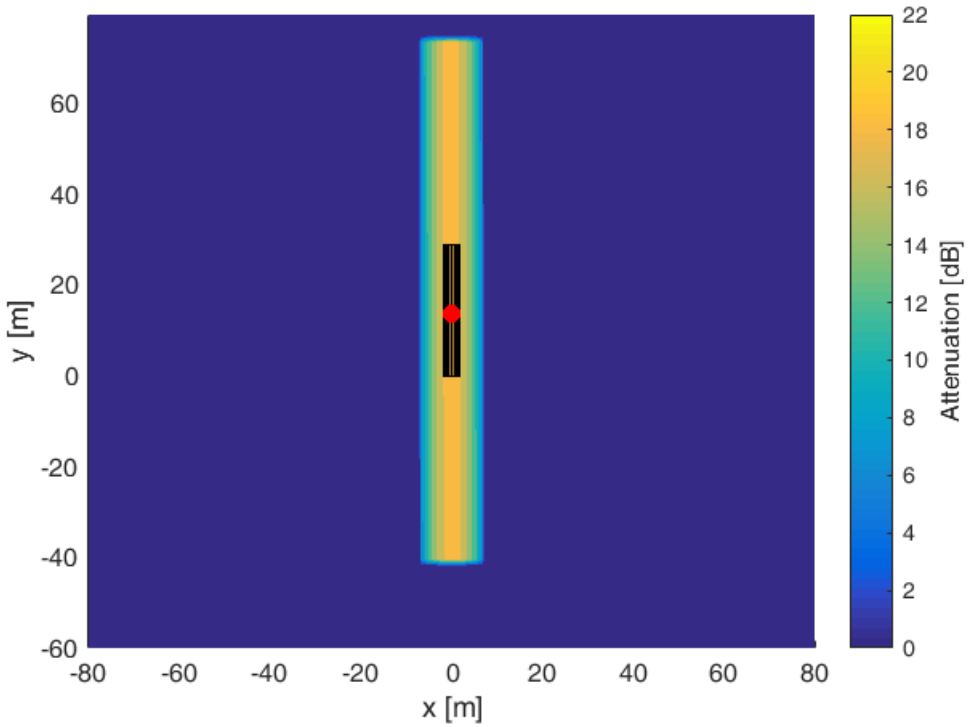

Figure 5.10: Noise Shielding of a Cylindrical Fuselage, f = 5000 [Hz]. radius = 1.88 [m]. The source is placed 10 [m] above the center of the fuselage and indicated with the red dot, observer plane is positioned 30 [m] below the fuselage center.

5.5. Cylindrical Fuselage and Wings

Now, the shielding of the wings need to be combined with the shielding of the cylindrical fuselage. When both the results are added together, the region where the wings and the fuselage connect give too low results as shown in Figure 5.11. This is the case because the sound that is shielded due to the cylinder is not shielded due to the wings as well, but goes in fact through the wings. This result is clearly not valid.

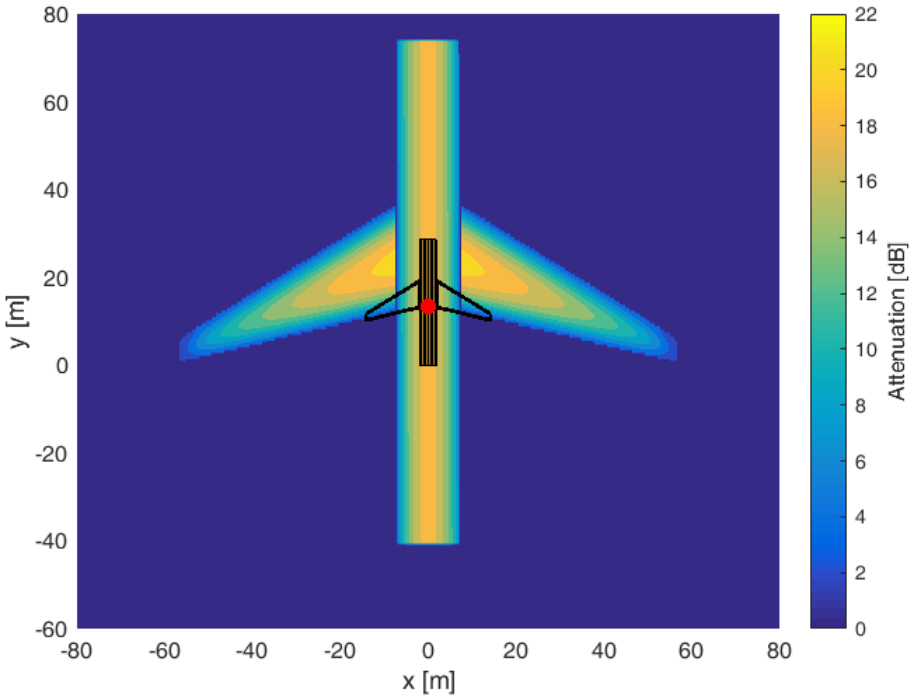

Figure 5.11: Noise Shielding of a cylindrical fuselage added with the wing shielding results, f = 5000 [Hz]. Source is positioned 10 [m] above the aircraft and the observer plane 30 [m] below the aircraft.

To overcome this error, the shielding calculation scheme shown in Figure 5.12 is used. First the shielding result of the wings with the plane fuselage is determined with the barrier shielding method. This is done to incorporate the rays that are diffracted from the fuselage and the wing. These rays are the ones diffracted by the wings shown in Figure 5.6. As stated before, those rays are taken into account when calculating the shielding of the complete aircraft with the barrier shielding method.

The rays that are diffracted from the plane fuselage itself, are not of interest. Therefore, the plane fuselage is subtracted from the total barrier shielding aircraft result. The result is the shielding due to the wings alone as if the fuselage would be present. Note that for this part, sharp edge diffraction is assumed. Next, to incorporate the fuselage shielding with the inclusion of the creeping rays, the analytic solution of the fuselage is added to the result of the wings.

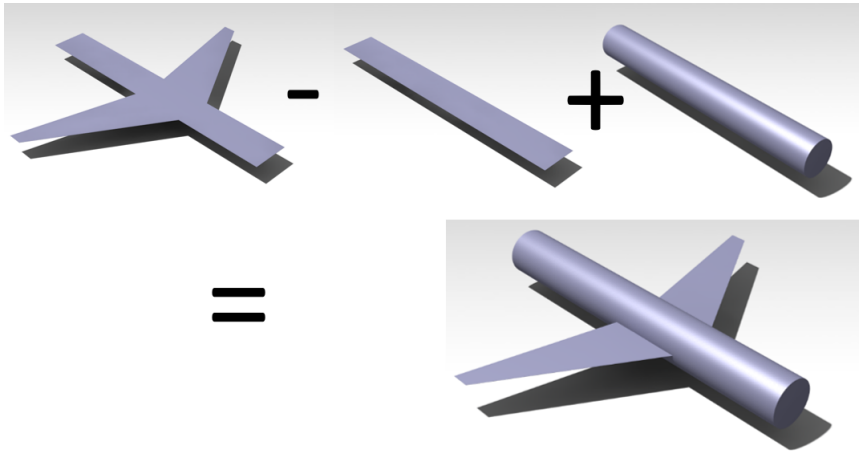

Figure 5.12: Graphical representation of the method of adding the wing and cylinder noise shielding together.

This addition technique indeed results in a smooth fuselage to wing transition as can be seen in Figure 5.13. This is the case because the rays that are diffracted by the fuselage and the wing as shown in Figure 5.5, are also taken into account. Note that the region of highest shielding of the fuselage is also increased at the wing height. This should be the case, since the wings accommodate for extra shielding at this location.

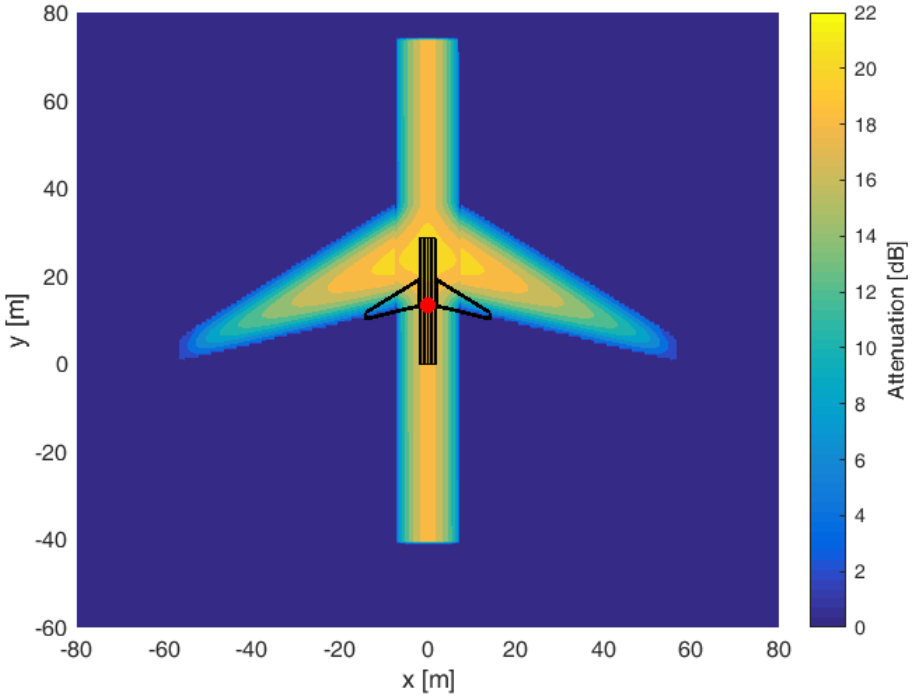

Figure 5.13: Noise shielding of a cylindrical fuselage with wings, f = 5000 [Hz]. Source is positioned 10 [m] above the aircraft and the observer plane is placed 30 [m] below the aircraft.

It has to be noted that this method adds unnecessary computational cost. The plane fuselage shielding needs to be calculated with and without the wings present. The computational cost is reduced by only using the part of the fuselage between the wings. If the fuselage part between the wings is intersected, the sound rays going from the source to the wing edges are taken into account. This gives the shielding result for the wing part as shown in Figure 5.14.

The result obtained from the modified wing shielding can then be added with the cylinder shielding. This results in the same complete aircraft shielding as shown in Figure 5.13. With this method, the complete plane fuselage noise shielding no longer needs to be calculated separately. Only part of the plane fuselage needs to be determined.

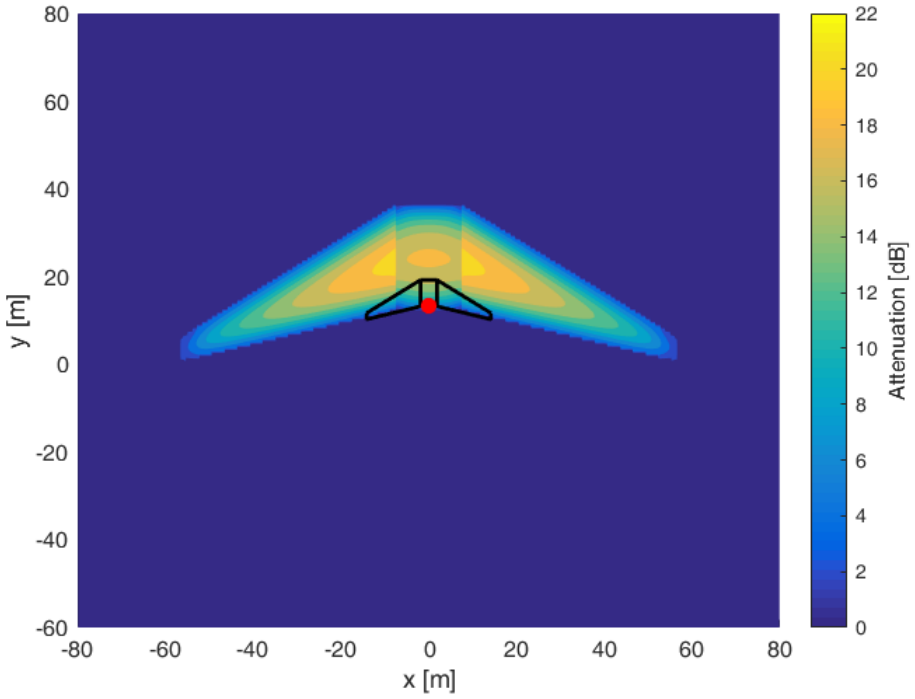

Figure 5.14: Noise Shielding of the wings as if part of the fuselage would be present, f = 5000 [Hz]. Source is positioned 5 [m] above the wings, the observer plane is located 30 [m] below the wings.

6

Noise Shielding Prediction Tool

In section 2.7, it was chosen to use a combination of two noise shielding methods. The barrier shielding method is used for the wings and the analytic solution of a cylinder for the fuselage. Since those are two separate methods, the two methods will first be implemented in an individual noise shielding prediction tool as shown in section 6.1 and 6.3. Creating the individual tools is done to asses the correct working of the methods separately. In section 6.2, a complete aircraft noise shielding program based on the barrier shielding method is created. To do this, the fuselage needs to be represented by a plane. Calculating the aircraft noise shielding with the barrier shielding method is done to give an indication of what the results of the barrier shielding method and analytic solution combined needs to be. Finally, the two methods are combined in section 6.4.

6.1. Wing Shielding

For the barrier shielding method, the theory as described in chapter 3 is used. In this section, the implementation of the wing shielding method in the noise shielding prediction tool is discussed.

6.1.1. Program Outline

First of all, the input of the prediction tool needs to be defined. The geometry of the wing is described by a three-dimensional point for each corner. The source and observer location are also defined by three-dimensional points. Since the noise shielding is frequency dependent, the frequency needs to be known. The source is modeled as a point source and a source directivity factor is not taken into account. The source strength is not an input, because the relative amount of shielding caused by the aircraft geometry is determined not the sound pressure level. This is independent of the source strength. Ground reflection is not taken into account which makes it unnecessary to specify the height of the wing with respect to the ground. Only the height until the observer needs to be known. An example input file is given in Appendix A.

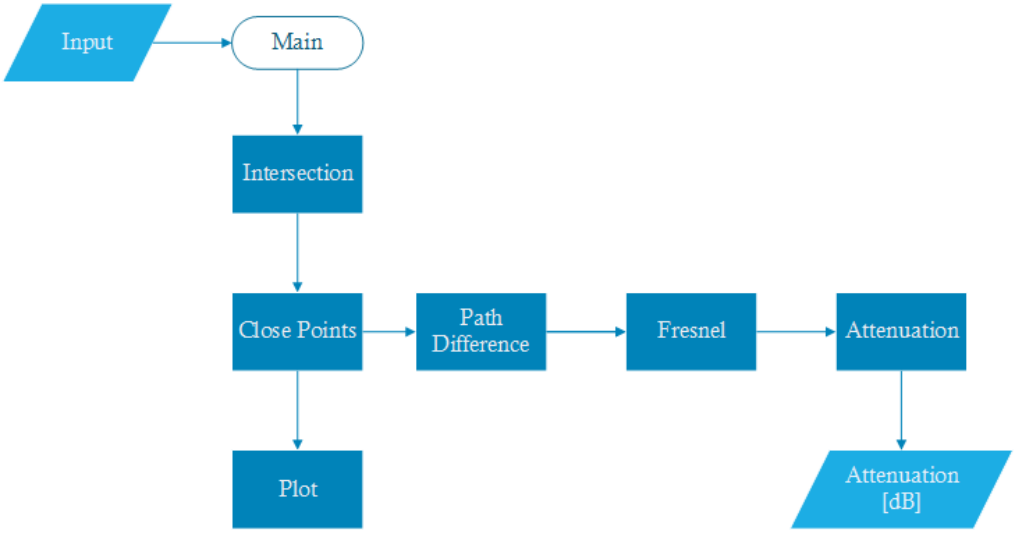

Figure 6.1: Wing shielding prediction tool flow chart

All the input data is entered into the main file as schematically indicated in the flow chart in Figure 6.1. The main file processes the data and runs all the other necessary files. First, the intersection point of the source observer line with the wing needs to be determined. This is determined by the intersection of a line with a plane described by three points. Then, it is determined if the intersection point is really on the wing, i.e. the point lies between the wing edges. This is all done in the program block intersection.

In the next program block, Close Points, the closest points to the intersection point on the wing edges are determined. Once these points are known, all the used sound rays can be plotted. This gives the user a clear indication of what is going on. An example is given in Figure 6.2.

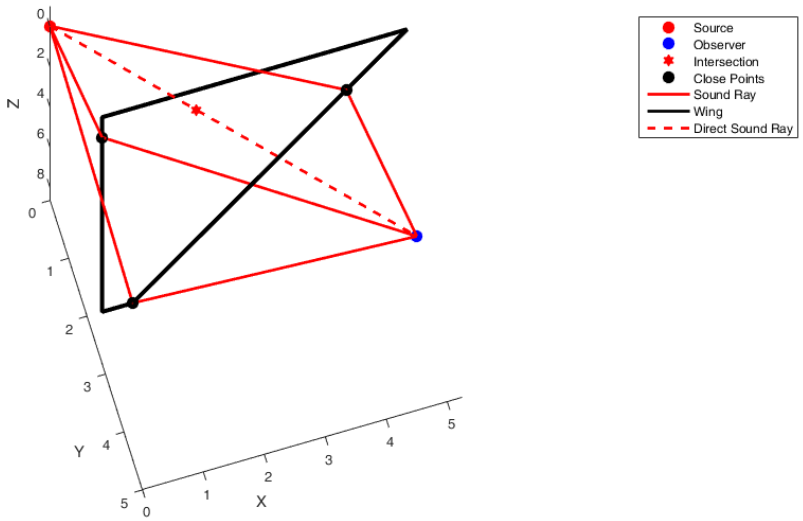

Figure 6.2: Plot of the used geometry, Intersection Point, close points, diffracted sound ray and direct sound ray.

From these obtained sound rays, the difference in path length with the direct and diffracted sound rays can be determined. This is done in Path Difference. In the program block Fresnel, the Fresnel number is determined with the use of the path length difference, the frequency and the speed of sound in free space. This is described in Equation 2.17. The attenuation of each wing edge with the use of Equation 2.18 and the total attenuation at the observer point with Equation 2.19 is determined in the

program block Attenuation. This is the final value which needs to be known. The procedure is repeated for different observer locations to create a noise shielding contour of the wing.

6.2. Aircraft with Plane Fuselage

Since the barrier shielding method for the wing alone works as expected, the same method will be used for the aircraft with a plane fuselage. This stage is done to get a good indication of what the final result of the cylindrical fuselage with plane wings will have to be. In other words, this makes it possible to do a verification of the shielding effects of the complete aircraft with cylindrical fuselage. The increase in accuracy and computational time of the analytic solution versus the barrier shielding method for the fuselage is assessed. This is done to see if it is worthwhile to implement the cylindrical fuselage. In this section, the fuselage will be represented by just one rectangular plane. This plane represents the cylinder that will be used later on.

6.2.1. Method

The method used for the wing and the plane has been already briefly discussed in section 5.3. In that section, a horizontal fuselage is used. Here, the method is explained again for a vertical fuselage. This because the noise shielding program can cope with both vertical and horizontal plane fuselages.
As for the shielding by the wing alone, the intersection point (I_{fus}) between the line from the origin ($point\ 1$) to the observer ($point\ 0$) and the shielding object is sought as shown in Figure 6.3. If this intersection point is on the fuselage plane, the closest points on the fuselage plane boundaries ($W_{up}, W_{low}, W_{front}, W_{back}$) are taken for the equivalent diffraction calculation [29]. However, it can happen that the ray from the source to one of the edge diffraction points intersects the wing (I_{wing}). When this happens, the same procedure for the sound rays as explained in section 5.3 is executed.

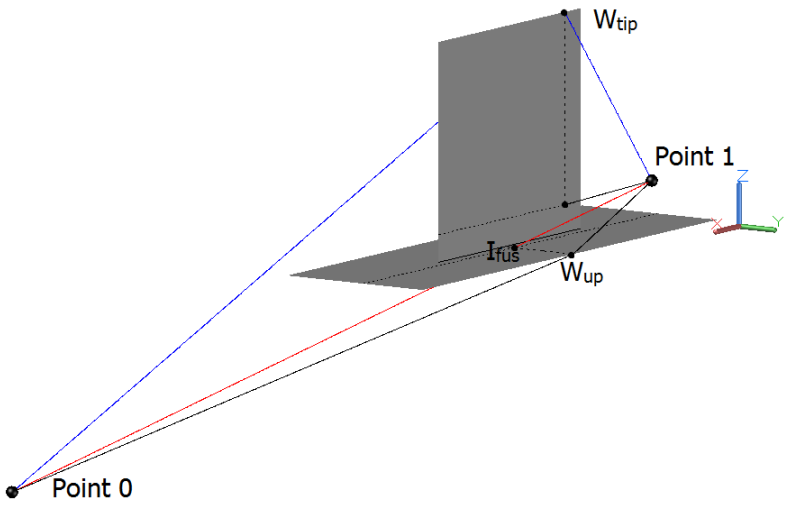

Figure 6.3: Sketch of diffraction rays of fuselage and wing

As can be seen in Figure 6.3, the ray of the source point 0 to W_{low} is intersected by the wing. In Figure 6.3, the closest points on the wing boundaries from this intersection point (I_{wing}) are shown. For the sake of clarity, only the sound ray from the tip is shown here. As can be seen, the sound ray that would go from the source to the lower fuselage (W_{low}), now needs to go from the source, to the tip of the wing (W_{wing}) and then to the observer point. Note that this needs to be done for each wing edge.

The attenuation is dependent on the Fresnel number, which is dependent on the distance the sound ray has to travel, as is explained in chapter 3. However, it is possible that the sound ray of the wing to the observer intersects the fuselage again. In this case, the same procedure of finding the closest points on the boundaries needs to be followed. This will increase the length of the sound ray even further. As a result, the amount of sound attenuation will increase.

6.2.2. Program Outline

The core of the program outline of the plane fuselage with wing is the same as that of the wing barrier shielding program. This can be seen from Figure 6.4 and Figure 6.1. The input is extended with the corner locations of the plane fuselage. The wing is mirrored so that the aircraft has two identical wings.

The inputs are loaded in the main file from which the program block Intersection Fuselage is started. When the fuselage is intersected by a sound ray, the closest points to the intersection point on the fuselage borders are determined. Once these points are known, it is checked if one of the sound rays of the source to one of the close points on the fuselage intersects the wing. If the intersection point exists, the close points on the wing are calculated and again it is checked if there is intersection with the fuselage.

If there is no intersection with the fuselage, it is checked if there is intersection with the wing and then again if there is intersection with the fuselage. This is repeated until no new intersection points are found as shown in Figure 6.4. When all the sound rays are known, the path difference with the source observer line can be determined. Once this is known, the Fresnel zone number is determined. With the Fresnel number, the attenuation is obtained. Once this is known, an attenuation plot can be plotted under the aircraft at any observer location of interest.

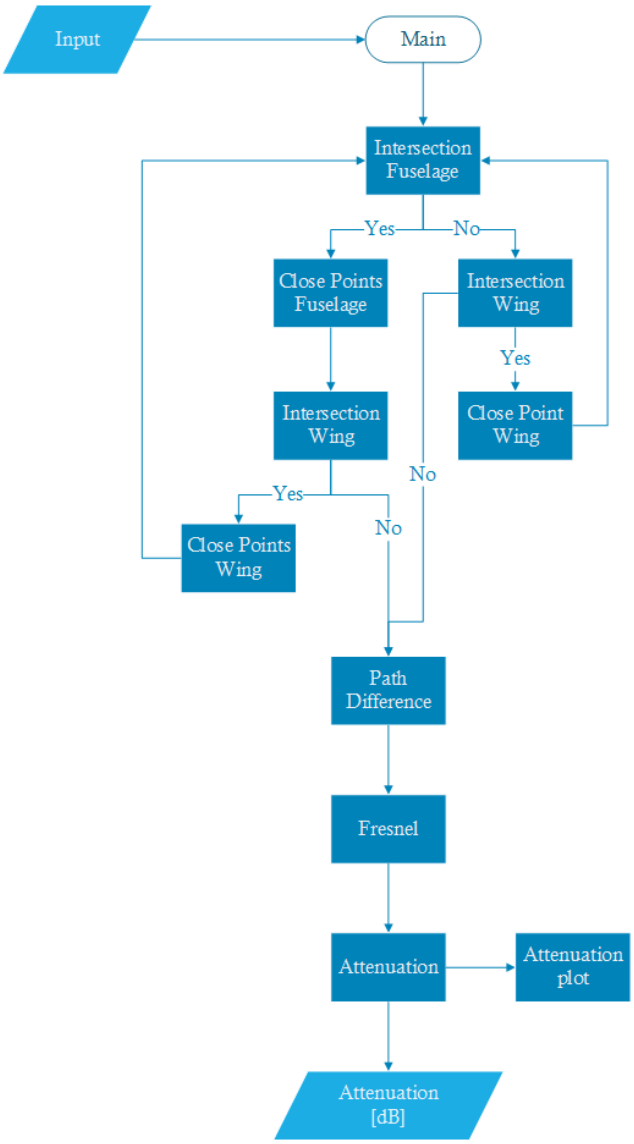

Figure 6.4: Noise shielding prediction tool of the wing with plane fuselage obtained with the barrier shielding method flow chart

6.3. Analytic Solution Fuselage

In this section, the program outline of the analytic solution of the cylindrical fuselage is discussed. For this analytic solution, the theory as described in section 4.6 is used. Since it is not necessary to trace the rays, the program build up is completely different. For the fuselage, the incident and scattered sound pressure field need to be combined and converted to noise attenuation.

6.3.1. Program Outline

For the fuselage, the analytic solution of a cylinder is used. As input one needs the cylinder length and radius. Also the distance from the source to the cylinder center and the distance to the observer location needs to be known. The magnitude of the source is irrelevant since here the relative attenuation due to the geometry is obtained. The noise attenuation is obtained by determining relative pressure difference with and without the presence of the cylinder.

To calculate the attenuation, the total pressure field with and without the cylinder needs to be known. Since the total pressure field with the cylinder present is built from an incident and a scattered pressure field, each of these fields is computed independently. Each pressure field has a separate program block. Once the incident and scattered pressures are known, the total pressure field can be calculated as shown in Figure 6.5. From the total and the incident pressure field, the attenuation is obtained. Finally, the attenuation results will be represented in a plot.

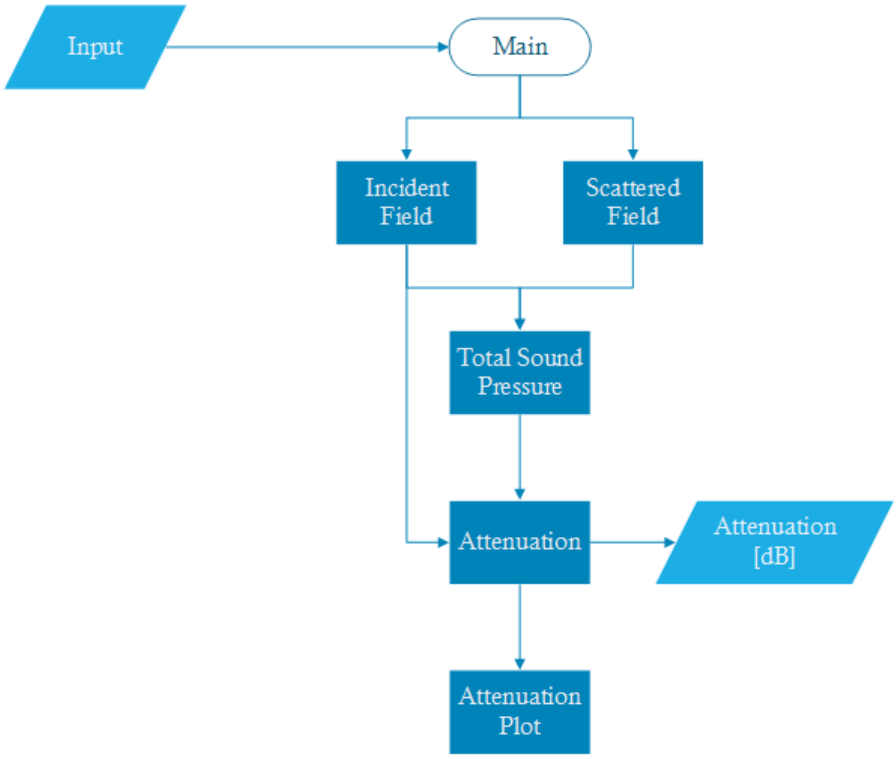

Figure 6.5: Flow chart of the analytic solution of the fuselage.

6.4. Barrier Shielding Method and Analytic Solution Combined

Finally, the cylindrical fuselage and the wings need to be combined. This means that the two methods need to be combined with each other. In chapter 5, the method used to do this is explained.

Firstly the attenuation of the aircraft wings combined with the part of the fuselage between the wings is calculated with the use of the barrier shielding method. At the same time, the noise attenuation of the plane fuselage part between the wings itself is calculated as well as the attenuation of the complete cylindrical fuselage.

In the program block Plane Fuselage and Wings, part of the plane fuselage shielding is included. As one wants to use the shielding result of the cylindrical fuselage, the plane fuselage attenuation needs to be subtracted. Then, the cylindrical fuselage shielding is added as shown in Figure 6.6. This procedure is done in order to take the sound rays that are diffracted from the fuselage followed by the wing into account. An example of such a sound ray is shown in Figure 5.6.

Each individual calculated part has a vector with their separate attenuation results in it. These data vectors are then summed with each other to obtain the total shielding result. From this result, a noise shielding plot can be made of the aircraft with a cylindrical fuselage.

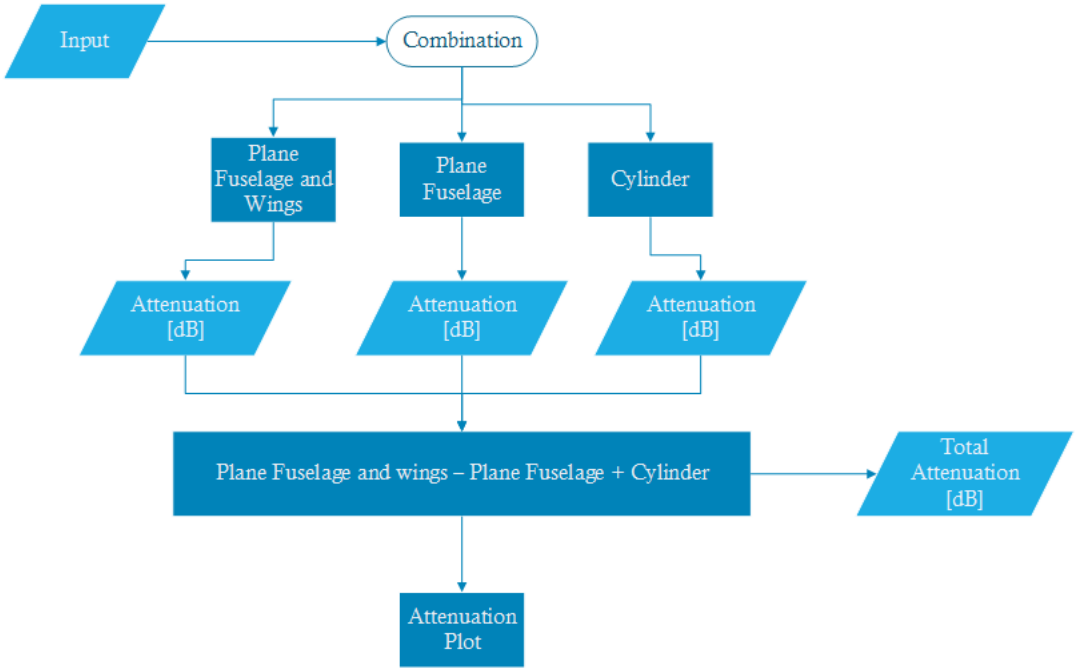

Figure 6.6: Flow chart of the fuselage and wing shielding combination noise shielding prediction tool.

7

Validation

To validate the noise shielding assessment tool developed in this thesis project, the results will be compared with the results of Leo W. T. Ng and Zoltán S. Spakovszky [6]. Ng and Spakovszky have used the Kirchhoff theory of diffraction to determine the aircraft engine noise shielding. This method is briefly discussed in section 2.2. With this method, the noise shielding of a Boeing 737 aircraft with the sound source placed above the left wing, is calculated. The validation is done step by step. Firstly the wings are looked at on their own. Then, the plane fuselage is added to the wing. Finally, the result of the aircraft with a cylindrical fuselage will be validated with one and two sources.

The overall amount of shielding is calculated over the 1/3 frequency octave band from 50 to 10 000 [Hz]. The amount of shielding for each frequency is then added with Equation 7.1 [58] for the 24 center frequencies.

$$\Delta OASPL_{attenuation} = 10 \log\left(\frac{1}{24}\sum 10^{\frac{\Delta SPL}{10}}\right) \tag{7.1}$$

The shielding outline used by the Kirchhoff theory of diffraction is indicated with the green line in Figure 7.1. The shielding results are shown in Figure 7.2.

It has to be kept in mind during this validation that the Kirchhoff theory of diffraction has several limitations. Since a contour integral is used to determine the shielding, this method only depends on the aircraft outline. In the Kirchhoff diffraction integral it is also assumed that there is no acoustic pressure on the shielding surface in the shadow zone. In the bright zone incident sound pressure is assumed. As a consequence, only sharp edge diffracted rays are taken into account. The method is also less accurate for low frequencies because it is based on high frequency geometric acoustics [58].

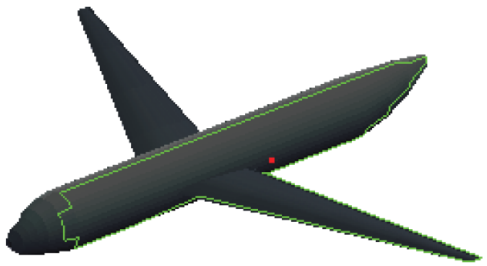

Figure 7.1: Kirchhoff Shielding contour used of a Boeing 737 with source above left wing [6]

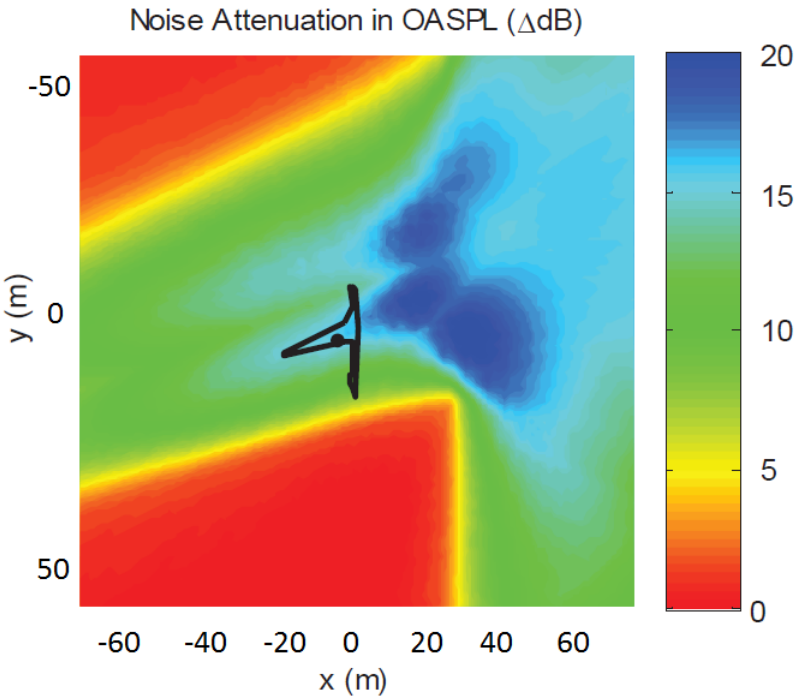

Figure 7.2: Noise Shielding of a Boeing 737 with source located above left wing, 1/3 octave band frequency range from 50 to 10 000 [Hz], the observer plane is located 30 [m] below the aircraft. [6]

Firstly the wing shielding over the 1/3 octave band frequency range is calculated. This is done to exclude the wing and fuselage combination method from the validation results. The geometric inputs used are given in Appendix A and are based on a Boeing 737 aircraft. The observer plane is positioned 30 [m] below the aircraft. This is the same height as used in the Kirchhoff diffraction integral results shown in Figure 7.2. In Figure 7.3, it can be seen that the wing shielding contour outline itself is very similar compared to Figure 7.2 but the attenuation levels are very different.

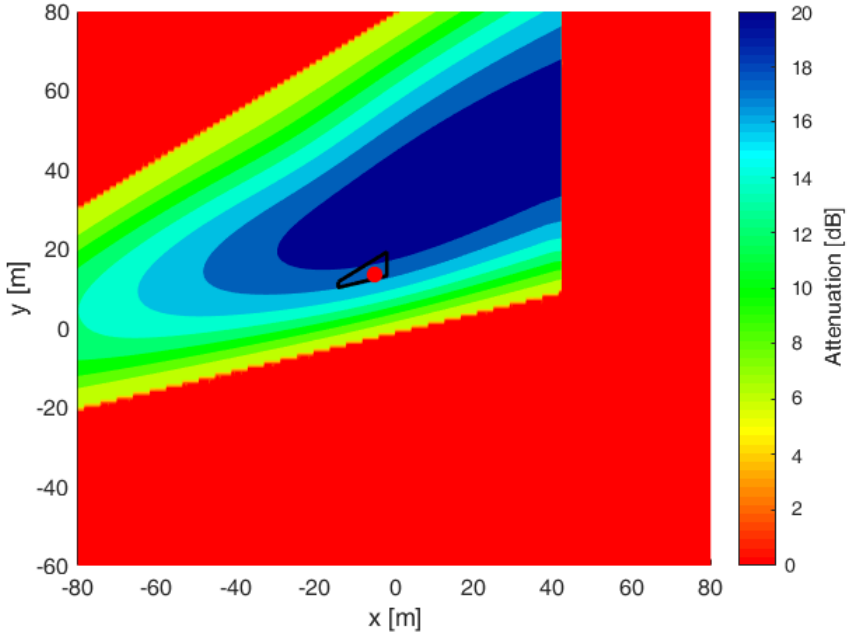

Figure 7.3: Wing Noise Shielding of a Boeing 737. 1/3 octave band frequency range from 50 [Hz] to 10 000 [Hz], the observer plane is located 30 [m] below the aircraft. The noise source is indicated with the red dot.

Both results have a shielding region of 10 [dB] and a highest shielding region of 20 [dB]. This region is a lot larger with the barrier shielding method than with the Kirchhoff theory of diffraction.

Both the Barrier shielding method and Kirchhoff diffraction method have similar limitations. Both methods only make use of sharp edge diffracted rays and only depend on the contour of the shielding object. The low frequency limitation of the Kirchhoff method is not suspected to cause this high difference in shielding over the frequency band used. This is because the amount of shielding at low frequencies is minor.

The main difference in the amount of shielding is caused by the finite plane modification. The barrier shielding method is modified to hold for a finite plane. Apparently, an overestimation is created by this. In subsection 3.1.2, the NASA ANOPP approach used, has already shown to indicate a higher region of maximum shielding than the method with the correction factor. Also, the assumption that there is no diffraction at the wing root increases the amount of shielding of the wing.

At the edge of the contour, both the results in Figure 7.2 and Figure 7.3 have a shielding of 5 [dB]. The 5 [dB] shielding occurs when the path difference is zero. When this occurs, the Fresnel number is zero and the attenuation will be 5 [dB] independent of the frequency. This phenomena is also described by Maekawa [3]. The 5 [dB] region is more prominent for the Kirchhoff theory. To show it more clearly, a zoomed image of the trailing edge of Figure 7.3 is shown in Figure 7.4.

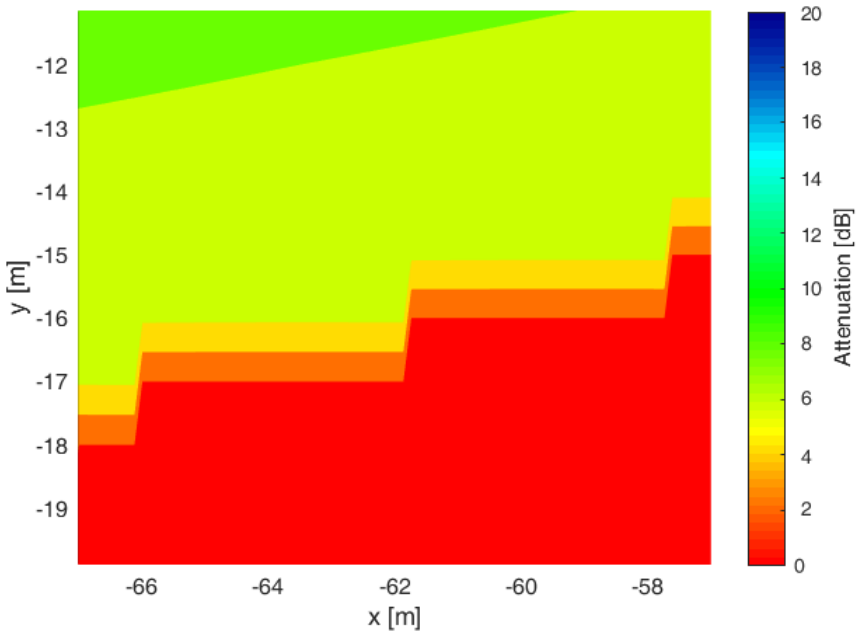

Figure 7.4: Trailing edge of the wing Noise Shielding of a Boeing 737, 1/3 octave band frequency range from 50 to 10 000 [Hz], the observer plane is located 30 [m] below the aircraft.

Since the Kirchhoff theory of diffraction does not take creeping rays into account, the results will be compared with that of a plane fuselage before comparing it with the cylindrical fuselage. The plane fuselage noise shielding is also calculated with the barrier shielding method. The results are shown in Figure 7.5. In this figure, the source is represented by the white dot. As can be seen, the fuselage shielding is around 10 [dB] over the complete fuselage.

The lower shielding in Figure 7.5 at the height of the wings compared with Figure 7.2 is caused due to the absence of the wing. As the wing is not present, the shielding object is smaller and thus the sound rays travel a shorter distance which results in a lower amount of shielding.

At the aft and front part of the fuselage, a region of higher shielding starts to occur again. This region is not present in Figure 7.2. This is an error in the amount of noise shielding caused by the fact that the horizontal plate is not a good representation of the fuselage if the source is not centered above the fuselage. At the outer end points of the fuselage, a kink in the diffracted sound rays start to occur. This kink results in higher shielding amounts and becomes greater closer to the end regions of the fuselage. This kink is not present if the source is located right above the horizontal plate.

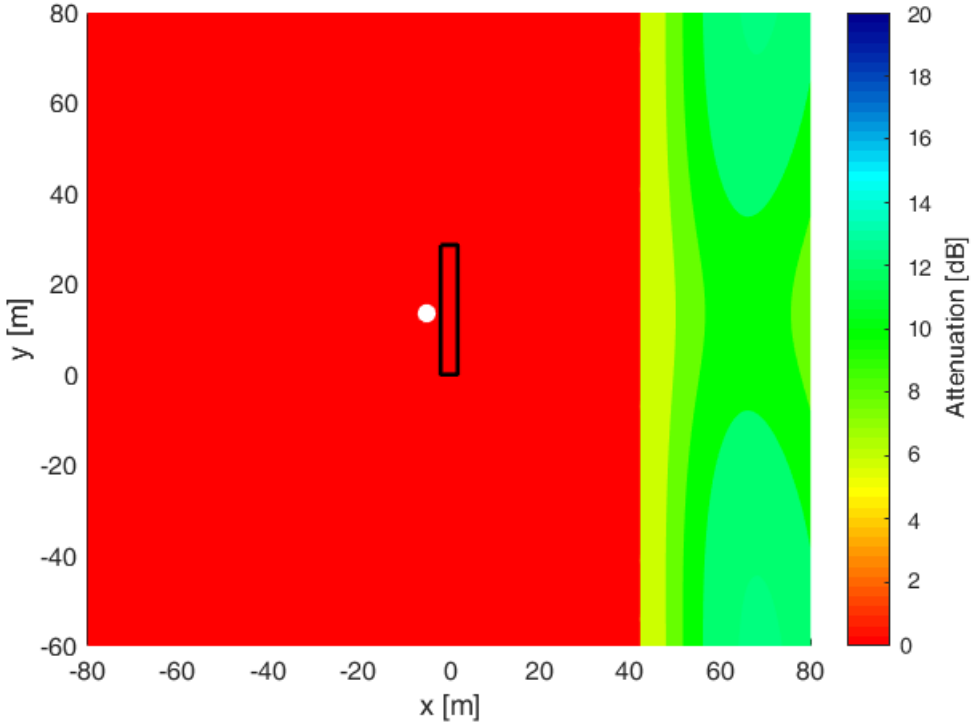

Figure 7.5: Noise Shielding of a Boeing 737 Fuselage represented by a plane. 1/3 octave band frequency range from 50 to 10 000 [Hz], the observer plane is located 30 [m] below the aircraft.

Now, the wings are added to the plane fuselage. The results of the aircraft with the fuselage represented by a flat horizontal plane is given in Figure 7.6. It has to be noted that in Figure 7.2 only one wing is represented. Only the shielding contour used by the Kirchhoff integral is represented in this plot. As for the barrier shielding method, the result is influenced by the complete aircraft geometry, the complete aircraft geometry used is plotted in the attenuation plot.

The shielding contour of the barrier shielding method is the same as that of the Kirchhoff theory of diffraction. The amount of shielding of the wing stays the same as in Figure 7.3. This means that the wing shielding remains an over estimation. In contrast with the wing, the fuselage shielding seems to be underestimated. This is the case because the horizontal plane is not a good representation of the fuselage when the source is not positioned right above the Fuselage. This means that when using the barrier shielding method to model other shapes, great care has to be taken in the geometry of the representative shielding plane.

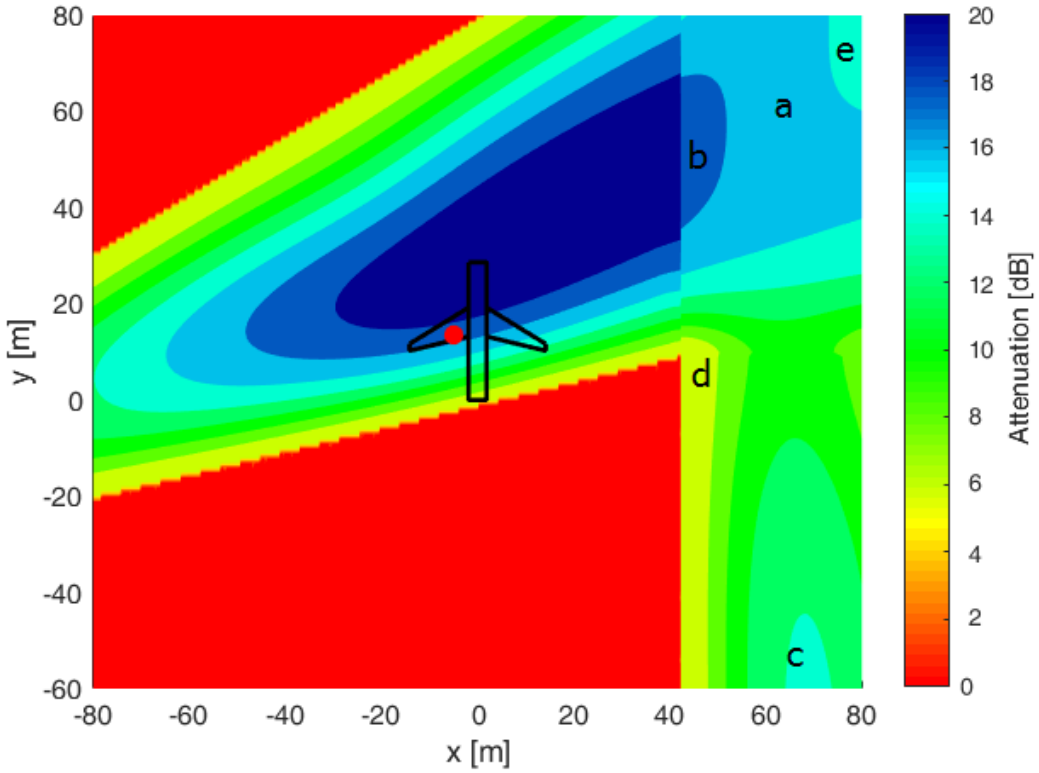

Figure 7.6: Aircraft Noise Shielding of a Boeing 737 as obtained with the barrier shielding method. 1/3 octave band frequency range from 50 to 10 000 [Hz]. The observer plane is located 30 [m] below the aircraft.

The maximum shielding of the fuselage is positioned at the location of the wing indicated by (a) as is the case for the Kirchhoff diffraction theory. The sudden change in the amount of shielding in the wing to the fuselage transition region at (b) originates from the fact that the wing root edge does not act as a diffraction edge. When the direct sound ray intersects the wing, it is assumed that no diffraction occurs at the fuselage. This assumption also contributes to the overestimation of the wing shielding. Note that when the fuselage is intersected with the direct sound ray and the diffracted sound ray intersects the wing, the wing will act as a diffraction barrier.

At the aft part of the fuselage (c), a region of higher shielding starts to occur again. This region is not present in Figure 7.2. This error is again caused by the fact that the flat plate is not a good representation of the fuselage if the source is not exactly above the fuselage. This is already discussed in the shielding validation of the fuselage alone.

At the fuselage side, where the wing stops indicated by (d), a sudden reduction in the amount of shielding occurs. This sudden change is caused due to the wing diffraction. At this region, the wing acts no longer as a second diffraction barrier of sound rays diffracted from the fuselage.

At (e) a region of lower shielding exists. This region is caused by the diffraction line at the leading edge of the right wing. The diffracted sound ray line approaches the direct sound ray. This means that the shielding at this edge approaches zero. The noise attenuation reduces close to this region because the diffraction edge of lowest shielding dominates the attenuation result.

Now, the flat plate fuselage needs to be substituted with the cylinder. Firstly the cylindrical fuselage is looked at on its own. The result is shown in Figure 7.7.

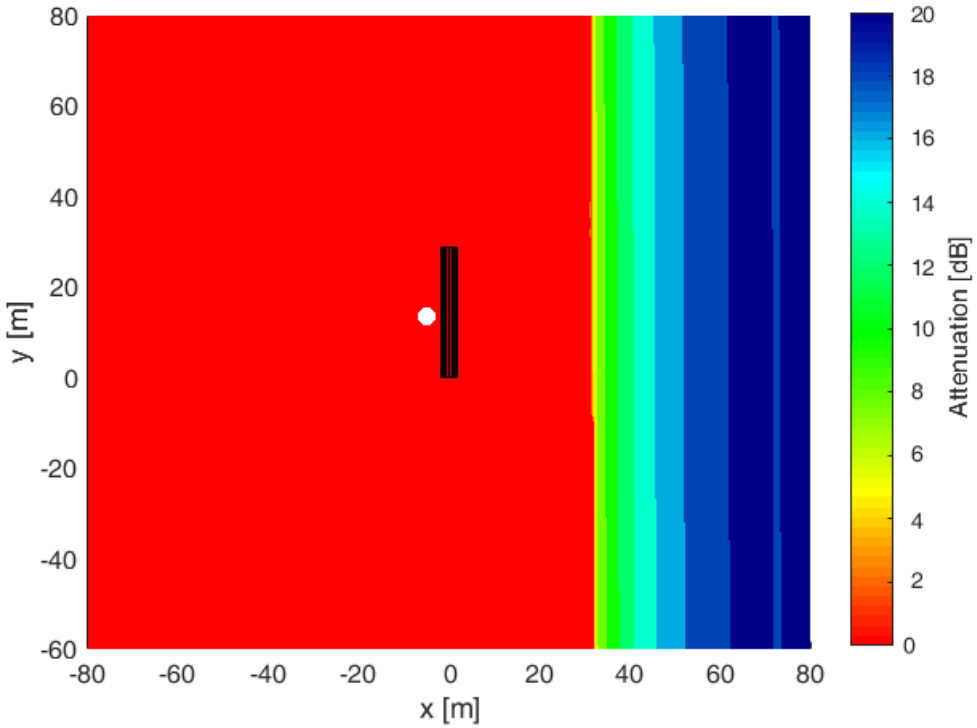

Figure 7.7: Cylindrical Fuselage Noise Shielding of a Boeing 737. 1/3 octave band frequency range from 50 to 10 000 [Hz]. The observer plane is located 30 [m] below the aircraft.

The more towards the center of the fuselage, the higher the amount of shielding becomes. After 50 [m] in x-direction, the fuselage shields more than the one represented in Figure 7.2, even without the wings present. At the center shielding region of the cylinder, a reduction of noise shielding takes place, The higher sound pressure at the center of the shielding region occurs because the sound pressure is reinforced there. A diffracted wave travels around both sides of the cylinder. At the center of the cylinder those two waves can collide and increase the pressure field. This results in a reduction in the shielding coefficient. This reduction in shielding at the back of the shielding object is also visible in Figure 4.7 and Figure 5.9.

The cylinder was expected to have higher shielding. This because creeping rays tend to give higher shielding results. This is shown in Figure 5.9. This is the case because the creeping rays continuously shed rays as it travels around the surface reducing the strength of the ray. The reduction in ray strength results in higher shielding. The highest difference in shielding between the flat plate and the cylinder is 10 [dB]. The results shown in Figure 7.2 are obtained with the Kirchhoff theory of diffraction. This theory is developed for flat shapes with sharp edge diffraction. The cylinder result is more realistic for round shapes. The method was already validated for a two dimensional plane in Figure 4.7 and has shown to provide good results.

At the edge of the contour there is a small region of 5 [dB] noise shielding. Although less prominent than in Figure 7.2. In Figure 7.8 it is zoomed in at the border region of the shielding contour of Figure 7.7. In the zoomed image, the 5 [dB] border is clearly visible.

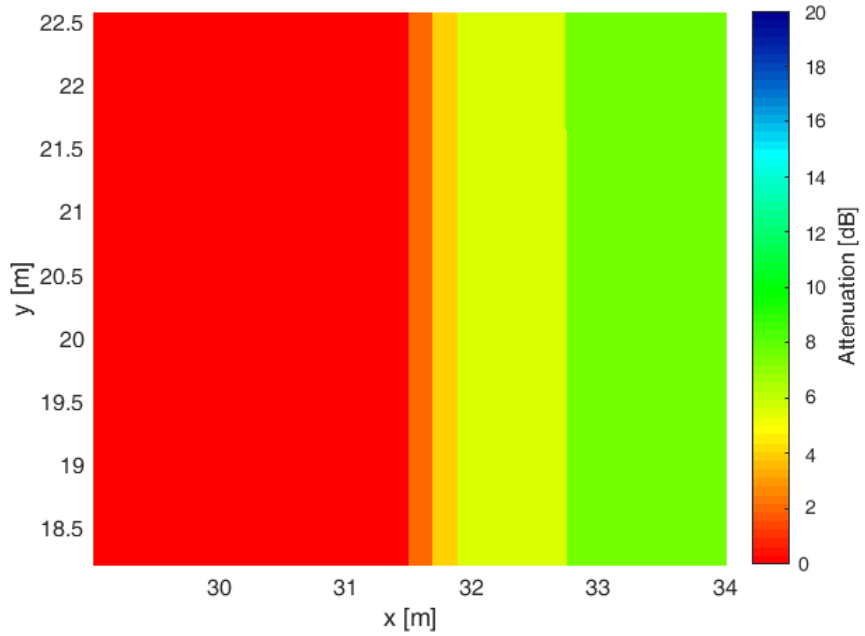

Figure 7.8: Cylindrical Fuselage Noise Shielding of a Boeing 737. 1/3 octave band frequency range from 50 to 10 000 [Hz]. The observer plane is located 30 [m] below the aircraft.

Next, wings are added to the cylindrical fuselage. The result is shown in Figure 7.9. The region of highest shielding at the location of the wing height is wider compared to the rest of the fuselage. This is to be expected and coincides with the highest shielding region of the wing. The error created by not taking the wing root diffraction into account becomes smaller here because the fuselage itself has higher shielding. However, an abrupt change in the highest shielding region from the wing to the fuselage still exists.

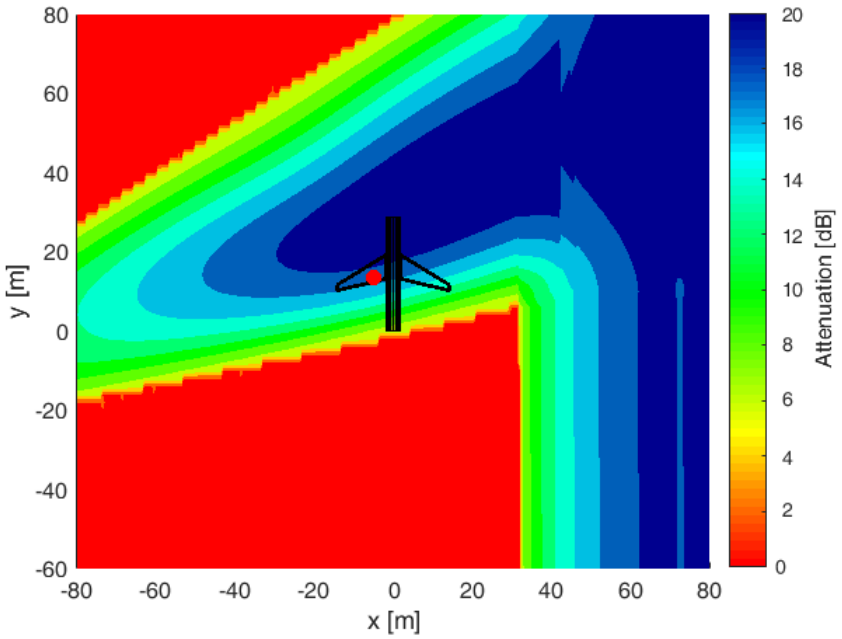

Figure 7.9: Aircraft Noise Shielding of a Boeing 737 With cylindrical Fuselage. 1/3 octave band frequency range from 50 to 10 000 [Hz]. The observer plane is located 30 [m] below the aircraft.

The lower shielding at the center of the fuselage is not present at the height of the wings, because the wings provide extra shielding at this location. The result is comparable to the results obtained with the barrier shielding method shown in Figure 7.6. Except the shielding towards the center of the fuselage is in the order of 10 [dB] higher with the cylindrical fuselage.

Finally, the shielding of two sources is looked at. The noise shielding with the two sources is also validated with the Kirchhoff theory of diffraction. The shielding result of this method is shown in Figure 7.10. It can be seen that the shielding is mainly caused due to the wings.

The result obtained with the noise shielding prediction tool developed in this thesis project is shown in Figure 7.11. The location of the highest shielding occurs at the same place as in Figure 7.10. The amount of highest shielding is 3 [dB] higher compared to the result shown in Figure 7.10. The shielding contour of the trailing edges is not straight as with the Kirchhoff theory of diffraction. This is because the straight trailing edge part is not implemented in the prediction tool. To be able to implemented more complex wing designs, a modular build-up of the wings is needed. The two longer parts in the shielding contour at the end of both wings occurs because the fuselage and wing shielding of both sources collide at these locations.

Overall, it can be concluded that the the noise shielding obtained with the prediction tool in this thesis project is comparable to the results with the Kirchhoff theory of diffraction shown in Figure 7.2 and Figure 7.10. The shielding of the fuselage is higher as expected when including the creeping rays and the wing shielding tends to be overestimated. However, to see how accurate the result is, it needs to be validated against a higher fidelity method such as the fast scattering code. From the results shown here, it is concluded that the noise shielding prediction tool gives a good first impression of the noise attenuation which is useful for the preliminary design phase.

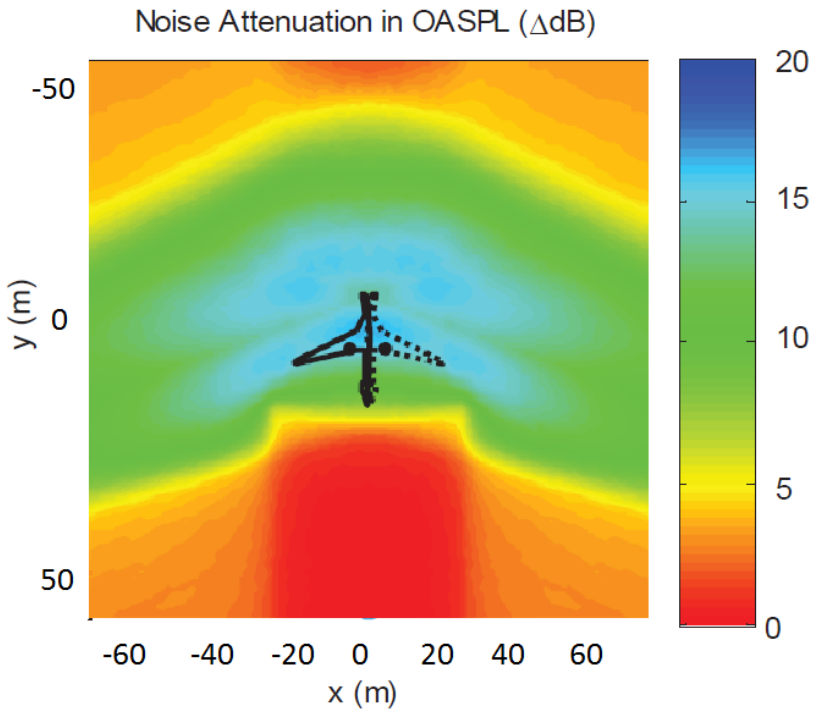

Figure 7.10: Noise Shielding of a Boeing 737 with two engines place on top of the wings. 1/3 octave band frequency range from 50 to 10 000 [Hz]. The observer plane is located 30 [m] below the aircraft. [6].

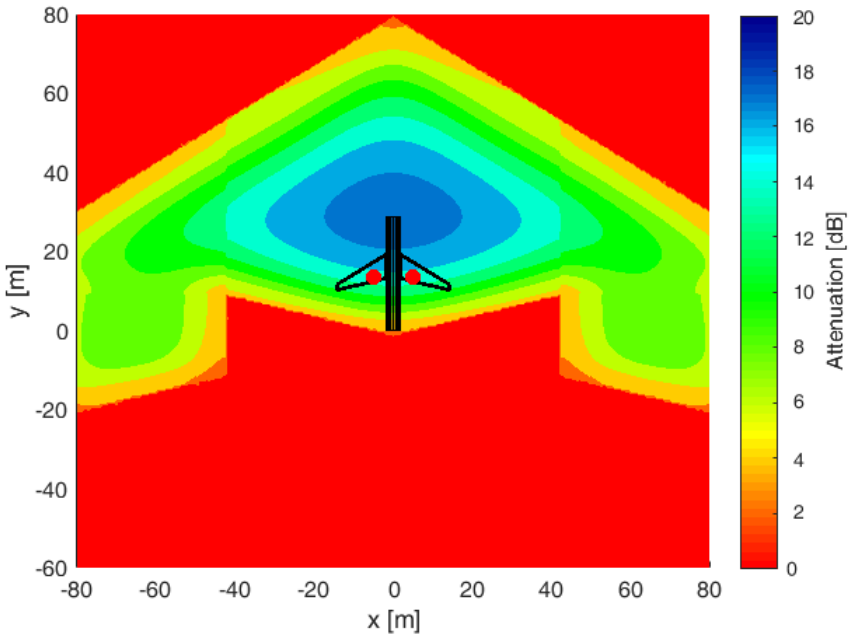

Figure 7.11: Noise Shielding of a Boeing 737 with two engines place on top of the wings. 1/3 octave band frequency range from 50 to 10 000 [Hz]. The observer plane is located 30 [m] below the aircraft.

8

Results

In this chapter, the results of a different aircraft configuration as used in chapter 7 will be discussed. The configuration makes use of the tail and the fuselage to perform the aircraft noise shielding.

8.1. Configuration

The aircraft configuration considered here is a rear fuselage nacelle configuration as shown in Figure 8.1. The purpose of this configuration is to shield the engine exhaust noise with the fuselage and the vertical and horizontal tail planes.

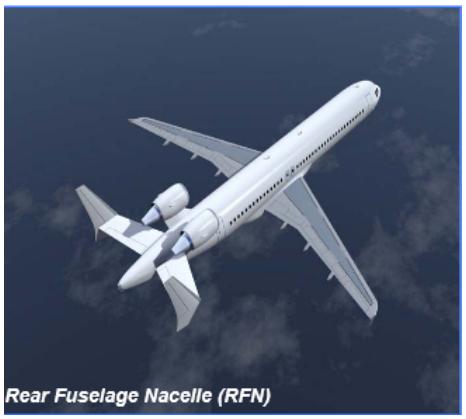

Figure 8.1: Representation of the used aircraft geometry [59].

In the noise shielding prediction tool developed in this thesis project, the fuselage is again modeled as a cylinder and the wings as barriers. For the tail planes, the same procedure as with the wing is followed. Both the vertical and horizontal tail are modeled as barriers from which the noise attenuation can be obtained with the barrier shielding method. In Figure 8.2, the aircraft as it is modeled in the aircraft prediction tool is shown.

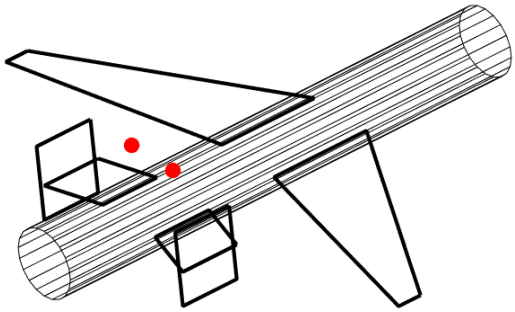

Figure 8.2: Representation of the aircraft as how it is modeled in the prediction tool. The red dots represent the two point sources. The tail-planes and wings are represented by barriers. The fuselage is represented by a cylinder.

The shielding result is shown in Figure 8.3. As can be seen from this figure, the shielding of the fuselage is limited to a small width region. The shielding of the tail plane is present over the complete width. This is the case because the vertical tail is higher than the sound source and thus blocks all the sound rays going downwards.

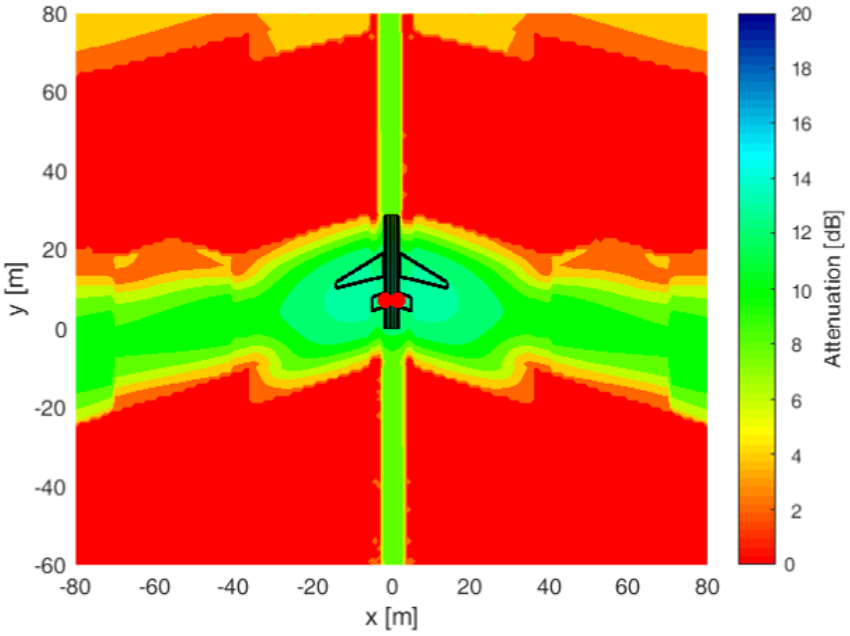

Figure 8.3: Noise shielding result of the rear fuselage nacelle configuration. OASPL over 1/3 octave band frequency range of 50 to 10000 [Hz]. The observer plane is located 30 [m] below the aircraft.

If the vertical tails are removed, the shielding width is decreased significantly as can be observed in Figure 8.4. Different aircraft configurations have a large effect on the aircraft noise shielding results. As shown with the results obtained, the noise shielding prediction tool is capable of determining the noise attenuation of various aircraft configurations.

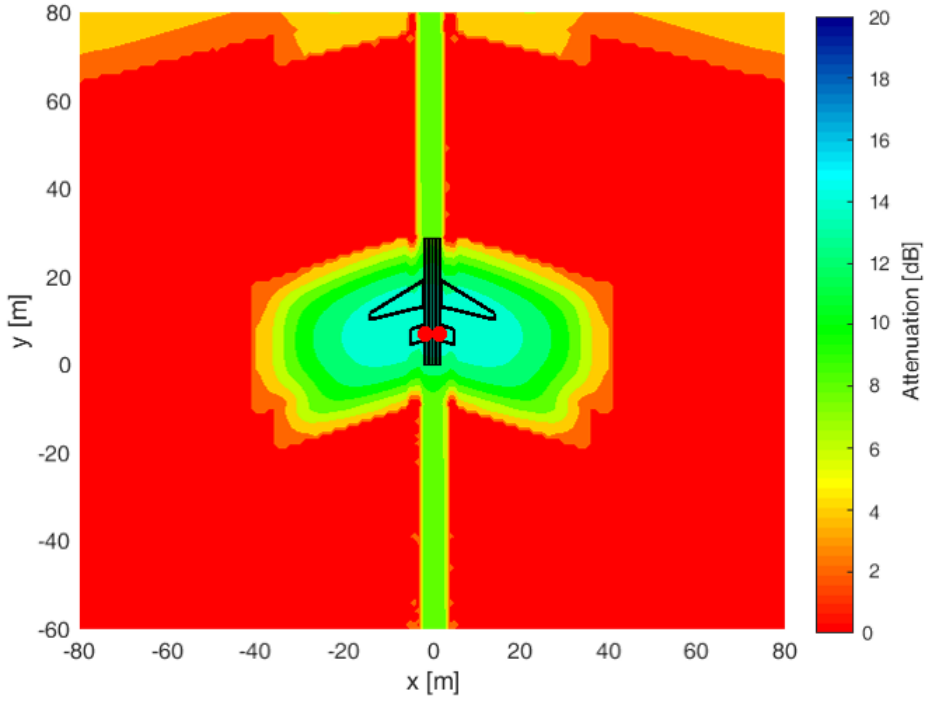

Figure 8.4: Noise shielding result of the rear fuselage nacelle configuration without vertical tail. OASPL over 1/3 octave frequency band of 50-10000 [Hz]. Observer plane located 30 [m] below aircraft.

9

Summary and Conclusions

In this thesis project, an aircraft engine noise shielding prediction tool has been developed. The requirements for this prediction tool are that the computational cost must be low while the accuracy must remain sufficiently high for the preliminary design phase. To achieve this, the barrier shielding method is used for the wings of the aircraft and the analytic solution of a cylinder for the fuselage.

The barrier shielding method is adjusted such that it holds for finite shielding screens. This is computationally the fastest method to determine noise shielding. However, it only considers sharp edge diffracted rays. This means that it is not as accurate for round shapes which will experience creeping rays. To increase the accuracy, the fuselage of a conventional aircraft is modeled as a cylinder. The noise shielding of an infinite cylinder can be obtained analytically. The analytic method incorporates creeping rays and is therefore more accurate. Since it is the result of an infinite cylinder, the diffraction at the front and aft of the fuselage are not taken into account. When the engines are not mounted close to the fuselage end points, the engine noise shielding at those points is of least interest. Finally, the barrier shielding method for the wings and the analytic solution for the fuselage are combined to obtain the complete aircraft noise attenuation. The noise attenuation is only based on the aircraft geometry. Sound absorption and ground reflection are not taken into account. The aircraft geometry is assumed acoustic hard and the engine sound source is modeled as a point source.

9.1. Summary of Results

To be able to use the barrier shielding method for the wings, it is modified to hold for a finite plane. There are two methods available to do this. The first one is used by the NASA Aircraft Noise Shielding Prediction Program. Where the attenuation of each edge is summed up in such a way that it holds for the finite plane. For the second method, the attenuation of the two longest edges of the plane are summed up. Both edges have a correction for the diffraction at the side edges based on their Fresnel numbers. The results are compared at a frequency of 5 [kHz]. When the same plane and same source distance is used, the results are very similar. However, the region of maximum shielding is stretched more in the length direction of the plane for the NASA ANOPP approach. The results are similar, but the NASA ANOPP aproach is more suitable for implementation on different screen shapes. Therefore, this method is used to obtain the wing shielding.

Next, the fuselage represented as a cylinder is looked at. The two-dimensional analytic case of the cylinder is validated. In the test case a shielding coefficient of a two dimensional cylinder of radius a with the point source positioned a distance $3a$ from the cylinder center is looked at. The ka value is set equal to 10 to compare the result with previous work. The prediction tool is found to give the same results as in previous studies.

The results of the fuselage with the barrier shielding method and the analytic solution are compared. To use the barrier shielding method for the fuselage, the fuselage is represented by a plane. Before comparing these two methods, the the shielding of a sphere from literature is looked at. This

is done with both the analytic solution and with the Kirchhoff theory of diffraction. The Kirchhoff theory only uses sharp edge diffracted rays. Therefore, the shielding only depends on the outline of the shielding object. The analytic solution also includes creeping rays. It was found that, when creeping rays are included, the amount of shielding will be higher. Especially at high frequencies. The creeping rays continuously shed rays as they travel around the surface, reducing the strength of the ray. As the frequency increases, more rays are shed reducing the strength even more. The reduction in ray strength results in higher shielding. This means that the analytic solution will result in higher shielding than the barrier shielding method and Kirchhoff theory of diffraction.

The shielding geometry used during this project is based on a Boeing 737 type aircraft. The frequency is 5 [kHz]. The source is located 10 [m] above the cylinder center. The height from the aircraft to the observer plane is 30 [m]. The diameter of the cylinder is set to be 3.76 [m]. As expected, the barrier shielding method gives lower shielding results than the analytic solution for the fuselage. The largest difference is 5 [dB] at the center of the cylinder. The sound rays that determine the shielding at the center, have the largest creeping distance over the cylinder. As a result, the strength of the rays is reduced the most in that region. The rest of the fuselage shielding contour is very similar. Except for the front and aft of the fuselage, because for the fuselage, the diffraction at the front and aft is not taken into account.

To obtain the complete aircraft noise shielding, the solution of the fuselage and wing need to be added together. When the separate results are added together a region of low shielding between the fuselage and wing exist. This is the case as the noise coming from the fuselage is not shielded by the wing. To incorporate the wing shielding of sound rays coming from the fuselage, part of the fuselage located between the wings is included.

When the direct sound ray from the source to the observer intersects this fuselage part, the sound rays diffracted by the fuselage, can also be diffracted by the wings. This part is obtained with the barrier shielding method. Next, the attenuation of that part of the fuselage is subtracted from the total result. Because this attenuation is not provided by the wings. Finally, the attenuation of the cylinder, obtained with the analytic solution, is added. In this way, the sound coming from the fuselage is also shielded by the wings.

The results of the noise shielding prediction tool are validated against the Kirchhoff theory of diffraction. Again, a Boeing 737 type aircraft is used as reference plane. A monopole sound source is placed 2 [m] above the left wing and 4.83 [m] away from the fuselage center. The attenuation is calculated over a 1/3 octave band frequency range from 50 to 10 000 [Hz].

It is concluded that the modification to the barrier shielding method for finite shapes overestimates the region of highest shielding for the wing. In addition, the horizontal plane is not a good representation of the fuselage. It underestimates the region of highest fuselage noise shielding. As expected, the cylindrical fuselage results in higher shielding. The maximum difference with the Kirchhoff theory of diffraction over the used frequency range is 10 [dB].

When a second source is placed on the reference aircraft, the result become very similar. The amount of maximum shielding is overestimated within 3 [dB]. The shielding contour deviates because the leading edge of the wing is assumed to be one straight line.

In conclusion the noise shielding obtained with the prediction tool in this thesis project is comparable to the results with the Kirchhoff theory of diffraction. The shielding of the fuselage is higher than expected when including the creeping rays. However, to see how accurate the result is, it needs to be tested against a higher fidelity method such as the fast scattering code. From the results shown here, it is concluded that the noise shielding prediction tool gives a good first impression of the noise attenuation which is useful for the preliminary design.

9.2. Contribution

The noise shielding prediction tool developed in this thesis project has shown to be able to determine the noise attenuation by a point source of a conventional aircraft with low computational cost. This for a 1/3 octave frequency band from 50 to 10 000 [Hz]. The computational cost needs to be low such that the aircraft noise shielding can be implemented in the design loop. Even with the use of parametric design methods. Once the design of the aircraft is known, a more accurate and computationally expensive noise shielding program can be used if the exact noise shielding results need to be known.

The addition of the analytic results of the cylinder to the barrier shielding method has increased the accuracy by including creeping rays. With this method, there is no need to determine the outline of the shielding object as is the case for the Kirchhoff theory of diffraction. It is also more accurate for the fuselage. Due to this, it is more applicable to conventional aircraft geometries.

9.3. Recommendations

The noise shielding prediction tool is validated against the Kirchhoff theory of diffraction. However, this method itself does have limitations. For instance, it does not incorporate creeping rays. As a result, the sound attenuation obtained with the Kirchhoff theory of diffraction is not completely accurate. To asses the accuracy of the prediction tool developed in this thesis project, it needs to be validated against a higher fidelity method such as the fast scattering code.

To increase the accuracy of the assessment tool, several adjustments can be considered. A modular build up of the wings can be implemented. This will make it possible to approach the shape of the real wing more closely. The diffraction at the front and aft of the fuselage should also be taken into account such that the results of the fuselage are for finite cylinders. To avoid over estimation of the wing shielding, also diffraction at the root edge over the fuselage needs to be considered. The cross section of the cylinder is assumed to be circular everywhere. However, when the sound waves are inclined on the cylinder this is no longer the case. To increase accuracy, oval cross sections may also be included in future work. All objects are assumed acoustic hard and ground reflection is not taken into account in this project. When these assumptions are no longer valid, adjustments to the prediction tool need to be made or another method needs to be used.

Furthermore, it needs to be stated that this method is only applicable to conventional aircraft geometries. When a hybrid wing body needs to be assessed, the substitution of the cylinder is no longer of use. In that case, the Kirchhoff theory of diffraction is assumed to give better results.

A

Input

	X [m]	Y [m]	Z [m]
Outboard Wing LE	14.175	0	11.68
Outboard Wing TE	14.175	0	10.26
Inboard Wing LE	1.88	0	19.23
Inboard Wing TE	1.88	0	13.23
Horizontal Fuselage top front	-1.88	0	28.65
Horizontal Fuselage low front	1.88	0	28.65
Horizontal Fuselage top aft	-1.88	0	0
Horizontal Fuselage low aft	1.88	0	0
Vertical Fuselage top front	0	-1.88	28.65
Vertical Fuselage low front	0	1.88	28.65
Vertical Fuselage top aft	0	-1.88	0
Vertical Fuselage low aft	0	1.88	0
Sound Source	-4.83	-2	13.5
Frequency [Hz]:	5000		
Speed of sound in free stream [m/s]:	340.29		
Fuselage diameter $[m]$:	3.76		
Fuselage length $[m]$:	28.65		
Density of air $[kg/m^3]$:	1.225		

Table A.1: Inputs of the noise shielding prediction tool

Bibliography

[1] M. J. Doty, T. F. Brooks, C. L. Burley, C. J. Bahr, and D. S. Pope, *Jet noise shielding provided by a hybrid wing body aircraft,* AIAA (2011).

[2] *Noise pollution,* (John Wiley and Sons Ltd, 1986) Chap. 3: Acoustic Shielding: Noise Reduction by Thin and Wide Barriers.

[3] Z. Maekawa, *Noise reduction by screens,* Applied Acoustics (1968).

[4] U. Kurze and G. Anderson, *Sound attenuation by bariers,* Applied Acoustics (1970).

[5] L. Lieber and D. Brown, *Small Engine Technology (SET) Task 23 ANOPP Noise Prediction for Small Engines*, Tech. Rep. (NASA, 2000).

[6] L. W. Ng and S. Spakovszky, *Noise shielding assessment of hybrid wing-body aircraft configurations,* AIAA **49**, 2444 (2011).

[7] A. F. Tinetti, M. Dunn, and D. S. Pope, *Fast Scattering Code (FSC) User's Manual*, NASA (2006).

[8] C. A. Reimann, A. F. Tinetti, and M. H. Dunn, *Noise prediction studies for the blended wing body using the fast scattering code,* AIAA/CEAS **11** (2005).

[9] A. F. Tinetti and M. H. Dunn, *Aeroacoustic noise prediction using the fast scattering code,* AIAA/CEAS **11** (2005).

[10] A. Agarwal and A. P. Dowling, *The calculation of acoustic shielding of engine noise by silent aircraft airframe,* AIAA/CEAS (2005).

[11] A. Agarwal, A. P. Dowling, H. C. Shin, W. Graham, and S. Sefi, *Ray-tracing approach to calculate acoustic shielding by a flying wing airframe,* **45** (2007).

[12] M. Lummer, M. Hepperle, and J. W. Delfs, *Towards a Tool for the Noise Assessment of Aircraft Configurations*, Tech. Rep. (DLR, 2004).

[13] D. F. M. Colas, *A Diffraction Integral Based Turbomachinery Noise Shielding Method*, Master's thesis, Massachusetts Intitute of Technology (2011).

[14] L. W.-T. Ng, *Design and Acoustic Shielding Prediction of Hybrid Wing-body Aircraft*, Master's thesis, University of Toronto (2009).

[15] M. Lummer, *Maggi-Rubinowicz diffraction correction for ray-tracing calculations of engine noise shielding,* AIAA/CEAS **14**, 2000 (2008).

[16] K. S. Rossignol, M. Lummer, and J. Delfs, *Validation of DLR's sound shielding prediction tool usig a novel sound source,* AIAA/CEAS **15** (2009).

[17] S. Chandler-Wilde and S. Langdon, *Boundary Element Methods for Acoustics*, Tech. Rep. (Department of Mathematics University of Reading, 2007).

[18] S. Kirkup, *The boundary element method in acoustics,* (Integrated Sound Software, 2007) Chap. 1.

[19] R. Visser, *A Boundary Element Approach to Acoustic Radiation and Source Identification*, Ph.D. thesis, University of Twente (2004).

[20] R. Seznec, *Diffraction of sound around barriers: use of the boundary elements technique,* Journal of Sound and Vibration **73**, 195 (1980).

[21] M. Lummer, *Calculation of Acoustic Shielding at Full-Scale Aircraft Configurations*, Tech. Rep. (DLR, 2012).

[22] A. Delnevo and S. Le Saint, *Numerical methods: Fast multipole method for shielding effects,* AIAA/CEAS **11** (2005).

[23] W. R. Wolf and S. K. Lele, *Fast acoustic scattering simulations with non-uniform potential flow effects,* AIAA/CEAS **16** (2010).

[24] M. Arntzen, *Aircraft Noise Calculation and Synthesis in a Non-Standard Atmosphere*, Ph.D. thesis, Technical University Delft (2014).

[25] P. H. Pathak, G. Carluccio, and M. Albani, *The uniform geometrical theory of diffraction and some of its applications,* IEEE **55** (2013).

[26] J. Keller, *Diffraction by an aperture,* Journal of applied physics **28**, 426 (1957).

[27] L. W.-T. Ng, *Design and Acoustic Shielding Prediction of Hybrid Wing-Body Aircraft*, Ph.D. thesis, Massachusetts Institute of Technology (2009).

[28] J. Keller, *Geometrical theory of diffraction,* Journal of the optical society of America **52**, 116 (1962).

[29] L. Lieber, *Small Engine Technology (SET) Task 13 ANOPP Noise Prediction for Small Engines*, Tech. Rep. (NASA, 2000).

[30] K. Kontos, B. Janardan, and P. Gliebe, *Improved NASA-ANOPP Noise Prediction Computer Code for Advanced Subsonic Propulsion Systems*, Tech. Rep. (NASA, 1996).

[31] O. Zaporozhets, V. Tokarev, and G. Golembievskiy, *Engine Installation and Sound Propagation Effects on Aircraft Noise Levels in Noise Control Points*, Tech. Rep. (National Aviation University, 2004).

[32] A. Pierce and W. J. Hadden, *Wing Shielding In Aircraft Noise Propagation*, Tech. Rep. (NASA, 1977).

[33] A. Filippone, *Aircraft noise prediction,* Progress in Aerospace Sciences (2014).

[34] J. J. Faran, *Sound scattering by solid cylinders and spheres,* Acoustical Society of America **23** (1951).

[35] T. Stanton, *Sound scattering by cylinders of finite length.* Acoustical Society of America (1988).

[36] L. V. Lopes, *A New Approach to Complete Aircraft Landing Gear Noise Prediction*, Ph.D. thesis, The Pennsylvania State University (2009).

[37] M. M. Morshed, A. Zander, and C. Hansen, *Two-dimensional and three-dimensionsl acoustic loading on cylinders due to a point source,* AIAA **49** (2011).

[38] W. Lui and K. Li, *The scattering of sound by a long cylinder above an impedance boundary,* Acoustic Society of America (2010).

[39] P. J. Morris, *The scattering of sound from spatially distributed axisymmetric cylindrical source by a circular cylinder,* Acoust. Soc. Am **97** (1995).

[40] M. M. M. Morshed, *Prediction of exterior sound pressure field of a cylinder using the boundary element method,* Procedia Engineering **56**, 857 (2013).

[41] M. M. M. Morshed, *Investigation of External Acoustic Loadings in a Launch Vehicle Fairing During Lift-off*, Ph.D. thesis, University of Adelaide (2008).

[42] Z. Shen and Y. Tao, *On plane-wave expansions of cylindrical waves,* IEEE (2010).

[43] T. Cavicchi and W. O'brien, *Acoustic scattering of an incident cylindrical wave by an infinite circular cylinder,* IEEE **35** (1988).

[44] P. Filippi, D. Habault, J. Lefebvre, and A. Begassoli, *Acoustics: Basic Physics, Theory and Methods*, 1st ed. (Academic Press, 1999).

[45] D. A. Russell, J. P. Titlow, and Y. J. Bemmen, *Acoustic monopoles, dipoles and quadrupoles: An experiment revisited,* American Journal of Physics (1998).

[46] M. H. Dunn and A. F. Tinetti, *Aeroacoustic scattering via the equivalent source method,* AIAA/CEAS **10** (2004).

[47] M. Ochmann, *The source simulation technique for acoustic radiation problems,* Acustica **81**, 512 (1995).

[48] M. H. Dunn and A. F. Tinetti, *Application of fast multipole methods to the NASA fast scattering code,* AIAA (2008).

[49] S. Mayoral and D. Papamoschou, *Prediction of jet noise shielding with forward flight effects,* AIAA (2013).

[50] W. R. Wolf and S. K. Lele, *Fast acoustic scattering simulations with non-uniform potential flow effects,* AIAA/CEAS (2010).

[51] C. Clancy and J. H. Rice, *Acoustic shielding in low Mach number potential flow incorporating a wake model using bem,* AIAA/CEAS (2009).

[52] E. Rathe, *Note on two common problems of sound propagation,* Sound Vibration **10**, 472 (1969).

[53] M. D. Nark, C. L. Burley, A. Tinetti, and J. W. J. Rawls, *Initial integration of noise prediction tools for acoustic scattering effects,* AIAA (2008).

[54] G. Butler, *A note on improving the attenuation given by a noise barrier,* Journal of Sound and Vibration **32**, 367 (1974).

[55] K. McDonald, *Sommerfeld's Diffraction Problem*, Tech. Rep. (Joseph Henry Laboratories, Princeton University, 2012).

[56] A. Ghiacci, *Excess attenuation: Barriers of finite length*, Tech. Rep. (University of Bologna, 2012).

[57] S. H. Schot, *Eighty years of sommerfled's radiation condition,* Historia Mathematica **19**, 385 (1992).

[58] L. W.-T. Ng, *Design and Acoustic Shielding Prediction of Hybrid Wing-Body Aircraft*, Master's thesis, Massachusetts Institute of Technology (2009).

[59] E. Manoha, S. Redonnet, R. Gaunanff, and X. Juvigny, *Numerical simulation of acoustic effect of engine installation for new concepts of aircrafts,* CEAS (2004).